ARCHITECTURE OF THE BACTERIAL FLAGELLAR ROTOR ELUCIDATED WITH X-RAY CRYSTALLOGRAPHY AND PULSED DIPOLAR ESR SPECTROSCOPY

A Dissertation

Presented to the Faculty of the Graduate School

of Cornell University

In Partial Fulfillment of the Requirements for the Degree of

Doctor of Philosophy

by

Ria Sircar

August 2013

ARCHITECTURE OF THE BACTERIAL FLAGELLAR ROTOR ELUCIDATED WITH X-RAY CRYSTALLOGRAPHY AND PULSED DIPOLAR ESR SPECTROSCOPY

Ria Sircar, Ph.D.

Cornell University 2013

Bacteria swim through liquid media propelled by rotating flagella, driven by a highly complex motor at the base. In response to stimuli, the motor can reverse rotation allowing the bacteria to stop and change direction almost instantaneously. The rotor proteins FliG, FliM, and FliN form the switch complex to generate the cytoplasmic rotor or C-ring. The switch complex is essential for torque generation, binding the response regulator phosphorylated CheY, and switching. Some bacteria contain FliY, which comprises of a FliN homologue and an additional domain with conserved residues from the CheC phosphatase family. There are crystal structures for most of the major rotor components, but not for FliY or complexes containing FliY. To advance our understanding of motor switching, more comprehensive structural information on the switch complex proteins and their assembly state is needed.

I determined the structure of FliY and characterized its biochemical properties. My studies show that FliY functions as an active phosphatase in *Thermotoga maritima* in spite of the presence of two other phosphatases in the chemotaxis signaling system. Interactions of FliY with other rotor proteins were studied. This information was used to develop a model of FliY arrangement in the switch complex.

I also investigated the arrangement of FliM and FliG in the C-ring with X-ray crystallography and pulsed dipolar electron spin resonance spectroscopy (PDS). I determined the crystal structure of a FliG:FliM complex that produces an arc with a radius consistent with the C-ring. However, the antiparallel arrangement of subunits in the crystal structure does not represent the interaction of components in solution phase. PDS data shows that FliM and FliG interact through their middle domains in a parallel fashion. Higher order complexes are mediated by interactions between the C-terminal domain of FliG and the middle domain of a neighboring FliG. Such cross-dimer interactions help to polymerize FliG around the C-ring and could explain the high degree of cooperativity observed upon rotational switching. PDS studies report changes the middle domain of FliM undergoes in the presence of phosphorylated CheY. The crystal structures and spectroscopic studies reported herein provided new insights about the architecture of the C-ring.

BIOGRAPHICAL SKETCH

Ria Sircar was born in Kolkata, India. From a very young age she was encouraged to think freely and pursue her own interest by her family members. In high school she realized her passion for chemistry and decided to pursue her career towards the learning of the subject. Ria attended the prestigious Presidency College, Calcutta to receive her bachelor's degree with an honors in Chemistry.

Next, she took admission in Indian Institute of Technology, Kanpur, Masters Program through a national level competitive examination in 2006. This changed her life. She was first exposed to research in the lab of Dr. P. K. Bharadwaj on metal organic frameworks. She loved the experience and she did not have any doubt about what she wanted to do in the future. To pursue her dreams she flew all the way across the globe to join the Department of Chemistry and Chemical Biology at Cornell University, Ithaca, NY. There she joined Prof. Brian Crane's lab and has worked on the architecture of rotor proteins.

Dedicated to my grandfather

ACKNOWLEDGMENTS

I would like to thank my parents for believing in me and supporting me in whatever I wanted to do. My husband has been my pillar of strength. I thank him for being there in good and bad times. Three people who I wished were alive to see this day is my grandparents. I am sure wherever they are, they are proud of me, and this achievement would not have been possible without their blessings.

I would like to thank all my teachers and professors from school and college for passing on their knowledge. I truly believe my chemistry teacher; Mr. Gautam Das made a huge impact in my life. He stirred the interest in me towards chemistry and from there this journey started.

I would like to express my gratitude to my advisor, Prof. Brian Crane, for his endless encouragement. It would have been very difficult to survive graduate school without his positive attitude. I have learnt a lot from him not only as a scientist but as a human being. I am grateful to have him as a mentor. My committee members Prof. Rick Cerione and Prof. Steve Ealick have been great help in terms to scientific discussion and invaluable suggestions.

A special thanks to Gaby and Jaya for mentoring me and Alex for teaching you how to determine a protein structure. It was great fun to work with my undergraduates Camille and Paul. The girl's squad- Anna, Bee, Alice, and Estella, it was wonderful sharing my everyday happiness and failures with you guys. I would specially like to thank Anna for the numerous radioassays she performed and proof reading. Among the junior members, I shared a lot of fun times with Greg. I really miss the late evening useless conversations with Anand, Greg and Ken. Thanks to Karen, who I really look up to, you are truly an example of how a postdoc should be. Two former members of the lab who I really miss are Xiaoxiao and Anand. I will cherish their friendship and

wonderful memories shared with them, specially the APS trip. Thanks to Joanne, Ken, Tom, Dipanjan, Craig, Mike, and Sarah for all their suggestions, guidance, and help.

I would like to thank Peter Borbat and Elka Georgieva from the Freed group for helping me with ESR experiments and data analysis. And I thank Laura Byrnes from the Sondermann laboratory for her immense help with MALS measurement and data processing. I have spent a lot of time at Cornell High Energy Synchrotron Source, I would like to thank everybody who helped me during data collection.

Five years here at Cornell has been a joyful experience which would not have been possible without the amazing group of friends I had. Thank you Anandarup, Arijit, Souvik, Romita, Abhimanyu, Trina, Joyjit, Saikat, Rima, and Anirudra for making my stay here a memorable one. Though I made new friends here I cannot forget my old friends Priyanka, Ananya, Pranabesh, Nipa, Shraboni, and Aritra (sorry if I missed out somebody) who I have shared my laughter and tears with. Lastly I would like to thank everyone who has touched my life in some way, it is impossible for me to mention everybody but I am grateful for this beautiful experience called life.

TABLE OF CONTENTS

Chapter 4: Probing the Structure of Flagellar Switch Complex from *Thermotoga maritima* using Pulsed ESR Spectroscopy

LIST OF FIGURES

LIST OF TABLES

Chapter 1

Introduction

1.1 Bacterial cell motility:

Bacteria swim through liquid media propelled by rotating flagella. Driven by a highly complex and efficient motor at their base, flagella run at speeds of up to several hundred cycles per second. More than twenty different proteins assemble to form an intricate machine that functions as the shaft, bushing, rotors, and stators of the flagella (Berg, 2003; Sowa and Berry, 2008). These motors can start, stop, and change rotational direction almost instantly, allowing the bacterium to rapidly respond to the environment. In the absence of a stimulus, the cells continue to swim smoothly or "run" for a second then stop, "tumble", and change rotational direction (Turner et al., 2000). In the presence of a repellent the run duration decreases, and tumbling occurs more frequently, which reorients the cell and helps it to move away from the unfavorable environment. When the cells swim smoothly, the flagella are bundled up together and rotate in a counter clockwise (CCW) direction. When the cell tumbles, one or more flagella separates from the bundle and rotate clockwise (CW) (Fig. 1.1) (Berg, 2003; Kojima and Blair, 2004; Sowa and Berry, 2008; Terashima et al., 2008).

1.2 Overview of the signaling pathway:

Decades of study on the chemotaxis signaling pathway in *Escherichia coli* has produced molecular level understanding of the pathway. Chemotaxis relies on a two-component system involving the histidine kinase CheA and the response regulator CheY. The binding of ligands to the methyl-accepting chemotaxis proteins (MCPs) in presence of a repellent triggers the autophosphorylation of CheA, which is coupled to CheW. Subsequent phosphorylation of the

response regulator CheY (CheY-P) by CheA on a specific aspartate residue activates CheY and favors the binding of CheY to the switch complex of the flagellar rotor. The amount of CheY-P bound to the rotor controls the bias of flagellar rotation between CCW to CW, with greater CheY-P favoring CW. Once the signal is relayed and the flagellar response takes place, the signal is terminated by the dephosphorylation of CheY-P, upon which the cells return back to the pre-stimulus level (Fig. 1.1). CheY has the ability to dephosphorylate itself; however, the rate becomes 100-fold faster in the presence of a specific phosphatase (Armitage, 1999; Wadhams and Armitage, 2004).

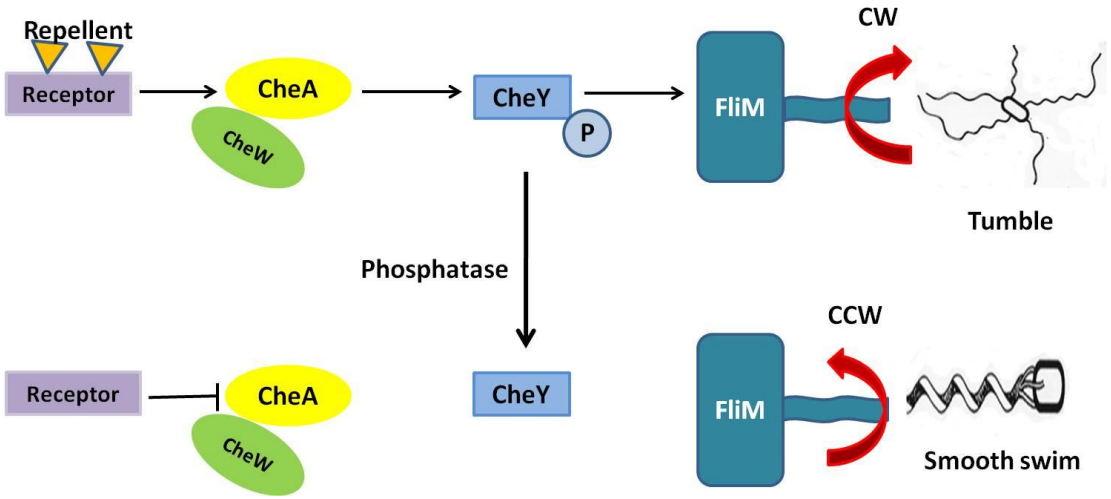

Figure 1.1. **Chemotaxis signaling pathway in *Escherichia coli.*** The schematic representation shows the important players involved in this pathway. The receptors undergo conformational changes after sensing the repellent or decrease in attractant concentration (Stewart, 2005). This activates autophosphorylation of CheA. CheA then phosphorylates CheY which binds to the rotor and causes the flagella to rotate clockwise, resulting in a tumble. This allows the bacteria to reorient and move away from the repellent. Once CheY is dephosphorylated the flagella rotates counter clockwise and cells continue to swim smoothly.

1.3 The flagellar motor:

The flagellar motor is the first direct evidence of a biological rotary machine (Sowa and Berry, 2008). Scientists have marveled for decades at how this nanomachine functions and converts

energy into mechanical work with such high efficiency. Unlike modern day motors which are powered by electricity or hydrocarbons, or biological ones such as actin and myosin which derive energy from ATP, the flagellar motors obtain their energy from the proton motive force (Paul et al., 2008). While the motors are as tiny as 45 nm, they can rotate at several hundred hertz, significantly faster than a Formula One engine (Berg, 2003; Thomas et al., 2006). Because the flagellar motor operates with very little friction and heat generation, they functions near the theoretical limit of an ideal machine. Understanding the mechanism of the flagellar motor may aid in the design of artificial nanoscale motors. Such motors could have important applications for drug delivery and cargo transport at cellular level.

1.3.1 Architecture: For over 40 years, flagella have been studied extensively in *E. coli* and *Salmonella typhimurium*. While these efforts have helped to further our understanding of the assemblies, much work is still needed to elucidate molecular aspects of this remarkable machine. The bacterial flagellum consists of an export apparatus, a reversible rotary motor, a universal joint, and filament (Berg, 2003; Kojima and Blair, 2004). Our understanding of the flagella is highly enhanced by the electron microscope (EM) images of an intact basal body from *S. typhimurium* at approximately 22 Å resolution (Fig. 1.2) (Thomas et al., 2006). The results indicate that the motor core or "basal body" comprises of a number of rings: L, P, MS, and C which together span several layers of the cytoplasmic and outer membrane (Fig. 1.2) (Berg, 2003; Suzuki et al., 2004). These rings are named after their location – lipopolysaccharide (L), peptidoglycan (P), membrane/supramembrane (MS), and cytoplasmic (C) layers respectively (DePamphilis and Adler, 1971). The MS-ring is assembled first, serving as the platform on which the other parts of the motor are built (Sowa and Berry, 2008). The MS-ring and C-ring are

thought to form the rotor, functioning together as one unit (Berg, 2003; Kojima and Blair, 2004; Terashima et al., 2008).

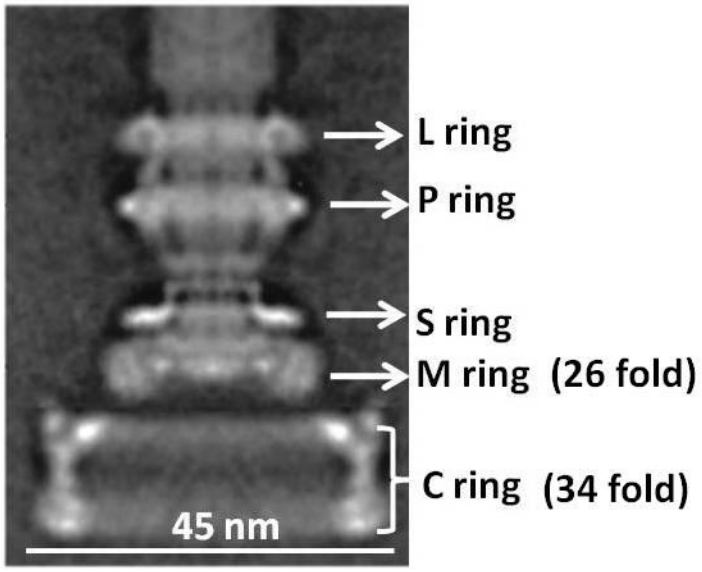

Figure 1.2. **Electron microscope image of an intact basal body from *Salmonella typhimurium***. Side view indicating the position of the different rings, adapted and modified from Thomas et al., 2006.

1.4 Switch complex:

The rotor proteins FliG, FliM, and FliN, each present in several copies, form the switch complex of the cytoplasmic C-ring (Fig. 1.3) (Kubori et al., 1997). The EM image measures the size of the C-ring to be 45 nm, and the symmetry within the EM reconstructions reports on the number of subunits present. Concentric rings of electron density of ~34-fold symmetry and 26-fold symmetry were observed for the C-ring and MS-ring respectively (Thomas et al., 2006). Interestingly, the feature of the C-ring closest to the MS-ring ("inner ring") has rotational symmetry similar to the MS-ring rather than the C-ring. This results in a symmetry mismatch among the components of the C-ring (Brown et al., 2007; Thomas et al., 2006). It is believed that there are 26 copies of FliG, 34 copies of FliM and 136 copies of FliN.

The switch complex composes of the rotor and is the site where the second messenger CheY-P binds in order to switch rotational sense (Dyer et al., 2009; Park et al., 2006). Mutations in the genes expressing FliG, FliM, and FliN lead to non-flagellate (Fla-), paralyzed (Mot-), and switch biased (either CCW or CW) phenotypes (Yamaguchi et al., 1986). However, non-motile mutations of *fliM*, *fliN* can be complemented by over-expression of these proteins (Berg, 2003). Combination of crystal structures, cross-linking experiments, and pull-down assays clearly indicate the interaction pattern of the conserved rotor proteins FliG, FliM, and FliN in the switch complex (Brown et al., 2002; Brown et al., 2007; Kubori et al., 1997; Lam et al., 2013; Lowder et al., 2005; Park et al., 2006; Paul et al., 2011b; Sarkar et al., 2010b; Vartanian et al., 2012). However, there is currently no consensus about the orientation of the protein domains in the switch complex (Brown et al., 2007; Paul et al., 2011b).

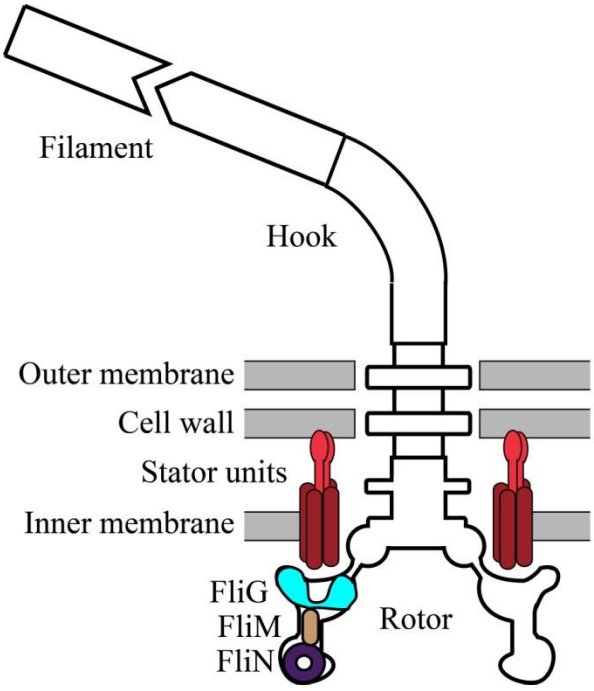

Figure 1.3. **Schematic representation of flagellar motor showing different components.** The arrangement of the different rotor proteins FliG, FliM, and FliN and the stator unit based on various biochemical assays is shown. Figure adapted from Sowa and Berry, 2008.

1.4.1 FliG: FliG acts as the connector between the C-ring and the MS-ring and plays the key role in flagellar rotation by interacting with the stator proton channel MotA (Fig. 1.3) (Lam et al., 2013; Lloyd et al., 1996). Crystal structures of FliG (Brown et al., 2002; Lam et al., 2013; Lee et al., 2010; Lloyd et al., 1999; Minamino et al., 2011) reveal three distinct globular domains (amino, middle, and C-terminal domains) comprised of α helices (Fig. 1.4). The MS-ring composed of FliF showed 26-fold symmetry. Since the N-terminus of FliG ($FliG_N$) interacts with FliF in the MS-ring (Grunenfelder et al., 2003; Kihara et al., 2000; Levenson et al., 2012), FliG is believed to have 26 copies (Suzuki et al., 2004; Thomas et al., 2001; Thomas et al., 2006). EM image of a FliF-FliG fused deletion mutant (FliF C-terminal 56 residues and FliG N-terminal 94 residues were deleted) showed an upward shift in the electron density when compared to the wild type EM image (Thomas et al., 2001). This indicates that $FliG_N$ contributes towards the electron density of the cytoplasmic face of the M-ring. The middle domain has a conserved EHPQR motif known to interact with FliM, which was observed in the co-crystal structures of FliM with FliG as well as in solution by NMR studies (Dyer et al., 2009; Lam et al., 2013; Paul et al., 2011b; Vartanian et al., 2012). The hydrophobic patch of the C-terminal domain of FliG ($FliG_C$) has also been implicated in interactions with FliM (Brown et al., 2007; Passmore et al., 2008; Paul et al., 2011b). The middle domain and the C-terminus are linked by a long α helix (referred as $Helix_{MC}$ in Fig. 1.4). A conserved Gly-Gly hinge at the C-terminal end of the linker renders the junction between the two domains highly flexible (Brown et al., 2002). Previous work has shown that mutation in this helix leads to phenotypes such as CW bias, defects in switching, and paused behavior. Thus, the junction helix plays a critical role in switching (Van Way et al., 2004). Crystal structure of different variants of FliG shows this $helix_{MC}$ in different orientations, (extended and closed) attributing each to different conformation that FliG could assume in CCW

and CW states (Brown et al., 2002; Lee et al., 2010; Minamino et al., 2011). Five conserved charged residues present along the ridge of $FliG_C$ interact with the stator, MotA (Lloyd and Blair, 1997; Lloyd et al., 1999; Zhou et al., 1998). These residues are not individually vital for rotation, but function collectively. The electrostatic interaction between these charged residues on MotA and FliG results in torque generation, thus allowing for the communication between the bound states of FliM to the motor.

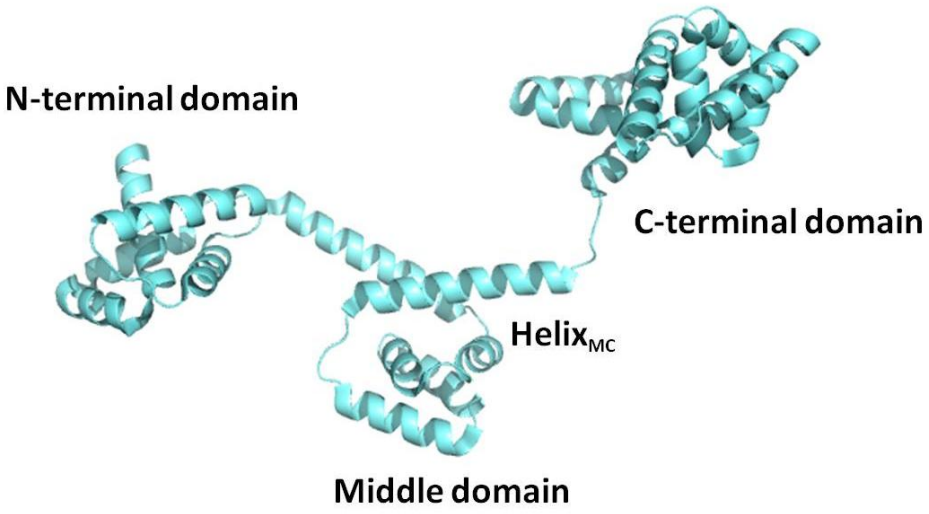

Figure 1.4. **Structure of full length FliG from *Aquifex aeolicus* is mostly helical.** Structure displays three distinct globular domains (PDB 3HJL).

1.4.2 FliM: Another component involved in switching is FliM, whose amino terminal is known to interact with CheY-P (Bren and Eisenbach, 1998; Park et al., 2006; Sockett et al., 1992; Toker and Macnab, 1997; Welch et al., 1993). The affinity for the N-terminal region however decreases many fold if CheY is not phosphorylated (Park et al., 2006). A recent study has shown that at higher local concentrations, CheY-P also interacts with the middle domain of FliM (Dyer et al., 2009). The structure of the middle domain of FliM ($FliM_M$) reveals a pseudosymmetric α/β globular protein similar to the CheC phosphatase family (Fig. 1.5). Cross-linking experiments on FliM shows that it self-associates in the C-ring via its α1 and α2′ helices. Based on the size of

$FliM_M$ structure, 35 copies of FliM can fit into the C-ring of diameter 45 nm (Park et al., 2006). The residues mediating the intersubunit contact between the FliM middle domains are also important for CCW/CW switching. All the CW bias mutants and some CCW bias mutants reside on surfaces mediating the FliM:FliM interaction. Many of the CCW biased mutants are located mostly at the bottom of the middle domain near the FliN interacting surface (Park et al., 2006; Paul et al., 2011b). The conserved GGXG motif in the middle domain is essential for binding FliG as evidenced from the FliG:FliM crystal structures (Lam et al., 2013; Paul et al., 2011b; Vartanian et al., 2012) and biochemical assays (Mathews et al., 1998). Insertion of a Proline residue in the conserved motif (GPGXG) reduces binding to FliG (Mathews et al., 1998). FliG is absolutely necessary for FliM localization as observed by fluorescence of FliM-YFP in cells (Sourjik and Berg, 2000). The C-terminal domain of FliM ($FliM_C$) interacts with the third rotor protein, FliN (Brown et al., 2005; Mathews et al., 1998; Sarkar et al., 2010b). FliM and FliN are the first proteins to be assembled acting as the foundation of the C-ring during the early stages of flagella formation (Brown et al., 2005; Gonzalez-Pedrajo et al., 2006).

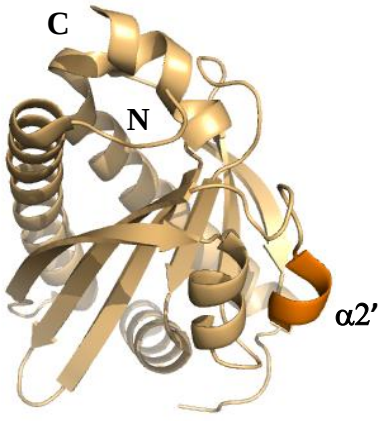

Figure 1.5. **Structure of middle domain of *Thermotoga maritima* FliM (46-226)**. The ribbon representation shows six helices and six β-strands intertwined to form the pseudosymmetric globular domain. The two-fold axis extends out of the plane from the central β sheet platform.

The electron density for the conserved GGXG motif is absent, seen here by the discontinuous loop at the bottom of the structure (PDB 2HP7).

1.4.3 FliN: FliN is thought to form the donut shaped ring at the bottom of the C-ring. This protein is involved mostly in switching and flagellar assembly. Crystal structure of the C-terminal two thirds of the protein is known (Fig. 1.6) (Brown et al., 2005). It is a tightly intertwined dimer formed mostly of β-sheets related by a twofold axis (Paul and Blair, 2006). The hydrophobic patch along the two fold symmetry axis is known to bind FliH, a protein involved in the export of filament subunits, thus implicating FliN in protein export as well as rotor architecture (Brown et al., 2005; Gonzalez-Pedrajo et al., 2006; McMurry et al., 2006; Yamaguchi et al., 1986). Switch-bias mutants are not as common in FliN, which suggests a minimum role for FliN in switching. FliN residues that when substituted do cause CCW bias are present around a hydrophobic patch (Sarkar et al., 2010a). However, a recent cross-linking study showed that after binding to $FliM_N$, CheY-P interacts with FliN (Sarkar et al., 2010a). FliM and FliN interact strongly in the ratio 1:4 with FliN tetramers alternating with $FliM_C$ (Brown et al., 2005; Sarkar et al., 2010b). Changes in the yield of $FliM_C$:FliN cross-linked product in presence of a repellent suggests a movement along the $FliM_C$:FliN surface during switching (Sarkar et al., 2010b). Biochemical assays and mutational studies show that the residues involved in this interaction are grouped in two different regions of FliN, one along the outer ridge and another along the inner edge of the donut (Sarkar et al., 2010b).

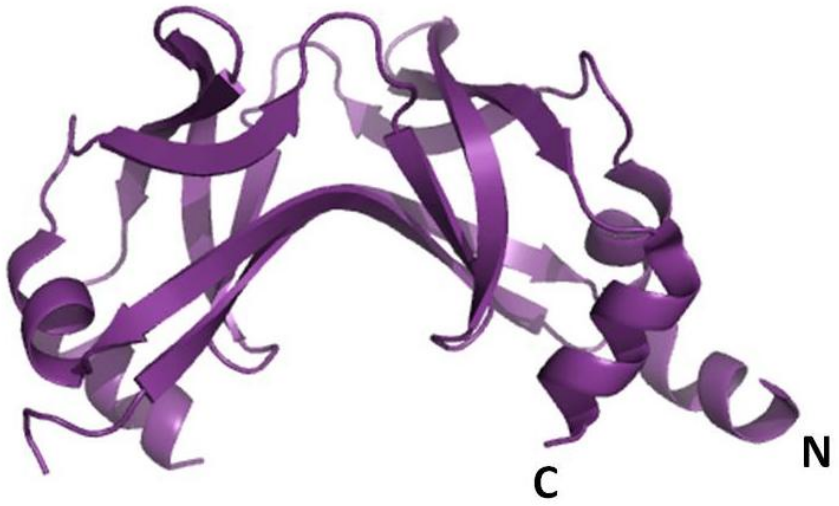

Figure 1.6. **Structure of C-terminus of FliN (64-158) dimer from *Thermotoga maritima***. The ribbon representation shows a saddle like structure composed mostly of β-sheets (PDB 106A).

1.4.4 The less-conserved rotor protein FliY: In some bacterial genera like *Thermotoga* and *Bacillus,* the amino terminus of FliN is fused to an additional phosphatase domain, known as FliY (Bischoff and Ordal, 1992b). FliY dephosphorylates CheY at the motor, thereby extinguishing the signal. It belongs to the CheC/CheX/FliY phosphatase family, with the structure of the central domain similar to CheC and the rotor protein FliM (Park et al., 2004; Park et al., 2006; Sircar et al., 2013). The conserved D/S–X_3-E-X_2-N-X_{22}-P motif defines the phosphatase active site (Muff and Ordal, 2008; Park et al., 2004; Silversmith, 2010). FliY has an amino-terminal CheY binding domain very similar in sequence to that of FliM (Park et al., 2006; Sircar et al., 2013). In *Bacillus subtilis,* this fragment is absolutely necessary to bind CheY-P but not in *T. maritima* (Sircar et al., 2013; Szurmant et al., 2003). Since FliY is able to complement the motility defect of *S. typhimurium fliN* null mutant, FliY is believed to be located at the rotor (Bischoff and Ordal, 1992b). Some bacterial species like *Thermotoga* and *Bacillus* encode only FliY whereas others like *Helicobacter* and *Leptospira* encode both FliN and FliY (Lowenthal et

al., 2009; Sircar et al., 2013). Encoding two or more proteins with redundant function is not uncommon in the chemotaxis signaling pathway.

1.5 Current switch complex model:

Structures of individual components, complemented with genetic analysis and biochemical studies by many groups enable the positioning of the C-ring components in the intact motor. Our best overall knowledge about the entire switch complex comes from high-resolution, single particle EM images. It is clear that FliG occupies the top most position of the C-ring followed by FliM and FliN. The charged residues of $FliG_C$ are present along the outer ridge of the C-ring so that they can interact with the stators. There is little agreement about the arrangement of $FliG_M$ and $FliG_N$ in the features observed in the EM images The Blair group favored positioning $FliG_C$ to the outer lobe of density and $FliG_{NM}$ to the inner lobe (Brown et al., 2007). The DeRosier group proposed that $FliG_C$ is present along the inner lobe and the remaining portions are present in MS-ring (Thomas et al., 2006). Recent work by the Namba and Stock groups predicted that $FliG_C$ (or $FliG_{C+1}$) and $FliG_M$ forms the outer lobe and $FliG_N$ forms the inner lobe (Fig. 1.7) (Lee et al., 2010; Minamino et al., 2011). FliG interacts with FliM's conserved GGXG motif. There are numerous models for FliM:FliG interaction as described below. FliN tetramers occupy the donut like electron density at the bottom of the C-ring right below FliM. The C-terminus of FliM is believed to bind between adjacent FliN tetramers.

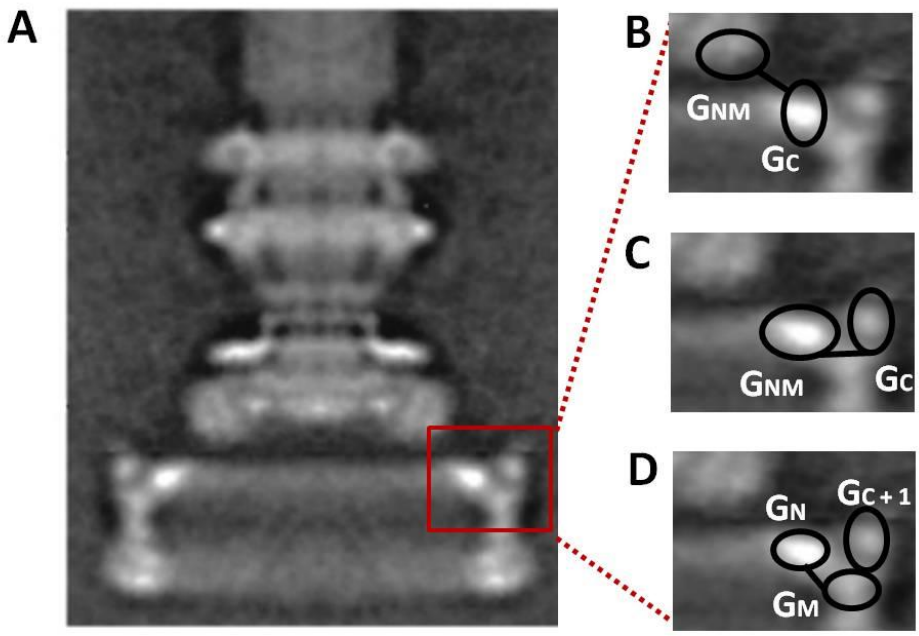

Figure 1.7. **Hypothesis for FliG arrangement in the rotor.** (A) EM image of intact flagella from WT *S. typhimurium* (Thomas et al., 2001). Red box indicates the position of FliG in the electron density. Arrangement of different domains of FliG proposed by Thomas et al., 2006 (B), Brown et al., 2007 (C) and Lee et al., 2010 or Minamino et al., 2011 (D). Figure adapted and modified from Paul et al., 2011b.

1.5.1 Model for FliM:FliG interaction: Different models have been proposed for the FliM:FliG complex. The Blair lab proposed a model based on the symmetry mismatch with evidence from biochemical assays. According to their model, 26 copies of FliM interact with 26 copies of FliG through the C-terminal hydrophobic patch and the remaining eight copies of FliM interact with the EHPQR motif present in the middle domain of FliG (Brown et al., 2007; Paul et al., 2011b) (Fig. 1.8 (A)). The co-crystal structure of $FliM_M$ with $FliG_M$ establishes the interaction via the middle domains. Using pull-down assays they were able to detect an interaction between $FliG_C$ (185-331) fragment and $FliM_M$ in cells (Paul et al., 2011b). The FliM molecules present along the outer edge of the C-ring change orientation during switching but the remaining eight copies form a more rigid inward region (Paul et al., 2011b). This model could explain results of

fluorescence photo bleaching where a major fraction of FliM was in rapid exchange with a free pool of FliM provided the cells were switching (Delalez et al., 2010). Accordingly, only the outward FliM molecules exchanged rapidly with cellular FliM.

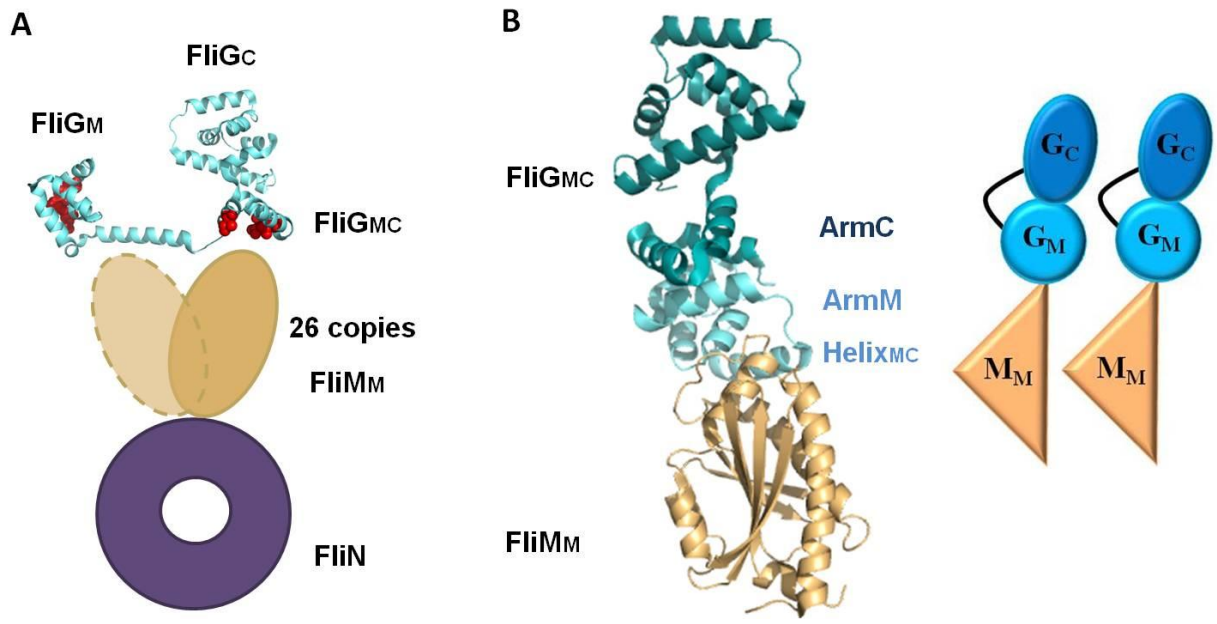

Figure 1.8. **Models for FliM:FliG interaction.** (A) Blair model based on the symmetry mismatch between FliG and FliM. More copies of FliM interact with FliG through the C-terminal domain ($FliG_C$), with fewer copies interacting with FliG through the middle domain ($FliG_M$). (B) Left: The $FliM_M$:$FliG_{MC}$ crystal structure from Dahlquist group (PDB 4FHR). FliM and FliG interaction is through the middle domains. The arm stacking between ArmM and ArmC is shown. Right: Schematic representation of the arrangement of FliM and FliG in the C-ring based on the crystal structure.

A recent co-crystal structure of $FliM_M$ with $FliG_{MC}$ from the Dahlquist lab shows that $FliG_M$ and $FliM_M$ interact in a 1:1 ratio through the EHPQR motif of $FliG_M$ and GGXG motif of $FliM_M$, much the same as was seen in the original structure of $FliG_M$ with $FliM_M$ (Lam et al., 2013; Paul et al., 2011b; Vartanian et al., 2012). The $FliG_C$ portion is present on top of $FliG_M$. The pseudo armadillo repeats from helices 1-4 (ArmM) and helices 6-8 (ArmC), stack on a single FliG protomer resulting in burial of 14 hydrophobic residues (Fig. 1.8 (B)) (Vartanian et al., 2012). Not observing any interaction between $FliM_M$ and $FliG_C$ in the crystal structure, they measured

the binding between these two domains. The dissociation constant value between FliM and $FliG_C$ was 580 μM indicating a weak interaction between them. This group predicted that the interaction between $FliG_C$ and FliM is either absent *in vivo* or applicable to a sub-population of the species (Vartanian et al., 2012).

1.6 Switching:

The reversible rotary motor efficiently converts proton-motive force to torque generated in either the CW or CCW direction. Switching between the CCW and CW directions dictates whether the bacteria will swim smoothly or tumble. The likelihood of spinning in the CW direction is governed by CheY-P (Silversmith and Bourret, 1999). Understanding the changes in molecular structure that causes switching will provide great insight into how the rotor is coupled to the stator for torque generation.

There are several mechanistic models for switching (Bai et al., 2010; Cluzel et al., 2000; Duke et al., 2001; Turner et al., 1999). However, none of these models are able to resolve how the CW/CCW configuration changes the shape of the basal body, what conformational changes are caused when CheY-P binds to FliM, or how the signal is transmitted to the rotor/stator interaction.

1.6.1 Switch associated movement in FliM, FliG and FliN: The model described here is the most extensive one involving all the switch proteins FliG, FliM, and FliN (Paul et al., 2011a; Paul et al., 2011b). According to the recent structural model there are two different types of FliM, one which is oriented outwards interacting with $FliG_C$ (26 copies of FliM) and the remaining eight copies oriented inwards interacting with $FliG_M$. Cross-linking experiments on FliG, FliM, and FliN in the presence of a stimulus (attractant or repellent) provided us with

insight into the switching mechanism. At first the signaling protein CheY-P is captured by the N-terminus of FliM. It then interacts with FliN and allows a conformational change to the FliN:$FliM_C$ interface. This acts as the initial steps of switching to CW direction. $FliM_M$ is directly placed above the FliN:$FliM_C$ array in the C-ring. Any conformational change that affects FliN:$FliM_C$ would also affect $FliM_M$. To test how the signal is transmitted towards FliG, cross-linking experiments were performed on FliM and FliG. Cross-linking yields were unaffected for $FliM_M$:$FliG_M$ and $FliG_M$:$FliG_M$ in presence of stimuli indicating that these collective domains behave as rigid units during switching. Residues cross-linked on the linker α helix of FliG and $FliM_M$ (FliG193/FliM74) yielded stronger repellent stimulated cross-linked bands (Lowder et al., 2005). Most of the $FliG_C$:FliM and $FliM_M$:$FliM_M$ cross-linked pairs showed a strong dependence on chemotactic stimuli. These results could be explained by the relative rotation of $FliG_C$ with respect to $FliM_M$ and a movement of the top of $FliM_M$, with the minor $FliG_M$:$FliM_M$ interaction providing a rigid support (Paul et al., 2011a). Rocking of $FliM_M$ in presence of activated CheY causes a large rotational change to $FliG_C$ which lies above (Fig. 1.9). According to this model, cooperativity is generated by the FliN:$FliM_C$ tetramer at the base of the ring along with the two-step binding mechanism of CheY-P. CheY-P binds to $FliM_N$ in a non-cooperative manner and then is recruited to the switch. However, the switch occurs only after a certain number of CheY-P molecules accumulate on the $FliM_N$ tethers. This model is based on studies in *E. coli*. Switch complex architecture in FliY containing bacteria might be different. Further studies would be necessary to show if this model is valid in such bacteria.

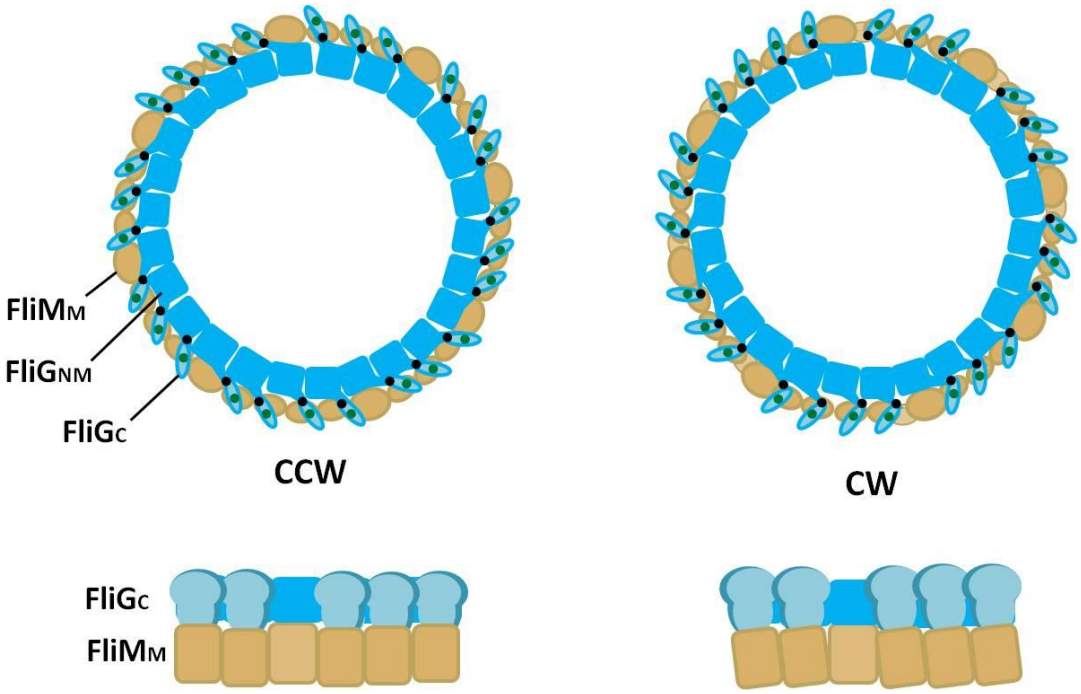

Figure 1.9. **Model for flagella switching.** Upper panel shows the tangential movement $FliG_C$ (light blue) undergoes after CheY-P binds to the lower part of C-ring. Green dots indicate the approximate positions about which $FliG_C$ pivots above FliM and black dots indicates the position of conserved Gly-Gly residues. Lower panel shows the tilting of $FliM_M$ (dark tan) and the rotation the supported $FliG_C$ (light blue) undergoes. The inner $FliM_M$ (light tan) and $FliG_{NM}$ (blue) are considered to be rigid and do not undergo any movement. Figure adapted from Paul et al., 2011a.

1.7 Diversity in C-ring structure across the bacterial kingdom:

Cryo EM images of bacterial flagella from 11 different bacteria shows the diversity in flagellar structure among varied species. Mostly the core structure is conserved, as is the relative position of the rings with respect to the membranes; however, there are remarkable differences in the overall size and appearances (Fig. 1.10). The C-ring from various bacteria shows different diameters, ranging from 37 nm to 54 nm (Chen et al., 2011; Murphy et al., 2006). Cryo EM of a *Leptospiral* motor shows additional electron density around the lower part of the C-ring (Raddi et al., 2012).

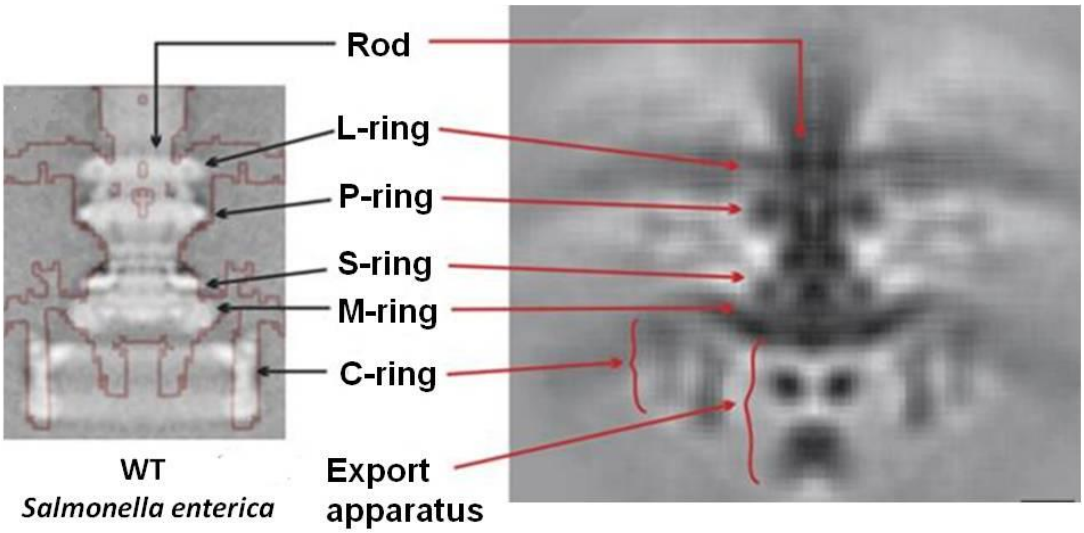

Figure 1.10. **Core structures of the motor from different bacteria.** Left: The isosurface of *S. enterica* motor (red line) aligned to the EM reconstruction of basal body. Right: The flagellar motor structure obtained by aligning motor images from 11 different bacterial species. The core structure aligns perfectly, however, the C-ring has different diameter, showing up as multiple C-rings in the average. Figure adapted and modified from Chen et al., 2011.

1.8 Discussion:

Studies of the chemotaxis pathway in *E. coli* over several decades have provided us knowledge about signal detection, amplification and adaption in bacterial motility (Hazelbauer et al., 2008; Tindall et al., 2012; Wadhams and Armitage, 2004). This dissertation is focused on the architecture of the flagellar C-ring, especially in Gram-positive and thermophilic bacteria. The sequence similarity between FliM and FliG amongst different bacteria indicates that the structure and interaction between these proteins were similar and conserved amongst different species. We have elucidated the arrangement of FliM and FliG in soluble complexes and find that they assemble in such a manner as to optimize cooperative interactions within the C-ring. The structure of the C-ring in Gram-positive bacteria and spirochetes differs from the paradigm *E. coli* or *S. typhimurium* due to the presence of FliY. Herein, we provide the first crystal structure of FliY and characterize its binding and reactivity toward CheY-P. So far the highest resolution

EM images of the basal body have been obtained from *S. typhimurium*. Lower-resolution cryo-EM images of the Gram-positive switch are available and they show a larger diameter of the C-ring, which may reflect the addition of FliY. Gram-positive and related bacteria are especially important in medicine because several motile species are involved in pathogenicity like *Helicobacter pylori*, *Vibrio cholera* (Howitt et al., 2011; Rolig et al., 2011; Schweinitzer and Josenhans, 2010; Terry et al., 2005). Understanding the architecture of the flagellar rotor in Gram-positive bacteria will help resolve remaining issues in overall C-ring architecture and provide molecular data on a key system required for medically important bacteria to sense and respond to their environment.

References:

Armitage, J.P. (1999). Bacterial tactic responses. Advances in microbial physiology *41*, 229-289.

Bai, F., Branch, R.W., Nicolau, D.V., Jr., Pilizota, T., Steel, B.C., Maini, P.K., and Berry, R.M. (2010). Conformational spread as a mechanism for cooperativity in the bacterial flagellar switch. Science *327*, 685-689.

Berg, H.C. (2003). The rotary motor of bacterial flagella. Annual review of biochemistry *72*, 19-54.

Bischoff, D.S., and Ordal, G.W. (1992). Identification and characterization of FliY, a novel component of the Bacillus subtilis flagellar switch complex. Molecular microbiology *6*, 2715-2723.

Bren, A., and Eisenbach, M. (1998). The N terminus of the flagellar switch protein, FliM, is the binding domain for the chemotactic response regulator, CheY. J Mol Biol *278*, 507-514.

Brown, P.N., Hill, C.P., and Blair, D.F. (2002). Crystal structure of the middle and C-terminal domains of the flagellar rotor protein FliG. The EMBO journal *21*, 3225-3234.

Brown, P.N., Mathews, M.A., Joss, L.A., Hill, C.P., and Blair, D.F. (2005). Crystal structure of the flagellar rotor protein FliN from Thermotoga maritima. J Bacteriol *187*, 2890-2902.

Brown, P.N., Terrazas, M., Paul, K., and Blair, D.F. (2007). Mutational analysis of the flagellar protein FliG: sites of interaction with FliM and implications for organization of the switch complex. J Bacteriol *189*, 305-312.

Chen, S., Beeby, M., Murphy, G.E., Leadbetter, J.R., Hendrixson, D.R., Briegel, A., Li, Z., Shi, J., Tocheva, E.I., Muller, A., *et al.* (2011). Structural diversity of bacterial flagellar motors. The EMBO journal *30*, 2972-2981.

Cluzel, P., Surette, M., and Leibler, S. (2000). An ultrasensitive bacterial motor revealed by monitoring signaling proteins in single cells. Science *287*, 1652-1655.

Delalez, N.J., Wadhams, G.H., Rosser, G., Xue, Q., Brown, M.T., Dobbie, I.M., Berry, R.M., Leake, M.C., and Armitage, J.P. (2010). Signal-dependent turnover of the bacterial flagellar switch protein FliM. Proc Natl Acad Sci U S A *107*, 11347-11351.

DePamphilis, M.L., and Adler, J. (1971). Purification of intact flagella from Escherichia coli and Bacillus subtilis. J Bacteriol *105*, 376-383.

Duke, T.A., Le Novere, N., and Bray, D. (2001). Conformational spread in a ring of proteins: a stochastic approach to allostery. J Mol Biol *308*, 541-553.

Dyer, C.M., Vartanian, A.S., Zhou, H., and Dahlquist, F.W. (2009). A molecular mechanism of bacterial flagellar motor switching. J Mol Biol *388*, 71-84.

Gonzalez-Pedrajo, B., Minamino, T., Kihara, M., and Namba, K. (2006). Interactions between C ring proteins and export apparatus components: a possible mechanism for facilitating type III protein export. Molecular microbiology *60*, 984-998.

Grunenfelder, B., Gehrig, S., and Jenal, U. (2003). Role of the cytoplasmic C terminus of the FliF motor protein in flagellar assembly and rotation. J Bacteriol *185*, 1624-1633.

Hazelbauer, G.L., Falke, J.J., and Parkinson, J.S. (2008). Bacterial chemoreceptors: high-performance signaling in networked arrays. Trends in biochemical sciences *33*, 9-19.

Howitt, M.R., Lee, J.Y., Lertsethtakarn, P., Vogelmann, R., Joubert, L.M., Ottemann, K.M., and Amieva, M.R. (2011). ChePep controls Helicobacter pylori Infection of the gastric glands and chemotaxis in the Epsilonproteobacteria. mBio *2*.

Kihara, M., Miller, G.U., and Macnab, R.M. (2000). Deletion analysis of the flagellar switch protein FliG of Salmonella. J Bacteriol *182*, 3022-3028.

Kojima, S., and Blair, D.F. (2004). The bacterial flagellar motor: structure and function of a complex molecular machine. International review of cytology *233*, 93-134.

Kubori, T., Yamaguchi, S., and Aizawa, S. (1997). Assembly of the switch complex onto the MS ring complex of Salmonella typhimurium does not require any other flagellar proteins. J Bacteriol *179*, 813-817.

Lam, K.H., Lam, W.W., Wong, J.Y., Chan, L.C., Kotaka, M., Ling, T.K., Jin, D.Y., Ottemann, K.M., and Au, S.W. (2013). Structural basis of FliG-FliM interaction in Helicobacter pylori. Molecular microbiology *88*, 798-812.

Lee, L.K., Ginsburg, M.A., Crovace, C., Donohoe, M., and Stock, D. (2010). Structure of the torque ring of the flagellar motor and the molecular basis for rotational switching. Nature *466*, 996-1000.

Levenson, R., Zhou, H., and Dahlquist, F.W. (2012). Structural insights into the interaction between the bacterial flagellar motor proteins FliF and FliG. Biochemistry *51*, 5052-5060.

Lloyd, S.A., and Blair, D.F. (1997). Charged residues of the rotor protein FliG essential for torque generation in the flagellar motor of Escherichia coli. J Mol Biol *266*, 733-744.

Lloyd, S.A., Tang, H., Wang, X., Billings, S., and Blair, D.F. (1996). Torque generation in the flagellar motor of Escherichia coli: evidence of a direct role for FliG but not for FliM or FliN. J Bacteriol *178*, 223-231.

Lloyd, S.A., Whitby, F.G., Blair, D.F., and Hill, C.P. (1999). Structure of the C-terminal domain of FliG, a component of the rotor in the bacterial flagellar motor. Nature *400*, 472-475.

Lowder, B.J., Duyvesteyn, M.D., and Blair, D.F. (2005). FliG subunit arrangement in the flagellar rotor probed by targeted cross-linking. J Bacteriol *187*, 5640-5647.

Lowenthal, A.C., Hill, M., Sycuro, L.K., Mehmood, K., Salama, N.R., and Ottemann, K.M. (2009). Functional analysis of the Helicobacter pylori flagellar switch proteins. J Bacteriol *191*, 7147-7156.

Mathews, M.A., Tang, H.L., and Blair, D.F. (1998). Domain analysis of the FliM protein of Escherichia coli. J Bacteriol *180*, 5580-5590.

McMurry, J.L., Murphy, J.W., and Gonzalez-Pedrajo, B. (2006). The FliN-FliH interaction mediates localization of flagellar export ATPase FliI to the C ring complex. Biochemistry *45*, 11790-11798.

Minamino, T., Imada, K., Kinoshita, M., Nakamura, S., Morimoto, Y.V., and Namba, K. (2011). Structural insight into the rotational switching mechanism of the bacterial flagellar motor. Plos Biol *9*, e1000616.

Muff, T.J., and Ordal, G.W. (2008). The diverse CheC-type phosphatases: chemotaxis and beyond. Molecular microbiology *70*, 1054-1061.

Murphy, G.E., Leadbetter, J.R., and Jensen, G.J. (2006). In situ structure of the complete Treponema primitia flagellar motor. Nature *442*, 1062-1064.

Park, S.Y., Chao, X., Gonzalez-Bonet, G., Beel, B.D., Bilwes, A.M., and Crane, B.R. (2004). Structure and function of an unusual family of protein phosphatases: the bacterial chemotaxis proteins CheC and CheX. Molecular cell *16*, 563-574.

Park, S.Y., Lowder, B., Bilwes, A.M., Blair, D.F., and Crane, B.R. (2006). Structure of FliM provides insight into assembly of the switch complex in the bacterial flagella motor. Proc Natl Acad Sci U S A *103*, 11886-11891.

Passmore, S.E., Meas, R., and Marykwas, D.L. (2008). Analysis of the FliM/FliG motor protein interaction by two-hybrid mutation suppression analysis. Microbiology *154*, 714-724.

Paul, K., and Blair, D.F. (2006). Organization of FliN subunits in the flagellar motor of Escherichia coli. J Bacteriol *188*, 2502-2511.

Paul, K., Brunstetter, D., Titen, S., and Blair, D.F. (2011a). A molecular mechanism of direction switching in the flagellar motor of Escherichia coli. Proc Natl Acad Sci U S A *108*, 17171-17176.

Paul, K., Erhardt, M., Hirano, T., Blair, D.F., and Hughes, K.T. (2008). Energy source of flagellar type III secretion. Nature *451*, 489-492.

Paul, K., Gonzalez-Bonet, G., Bilwes, A.M., Crane, B.R., and Blair, D. (2011b). Architecture of the flagellar rotor. The EMBO journal *30*, 2962-2971.

Raddi, G., Morado, D.R., Yan, J., Haake, D.A., Yang, X.F., and Liu, J. (2012). Three-dimensional structures of pathogenic and saprophytic Leptospira species revealed by cryo-electron tomography. J Bacteriol *194*, 1299-1306.

Rolig, A.S., Carter, J.E., and Ottemann, K.M. (2011). Bacterial chemotaxis modulates host cell apoptosis to establish a T-helper cell, type 17 (Th17)-dominant immune response in Helicobacter pylori infection. Proc Natl Acad Sci U S A *108*, 19749-19754.

Sarkar, M.K., Paul, K., and Blair, D. (2010a). Chemotaxis signaling protein CheY binds to the rotor protein FliN to control the direction of flagellar rotation in Escherichia coli. Proc Natl Acad Sci U S A *107*, 9370-9375.

Sarkar, M.K., Paul, K., and Blair, D.F. (2010b). Subunit organization and reversal-associated movements in the flagellar switch of Escherichia coli. J Biol Chem *285*, 675-684.

Schweinitzer, T., and Josenhans, C. (2010). Bacterial energy taxis: a global strategy? Archives of microbiology *192*, 507-520.

Silversmith, R.E. (2010). Auxiliary phosphatases in two-component signal transduction. Current opinion in microbiology *13*, 177-183.

Silversmith, R.E., and Bourret, R.B. (1999). Throwing the switch in bacterial chemotaxis. Trends in microbiology *7*, 16-22.

Sircar, R., Greenswag, A.R., Bilwes, A.M., Gonzalez-Bonet, G., and Crane, B.R. (2013). Structure and activity of the flagellar rotor protein FliY: a member of the CheC phosphatase family. J Biol Chem *288*, 13493-13502.

Sockett, H., Yamaguchi, S., Kihara, M., Irikura, V.M., and Macnab, R.M. (1992). Molecular analysis of the flagellar switch protein FliM of Salmonella typhimurium. J Bacteriol *174*, 793-806.

Sourjik, V., and Berg, H.C. (2000). Localization of components of the chemotaxis machinery of Escherichia coli using fluorescent protein fusions. Molecular microbiology *37*, 740-751.

Sowa, Y., and Berry, R.M. (2008). Bacterial flagellar motor. Quarterly reviews of biophysics *41*, 103-132.

Stewart, R.C. (2005). Analysis of ATP binding to CheA containing tryptophan substitutions near the active site. Biochemistry *44*, 4375-4385.

Suzuki, H., Yonekura, K., and Namba, K. (2004). Structure of the rotor of the bacterial flagellar motor revealed by electron cryomicroscopy and single-particle image analysis. J Mol Biol *337*, 105-113.

Szurmant, H., Bunn, M.W., Cannistraro, V.J., and Ordal, G.W. (2003). Bacillus subtilis hydrolyzes CheY-P at the location of its action, the flagellar switch. J Biol Chem *278*, 48611-48616.

Terashima, H., Kojima, S., and Homma, M. (2008). Flagellar motility in bacteria structure and function of flagellar motor. International review of cell and molecular biology *270*, 39-85.

Terry, K., Williams, S.M., Connolly, L., and Ottemann, K.M. (2005). Chemotaxis plays multiple roles during Helicobacter pylori animal infection. Infection and immunity *73*, 803-811.

Thomas, D., Morgan, D.G., and DeRosier, D.J. (2001). Structures of bacterial flagellar motors from two FliF-FliG gene fusion mutants. J Bacteriol *183*, 6404-6412.

Thomas, D.R., Francis, N.R., Xu, C., and DeRosier, D.J. (2006). The three-dimensional structure of the flagellar rotor from a clockwise-locked mutant of Salmonella enterica serovar Typhimurium. J Bacteriol *188*, 7039-7048.

Tindall, M.J., Gaffney, E.A., Maini, P.K., and Armitage, J.P. (2012). Theoretical insights into bacterial chemotaxis. Wiley interdisciplinary reviews Systems biology and medicine *4*, 247-259.

Toker, A.S., and Macnab, R.M. (1997). Distinct regions of bacterial flagellar switch protein FliM interact with FliG, FliN and CheY. J Mol Biol *273*, 623-634.

Turner, L., Ryu, W.S., and Berg, H.C. (2000). Real-time imaging of fluorescent flagellar filaments. J Bacteriol *182*, 2793-2801.

Turner, L., Samuel, A.D., Stern, A.S., and Berg, H.C. (1999). Temperature dependence of switching of the bacterial flagellar motor by the protein CheY(13DK106YW). Biophysical journal *77*, 597-603.

Van Way, S.M., Millas, S.G., Lee, A.H., and Manson, M.D. (2004). Rusty, jammed, and well-oiled hinges: Mutations affecting the interdomain region of FliG, a rotor element of the Escherichia coli flagellar motor. J Bacteriol *186*, 3173-3181.

Vartanian, A.S., Paz, A., Fortgang, E.A., Abramson, J., and Dahlquist, F.W. (2012). Structure of flagellar motor proteins in complex allows for insights into motor structure and switching. J Biol Chem *287*, 35779-35783.

Wadhams, G.H., and Armitage, J.P. (2004). Making sense of it all: bacterial chemotaxis. Nature reviews Molecular cell biology *5*, 1024-1037.

Welch, M., Oosawa, K., Aizawa, S., and Eisenbach, M. (1993). Phosphorylation-dependent binding of a signal molecule to the flagellar switch of bacteria. Proc Natl Acad Sci U S A *90*, 8787-8791.

Yamaguchi, S., Aizawa, S., Kihara, M., Isomura, M., Jones, C.J., and Macnab, R.M. (1986). Genetic evidence for a switching and energy-transducing complex in the flagellar motor of Salmonella typhimurium. J Bacteriol *168*, 1172-1179.

Zhou, J., Lloyd, S.A., and Blair, D.F. (1998). Electrostatic interactions between rotor and stator in the bacterial flagellar motor. Proc Natl Acad Sci U S A *95*, 6436-6441.

Chapter 2

Structure and activity of the flagellar rotor protein FliY: A member of the CheC phosphatase family *

Background: FliY is a flagellar rotor protein of the CheC phosphatase family.

Results: The FliY structure resembles that of the rotor protein FliM but contains two active centers for CheY dephosphorylation.

Conclusion: FliY incorporates properties of the FliM/FliN rotor proteins and the CheC/CheX phosphatases to serve multiple functions in the flagellar switch.

Significance: FliY distinguishes flagellar architecture and function in different types of bacteria.

SUMMARY:

Rotating flagella propel bacteria toward favorable environments. Sense of rotation is determined by the intracellular response regulator CheY, which when phosphorylated (CheY-P) interacts directly with the flagellar motor. In many different types of bacteria the CheC/CheX/FliY (CXY) family of phosphatases terminates the CheY-P signal. Unlike CheC and CheX, FliY is localized in the flagellar switch complex, which also contains the stator-coupling protein FliG and the target of CheY-P, FliM. The 2.5 Å resolution crystal structure of the FliY catalytic domain from *Thermotoga maritima* bears strong resemblance to the middle domain of FliM. Regions of FliM that mediate contacts within the rotor compose the phosphatase active sites in FliY. Despite the

similarity between FliY and FliM, FliY does not bind FliG and thus is unlikely to be a substitute for FliM in the center of the switch complex. Solution studies indicate that FliY dimerizes through its C-terminal domains, which resemble the *Escherichia coli* switch complex component FliN. FliY differs topologically from the *E. coli* chemotaxis phosphatase CheZ, but appears to utilize similar structural motifs for CheY dephosphorylation in close analogy to CheX. Recognition properties and phosphatase activities of site-directed mutants identify two pseudosymmetric active sites in FliY (Glu35/Asn38 and Glu132/Asn135), with the second site (Glu132/Asn135) being more active. A putative N-terminal CheY binding domain conserved with FliM is not required for binding CheY-P or phosphatase activity.

---

*"This research was originally published in Journal of Biological Chemistry. Ria Sircar, Anna R. Greenswag, Alexandrine M. Bilwes, Gabriela Gonzalez-Bonet and Brian R. Crane. Structure and Activity of the flagellar rotor protein FliY: A member of the CheC phosphatase family. *Journal of biological chemistry*. 2013; 288: 13493-13502. © the American Society for Biochemistry and Molecular Biology".

2.1 Introduction:

Bacterial chemotaxis, the movement of cells in response to the surrounding environment, is achieved through a coordinated network of over twenty proteins that link receptors in the cytoplasmic membrane with the flagellar motor (Wadhams and Armitage, 2004). Central to the network, the intracellular messenger protein CheY undergoes receptor-regulated phosphorylation on a conserved aspartate residue by the histidine kinase CheA and then binds to the flagellar rotor to change its direction of rotation (Wadhams and Armitage, 2004; Bilwes et al., 2003). To maintain an optimal concentration of phosphorylated CheY (CheY-P) for signal transmission and adaptation, phosphatases are required to dephosphorylate CheY-P (Clausznitzer et al., 2010; Sourjik and Berg, 2002; Kuo and Koshland, 1987; Silversmith et al., 2003). For example, in *E. coli*, the phosphatase CheZ decreases the CheY-P lifetime from ~ 20 seconds to ~ 200 milliseconds (Wadhams and Armitage, 2004). CheZ is generally found in proteobacteria; other types of bacteria such as those of genera *Thermotoga* and *Bacillus* do not have CheZ but instead encode phosphatases of the CheC/CheX/FliY (CXY) family (Fig. 2.1 (A)) (Muff and Ordal, 2008; Szurmant and Ordal, 2004; Silversmith, 2010; Wuichet and Zhulin, 2010).

Structure function studies have been carried out on CheC and CheX (Silversmith et al., 2003; Muff and Ordal, 2008; Szurmant and Ordal, 2004; Silversmith, 2010; Wuichet and Zhulin, 2010) but not FliY, the last member of the family to have its crystallographic structure determined. The CXY family contains a consensus sequence D/S–X3-**E**-X2-**N**-X22-P that defines the phosphatase active site, with CheC and FliY having two such repeats and CheX only one (Muff and Ordal, 2008; Szurmant and Ordal, 2004; Silversmith, 2010; Park et al., 2004). CheX dimerization generates two active sites per dimer (Park et al., 2004), but the recent crystal structure of the complex between CheX and BeF_3^--activated CheY3 from *Borrelia burgdorferi*

shows CheY3 bound to a single subunit of CheX, which suggests that binding CheY-P may dissociate the CheX dimer (Pazy et al., 2010). In CheC and CheX, the invariant Glu residue in the consensus sequence (bolded above) is essential for binding CheY-P, whereas the invariant Asn residue (also bold) is critical for the phosphatase activity (Fig. 2.2 (A)) (Park et al., 2004; Pazy et al., 2010). These residues structurally mimic the conserved Asp and Gln residues essential for phosphatase activity in CheZ (Zhao et al., 2002). In the structure of the CheX•CheY3•BeF_3^-•Mg^{2+} complex, the helix bearing the conserved Glu/Asn residues on CheX adopts a perpendicular orientation with respect to CheY3 α1 (Pazy et al., 2010). The Glu/Asn residues themselves participate in an extensive hydrogen bond network with the aspartyl-phosphate and surrounding residues of CheY. The Asn residue hydrogen bonds with an ordered water molecule, which is positioned for in-line attack of the phosphate mimic group BeF_3^-. Alone, CheC is a weak phosphatase (Park et al., 2004; Szurmant et al., 2004), but its affinity for CheY-P increases in complex with CheD, a chemoreceptor deamidase (Park et al., 2004; Szurmant et al., 2004; Chao et al., 2006; Muff and Ordal, 2007b). Formation of the CheD:CheC complex is proposed to allow levels of CheY-P to influence receptor modification state by sequestering CheD (Chao et al., 2006; Glekas et al., 2012).

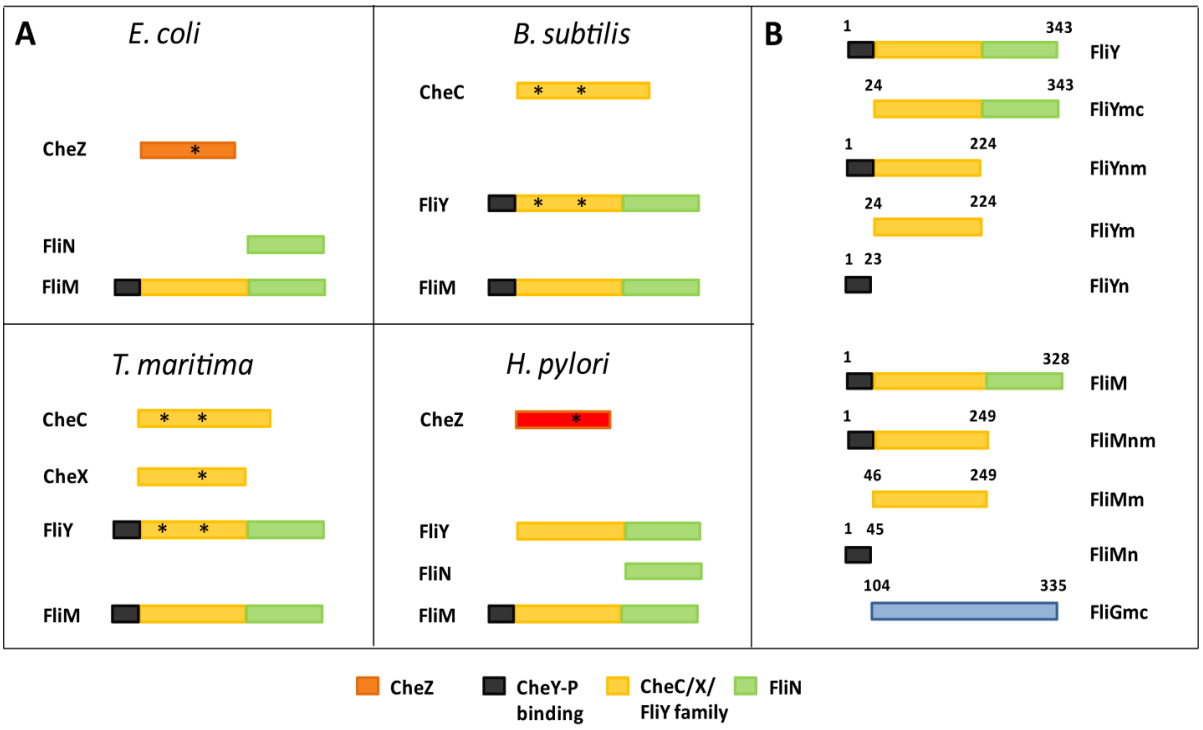

Figure 2.1. **Domain arrangement of the CheC family and related proteins.** (A) Domain organization of CheC family and related proteins in *E. coli*, *H. pylori*, *T. maritima*, and *B. subtilis*. Structurally unrelated CheY phosphatases *E. coli* CheZ (orange) and *H. pylori* (red) are found in proteobacteria. The asterisk indicates active centers. (B) Schematic representation of different constructs of FliY, FliM, and FliG from *T. maritima* used in this study. Black shading denotes CheY-P binding domain, yellow shading denotes CheC homology domain, and green shading represents the rotor protein FliN homology domain.

Many non-proteobacteria encode the third member of this phosphatase family, FliY (Muff and Ordal, 2008; Silversmith, 2010; Szurmant et al., 2004; Bischoff and Ordal, 1992b). For example, FliY is found in pathogenic Gram-positive bacteria from the geni *Bacillus* or *Helicobacter* and pathogenic spirochetes from the geni *Leptospira* and *Treponema.* Lower pathogenicity of *Leptospira* has been associated with inactivation of *fliY* gene (Liao et al., 2009). FliY is thought to localize in the switch complex that composes the flagellar C-ring (Muff and Ordal, 2008; Silversmith, 2010; Szurmant et al., 2004; Bischoff and Ordal, 1992b). In *E. coli*, the switch complex contains many copies of FliG, FliM and FliN (see Fig. 2.1 for domain designations and relationships of rotor proteins and phosphatases). FliG connects the C-ring to the MS-ring and

interacts with the stator to allow rotation (Brown et al., 2002). Structures of FliG from various organisms (Brown et al., 2002; Lloyd et al., 1999; Lee et al., 2010; Minamino et al., 2011; Paul et al., 2011) reveal three globular domains linked by flexible linkers. FliM is sandwiched between FliG and FliN in the C-ring and is directly involved in binding CheY-P (Mathews et al., 1998; Sockett et al., 1992; Toker and Macnab, 1997). The middle and C-terminal domains of FliG interact with FliM (Paul et al., 2011; Brown et al., 2007). FliM contains an amino terminal CheY-binding motif ($FliM_N$) that recruits CheY-P to the motor (Mathews et al., 1998; Sockett et al., 1992; Toker and Macnab, 1997). NMR studies have shown that in addition to CheY-P binding to the N-terminal motif, it also interacts with the middle domain of FliM, albeit weakly (Dyer et al., 2009). The crystal structure of the middle domain of FliM ($FliM_M$) reveals a topology similar to CheC (Park et al., 2006). The conserved GGXG motif is essential for binding FliG as evident in the FliG:FliM complex structure (Paul et al., 2011; Vartanian et al., 2012). The C-terminal domain of FliM interacts with the third rotor protein, FliN (Mathews et al., 1998; Toker and Macnab, 1997; Brown et al., 2005). FliN represents the donut shaped structure present at the bottom of the C-ring membrane distal in EM reconstructions (Brown et al., 2005; Thomas et al., 2006). Recent crosslinking studies in *E. coli* show that CheY interacts with FliN and in doing so transmits conformational signals to FliG (Sarkar et al., 2010). Crystal structures of the C-terminal two thirds of *T. maritima* FliN reveal a tightly intertwined dimer formed mostly of β-sheets (Brown et al., 2005). Nonetheless, *E. coli* FliN is a tetramer in solution, which is assumed to be the assembly state found in the C-ring (Brown et al., 2005).

The FliY gene was first identified and characterized in *Bacillus subtilis* as a multidomain protein, with an amino terminal CheY-P binding domain ($FliY_N$), a middle domain ($FliY_M$) similar to FliM and a C-terminal domain similar to FliN ($FliY_C$, Fig. 2.1) (Bischoff and Ordal,

1992; Park et al., 2006). The deletion mutant FliYΔ 6-15 of *B. subtilis* FliY cannot bind CheY-P (Szurmant et al., 2003). The large middle domain ($FliY_M$) has structural homology to the CheC phosphatase family. It has been suggested that CheC/CheX phosphatases and the FliM/FliY flagellar rotor proteins all evolved from a common ancestor (Kirby et al., 2001). FliY conserves the dephosphorylation sites of CheC and CheX, but FliM does not. *B. subtilis* FliY has greater phosphatase activity than CheC alone (Szurmant et al., 2004). Some bacteria such as *B. subtilis* and *T. maritima*, do not contain a separate FliN, presumably deriving this function solely from FliY; whereas in other bacteria, such as *H. pylori* FliY and FliN are expressed as separate proteins (Lowenthal et al., 2009). *B. subtilis* FliY can complement the motility defect in a *Salmonella* FliN mutant (Bischoff and Ordal, 1992), which suggests redundant functions for FliY and FliN, as well as localization of FliY in the C-ring. The importance of having the primary CheY-P phosphatase localized to the switch is currently not well understood.

Herein we report the crystallographic structure of *T. maritima* $FliY_M$, characterize its phosphatase activity and investigate the interaction properties of full-length FliY. The structure reveals how a variable α/β/coil2′ region diverges among the CXY family members to impart specific functions. We verify that both putative active sites of FliY bind phosphorylated CheY and have CheY phosphatase activity but that the second site is more active than the first. $FliY_N$ does not increase the binding affinity of CheY-P and $FliY_M$ does not appear to associate with FliG. These findings have implications for the function and architecture of the flagellar rotor in non-enteric bacteria.

2.2 Experimental Procedures:

2.2.1 Protein preparation: The genes encoding *T. maritima* FliY (residues 1-343), $FliY_{MC}$ (residues 24-343), $FliY_{NM}$ (residues 1-224), $FliY_{M}$ (residues 24-224), CheA, CheY were PCR cloned from *T. maritima* genomic DNA (obtained from the American Type Culture Collection) into the vector pET28a (Novagen) and expressed with a His_6-tag in *E. coli* strain BL21-DE3. Cells were induced with 100 μM Isopropyl β-D-1-thiogalactopyranoside (IPTG) at OD = 0.6 and grown at 37 °C for 6-10 hrs. Point mutations on $FliY_{NM}$ were introduced by quick change or overlap PCR and verified by sequencing.

Proteins were purified with Nickel-NTA affinity chromatography and the His_6-tags were subsequently cleaved with thrombin. Samples were then run on size exclusion chromatography (Superdex 75 or Superdex 200; Pharmacia Biotech) and concentrated in GF buffer (50 mM TRIS, pH=7.5, 150 mM NaCl).

Seleno-methionine substituted $FliY_{M}$ was grown in minimal media supplemented with 16 amino acids. 100 mg of L-seleno-methionine was added to 2 L of media. Cells were induced with 100 μM IPTG at OD= 0.6 and grown overnight at room temperature. The protein purification carried out as described above, except that 10 mM DTT was added to all the buffers.

2.2.2 Crystallization and data collection: Crystals were obtained from vapor diffusion of 2 μL drops containing 1 μL of reservoir solution (0.2 M ammonium sulfate, 30% w/v PEG 8000 (Hampton screen)) and 1 μL of the $FliY_{M}$ protein in GF buffer. A single anomalous diffraction (SAD) dataset was collected at the peak wavelength of Se (0.97670 Å) at Cornell High Energy Synchrotron Source (CHESS), station A1. Crystals were soaked in the cryoprotectant (15% glycerol) briefly before flash cooling in a N_2 cold stream.

2.2.3 Structural Determination and Refinement: Diffraction data were scaled with HKL2000 (Otwinowski and Minor, 1997) and the structure determined with SOLVE (Terwilliger and Berendzen, 1999). The initial model produced by automatic chain-tracing in SOLVE/RESOLVE provide the foundation to build the complete model manually with XFIT (McRee, 1999) and refined with CNS (Brunger, 2007). Water were added with water picking algorithms in CNS and adjusted manually amidst cycles of refinement.

2.2.4 Phosphatase Assays: CheA (12-30 μM) and CheY (33-300 μM) were premixed with 5 μL of TKM buffer (50 mM TRIS, pH 7.5, 200 mM KCl, 10 mM $MgCl_2$) with various volumes of GF buffer. The samples were incubated with 2 μL of an ATP solution (15 μL of an 11 μM cold ATP solution, 3-8 μL of [γ-^{32}P] ATP (3000 Ci/mmol, Perkin-Elmer)) made to a total volume of 75 μL with filtered nanopure water. For the control containing no FliY, the sample was quenched at 15 minutes with 25 μL of 3×SDS buffer containing 50 mM EDTA [pH 8]. Once the samples were incubated for 15 minutes, 2.5 μL of FliY (5 or 10 μM, native or mutants) was added to a total volume of 25 μL per sample and quenched at various time points with the same SDS buffer as the control. The proteins were separated on a 4-20% Tris-glycine SDS-PAGE at 120 V for two hours. The proteins were affixed with water, then stained with Coomassie for 10 minutes, and de-stained with water for three hours. The gels were dried in a GelAir Drying System for three hours, placed in a cassette and the film exposed for a minimum of twenty-four hours before visualization using a STORM phosphoimager.

2.2.5 Multiangle light scattering: Size-exclusion chromatography coupled with multiangle light scattering was used to study the molar mass of the various protein fragments. Proteins (2 mg / mL) were run at room temperature on the column (BioSep-SEC-S 3000 column (Phenomenex))

pre-equilibrated with GF buffer. Analysis and molecular weight determination was carried out with Wyatt technologies ASTRA. Bovine serum albumin (Sigma) was used as a control for data quality.

2.2.6 Pull-down assays: Assays were carried out in binding buffer (25 mM HEPES, pH= 7.5, 500 mM NaCl, and 50mM Imidazole). Proteins were incubated in 30 μL Ni-NTA with the binding buffer for 30 minutes at room temperature. The beads were washed with binding buffer thrice and once with binding buffer containing 1% Triton X-100 to minimize non-specific binding. 2x SDS loading dye was added to the resin and boiled for 5 minutes at 90 °C, centrifuged at 13000 rpm for 5 minutes. The supernatant was used for SDS-PAGE analysis. To demonstrate the binding of various constructs of FliY (100 μM) to CheY (75 μM) and CheY-P (75 μM), pull-down assays were performed with His-tagged proteins as described previously (Muff et al., 2007; Muff and Ordal, 2007a) with minor modifications. The samples which required phosphorylation of CheY, 20 mM acetyl phosphate (Sigma-Aldrich) in presence of 20 mM $MgCl_2.6H_2O$ was added for incubation and wash steps to the binding buffer to ensure complete phosphorylation of CheY.

2.3 Results:

2.3.1 Gene structure of *T. maritima* FliY: In the annotated genome of *T. maritima* two adjacent flagellar genes demarked by an authentic frameshift have been designated as FliY1 and FliY2 (gene id 897481 and 897793 respectively), FliY1 corresponds to $FliY_{NM}$, whereas FliY2 corresponds to *E. coli* FliN. FliY2 was cloned, characterized and its structure determined (Brown et al., 2005). As annotated, all the reading frames indicate a stop codon between FliY1 and FliY2. However, PCR cloning from genomic DNA and subsequent sequencing revealed an

additional guanine nucleotide (# 479) between the two reading frames that abrogates the stop codon and allowed for expression of a fused FliY1-FliY2. The composite full-length FliY (343 residues) was expressed in E. *coli* and found to be fully soluble and well behaved (supplemental Fig. 2.7).

2.3.2 $FliY_M$ is a α/β globular protein with a fold similar to CheC and CheX: The structure of *T. maritima* $FliY_M$ (residues 24 - 223) was determined at 2.5 Å resolution by single anomalous diffraction of selenomethionine substituted protein (Table 2.1). The two FliY molecules in the asymmetric unit have a nearly identical structure with a main chain Cα RMSD of 0.6 Å. The structure of $FliY_M$ shares a pseudo symmetric topology with the phosphatases CheC and CheX, and the rotor protein $FliM_M$ (Fig. 2.2 (B)). In all cases, the first half of the protein relates to the second half both in sequence and structure by a pseudo-twofold rotation axis roughly perpendicular to the central β-sheet (supplemental Fig. 2.8). The $FliY_M$ α/β globular fold comprises five α helices and six β-strands. The six β-strands (β1-β2′-β3′-β3-β2-β1′; primes denote symmetry-related features) form a continuous antiparallel β-sheet and are very similar in structure to those of the other family members. Two long helices (α1 and α1′) pack against and run diagonal to the central β-sheet, two medium length helices (α3 and α3′) cap the hydrophobic core generated by the β-sheet and α1/α1′. The fifth small helix (α2) packs on the opposite face of the β-sheet as α1/α1′ (Fig. 2.2 (B)). Notably, the symmetry-related feature to α2 (hereafter referred to as c2′), is not a helix, but rather an extended loop that has β-like geometry, yet does not main-chain hydrogen bond with β1′, the neighboring β−strand. In CheC, this region is helical (α2′) and pseudosymmetric to α2; whereas in CheX, this region also displays pseudosymmetry but rather forms a β-strand (βx2′/βx2) that mediates CheX dimerization by allowing for a

continuous 7-stranded β-sheet across the dimer interface. Thus, FliY appears to be a hybrid between CheC and CheX, where α2 is CheC-like, but the symmetry related region, c2′, is not helical and instead more closely resembles βx2′ in CheX. As predicted from sequence alignments of $FliY_M$ with CheX and CheC (Park et al., 2004), $FliY_M$ lacks a Gly residue following β1′ that would allow for the extended loop to align with the β-sheet and become βx2′. Thus, $FliY_M$ remains monomeric and shows greater overall resemblance to CheC than to CheX (supplemental Fig. 2.9).

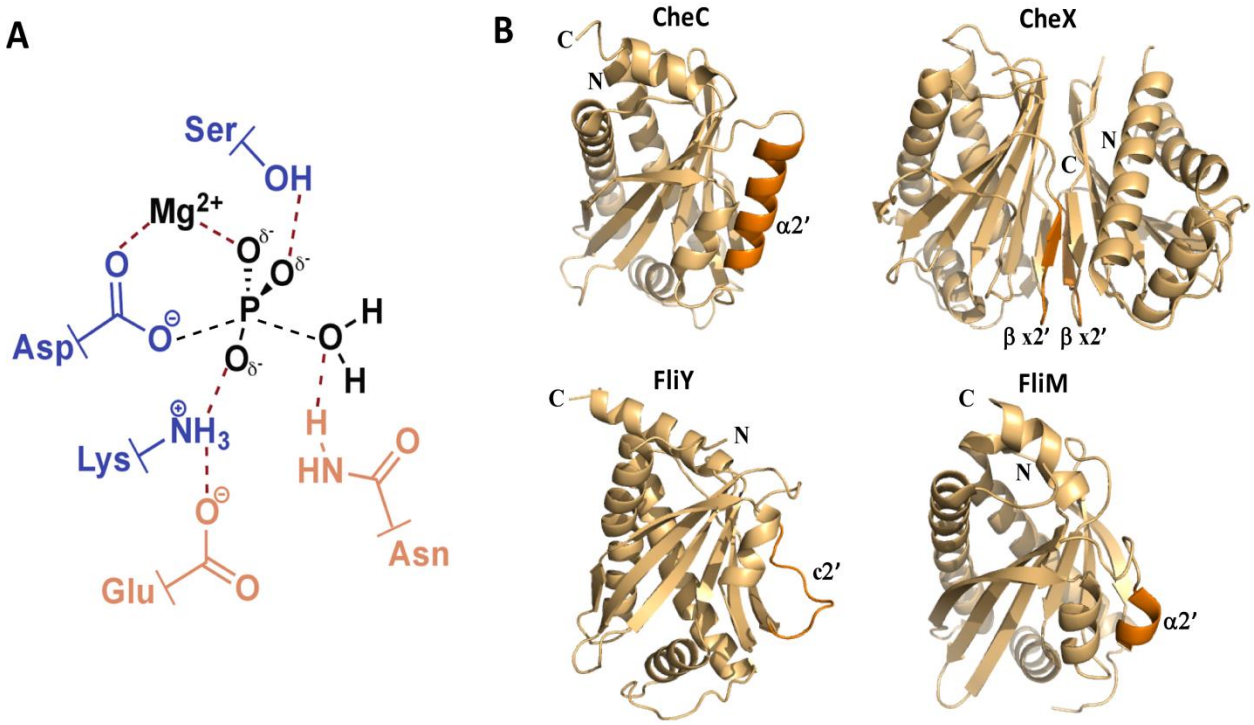

Figure 2.2. **The CXY phosphatase family.** (A) Proposed transition state for CheY-P dephosphorylation (adapted from Pazy et al., 2010) highlighting the role of the essential Glu and Asn side chains (orange) and contributing residues from CheY (blue). (B) Structural comparison within the CXY family and $FliM_M$. Secondary structural elements of each protein are shown as ribbons. The α2′/βx′/c2′ regions differentiate the members from each other (dark orange).

Table 2.1. Data collection, phasing and refinement statistics

Data Collection	
Space group	$P2_12_12_1$
Unit cell (Å)	a = 49.75, b = 85.89, c = 119.94
Resolution range (Å)	50 - 2.5 (2.54- 2.50)[a]
†R_{merge} [b]	0.090 (0.157) [a]
I/σI	19.4 (13.6) [a]
Completeness (%)	99.9 (99.3) [a]
Redundancy	7.4 (6.8) [a]
Phasing FOM[c]	0.37 (0.39) [a]
Refinement	
No. of reflections	33692
R work/R free	0.213/0.261
No. of atoms	
Residues	200 (#24-223) for chain A,
	198 (#24-220) for chain B
Water	175
B-factors (Å^2)	
Wilson	27.1
Main chain	25.2
Side chain	28.8
Water	30.2
Geometry (r.m.s.d.)[c]	
Bond lengths (Å)	0.007
Bond angles	1.3°

[a]Highest resolution range for compiling statistics

[b]$R_{merge} = \Sigma\Sigma_i \, |I_i - \langle I \rangle| \, / \, \Sigma\Sigma_i I_i$

[c]r.m.s.d., root mean square deviation, FOM, figure of merit.

2.3.3 Association state of FliY: Multiangle Light Scattering (MALS) coupled to size-exclusion chromatography indicated that full-length FliY behaves as a single species in solution (Table 2.2), with a molar mass of ~80 kDa, which is consistent with a dimer (subunit molecular weight = 37.8 kDa). However, $FliY_{NM}$ and $FliY_M$ were both monomeric with molar masses of 22.2 and 19.8 kDa respectively (Table 2.2 and supplemental Fig. 2.10). Thus, the C-terminus of FliY mediates dimerization, which is consistent with the dimeric state of $FliY_C$ in solution and in crystal structures, where it folds as an intertwined, domain-swapped dimer (Brown et al., 2005).

Table 2.2. Multiangle Light Scattering Data

Mw, weight average molar mass, Mn, number average molar mass

	Predicted Subunit Molar mass (kDa)	Observed Molar mass (kDa)	Polydispersity Mw/Mn
$FliY_{FL}$	37.8	80.3 (1%)	1.012
$FliY_{NM}$	24.4	22.2 (4%)	1.005
$FliY_M$	21.9	19.8 (3%)	1.002

2.3.4 FliY is a CheY phosphatase: *T. maritima* FliY actively dephosphorylates CheY as monitored under conditions of steady-state phosphotransfer from CheA with γ^{32}P-ATP. CheA is included in the assay because of the instability of CheY-P, which requires it's *in situ* production (Park et al., 2004; Szurmant et al., 2004; Muff et al., 2007; Muff and Ordal, 2007a). FliY does not affect CheA autophosphorylation (Fig. 2.3 (A), lanes 7 and 8). The rate of FliY phosphatase activity greatly exceeds the rate of CheA phosphorylation of CheY when 33 μM CheY is treated with 12 μM CheA and 5 μM FliY (Fig. 2.3 (A)). At CheY levels as great as 300 μM, sub-stoichiometric amounts of FliY (5 μM) dephosphorylate nearly all available CheY-P and hence the reaction requires catalytic turnover by FliY. $FliY_{MC}$, $FliY_{NM,}$ and $FliY_{M}$ behave very similarly to FliY under similar conditions, and thus the N- and C-terminal domains of FliY have little effect on phosphatase activity (Fig. 2.3 (B)). Furthermore, FliY dimerization, which is disrupted in the absence of $FliY_{C}$, is not important for dephosphorylation of CheY-P.

Based on homology to CheX and CheC (Park et al., 2004), FliY has two potential active centers that are composed from conserved residues containing acidic and amide side chains. α1 and α1′ harbor the putative catalytic residues Glu35/Asn38 and Glu132/Asn135, respectively (Fig. 2.3 (C)). In order to evaluate the importance of each active site for CheY-P hydrolysis, phosphatase activity was measured in $FliY_{NM}$ variants where Glu35, Asn38, Glu132, and Asn135 were mutated to Ser individually, in pairs, and in totality. The time points and relative concentrations of each protein were optimized such that a comparison could be made between fully phosphorylated and dephosphorylated levels of CheY-P under steady state phosphorylation by CheA. The Asn35Ser/Glu38Ser/Asn132Ser/Glu135Ser mutant had no phosphatase activity (Fig. 2.3 (E)). When each active site was examined separately, the Glu35Ser/Asn38Ser mutant had reduced phosphatase activity compared to WT $FliY_{NM}$, however the phosphatase activity of

Glu132Ser/Asn135Ser was severely impaired. The single mutants Glu132Ser and Asn135Ser had similar, albeit lesser effects (Fig. 2.3 (D)). Thus, both putative active centers contribute to FliY phosphatase activity; however, the second Glu132/Asn135 site is dominant.

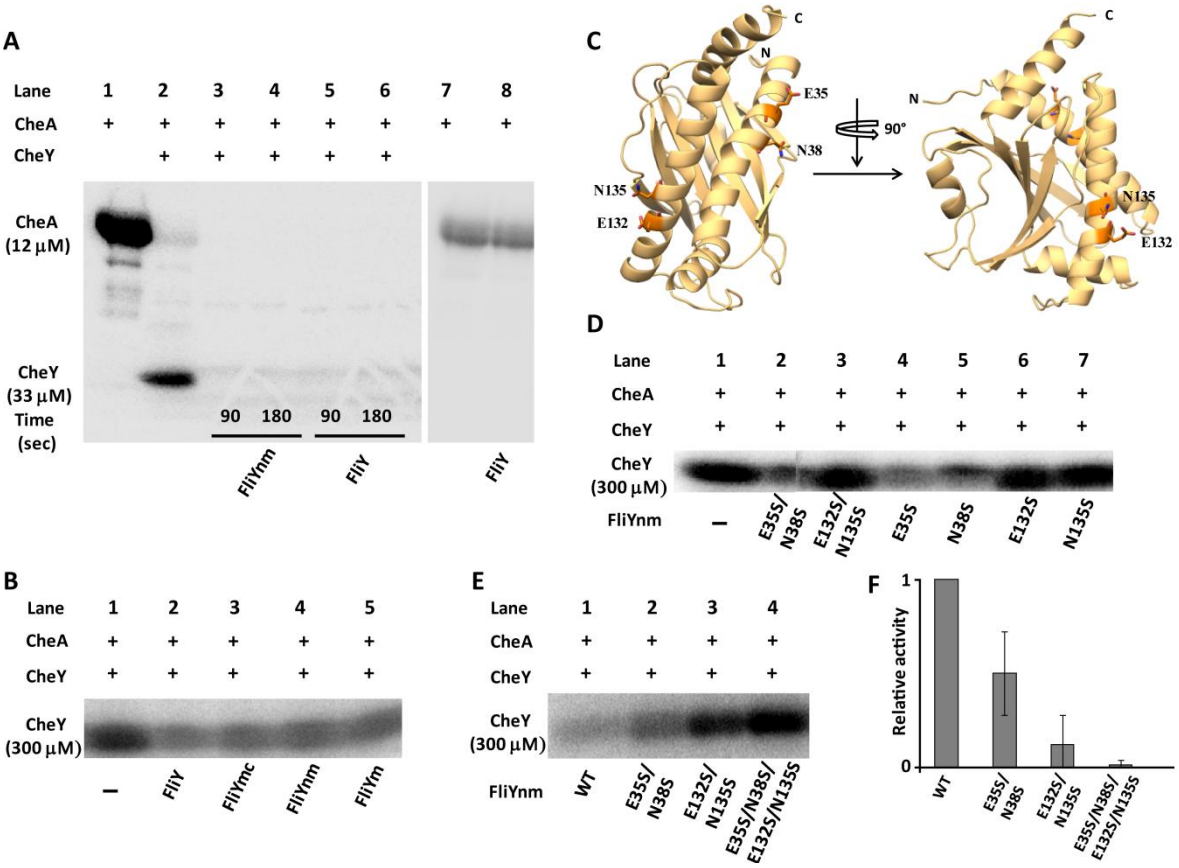

Figure. 2.3. **FliY phosphatase activity.** (A) Autophosphorylated *T. maritima* CheA (12 μM; lane 1) transfers ^{32}P to 33 μM CheY (lanes 2–6). 5 μM $FliY_{NM}$ (lanes 3 and 4) or 5 μM FliY (lanes 5 and 6) dephosphorylates CheY-P. 90 s and 180 s time points were measured after FliY addition. FliY does not affect CheA autophosphorylation (lanes 7 and 8). (B) Effect of N-terminal CheY binding domain ($FliY_N$) on CheY-^{32}P dephosphorylation: All reactions contained 30 μM CheA and 300 μM CheY. Bands correspond to CheY-^{32}P after transfer from CheA, measured at 45 s after addition of 5 μM FliY (lane 2), 5 μM $FliY_{MC}$ (lane 3), 5 μM $FliY_{NM}$ (lane 4), and 5 μM $FliY_M$ (lane 5). (C) Ribbon diagram of the $FliY_M$ topology with active site Glu and Asn residues shown as sticks. (D) Effects of FliY double and single mutants on phosphatase activity measured 45 s after addition of 5 μM FliY variants. (E) Effect of $FliY_{NM}$ mutants on CheY-^{32}P dephosphorylation. Reactions contained 30 μM CheA and 300 μM CheY. Bands correspond to CheY-^{32}P after transfer from CheA measured 5 min after addition of 10 μM $FliY_{NM}$ (WT and variants). (F) Relative phosphatase activities of FliY mutants measured as the ratio of CheY-P dephosphorylated per unit time relative to WT activity. The experiments were performed in quadruplicate; error bars indicate S.D. For ease of visualization, the gel images have different contrast ratios.

To study the contributions of the FliY domains on phosphatase activity we performed the dephosphorylation assay with various FliY variants (FliY, $FliY_{MC}$, $FliY_{NM}$, and $FliY_{M}$). The full-length and FliY domain fragments were all able to dephosphorylate CheY-P with similar activity provided they contained the FliY middle domain (Fig. 2.3 (B)). Thus FliY dimerization, which is disrupted in the absence of $FliY_{C}$, does not largely influence phosphatase activity and surprisingly, neither does the putative N-terminal CheY binding domain ($FliY_{N}$). We then tested whether purified FliY required the N-terminal domain to interact with CheY in pull-down experiments. Strong interaction between FliY and affinity tagged CheY is only observed when CheY is phosphorylated by the phosphate donor acetyl phosphate. This interaction did not depend on the presence of $FliY_{N}$ (Fig. 2.4 (A)). In contrast, $FliM_{M}$ alone showed no interaction with CheY-P or CheY; however, $FliM_{NM}$, which contains the N-terminal peptide, bound both CheY-P and CheY, the former most strongly.

Mutation studies showed that each FliY active site binds CheY-P (Fig. 2.4 (B)). Alteration of residues in both active sites (Glu35Ser/Asn38Ser/Glu132Ser/Asn135Ser) greatly reduced binding but did not abrogate it entirely (Fig. 2.4 (B)). This indicates that the Ser replacements can still mediate some interaction with CheY-P or that other peripheral residues are also involved in binding. Binding to CheY-P was increased when either the first or second active site was restored in the absence of the other; however, restoration of the first active site alone showed the greatest increase in CheY-P binding (Glu132Ser/Asn135Ser; Fig. 2.4 (B)). Thus, the more active dephosphorylation center (Glu132/Asn135) exhibits lower apparent CheY-P affinity than the less active center (Glu35Ser/Asn38). Given the very low affinity of unphopshorylated CheY for FliY, the weaker apparent binding at the second site may reflect its ability to turnover substrate more quickly.

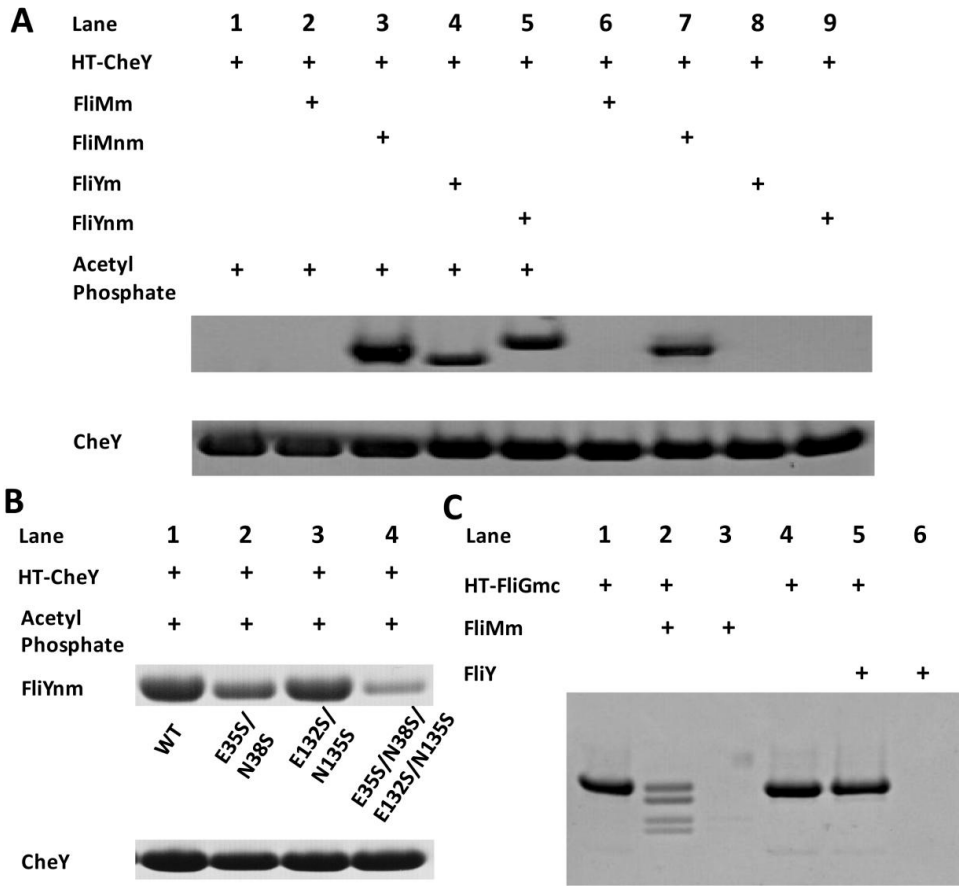

Figure 2.4. **Interaction between CheY and FliY domains.** (A) Pull-down assay of $FliY_{NM}$ (100 μM) and $FliY_{M}$ (100 μM) with His-tagged CheY (75 μM) in presence of acetyl phosphate where indicated. Shown is His-tagged CheY in presence of acetyl phosphate (lane 1). Negative and positive controls are shown: interaction of $FliM_{M}$ (lane 2) and $FliM_{NM}$ (lane 3), respectively, with CheY in presence of acetyl phosphate. $FliY_{M}$ (lane 4) and $FliY_{NM}$ (lane 5) interacted strongly with CheY only in presence of acetyl phosphate. No interaction was observed between CheY and $FliM_{M}$ (lane 6), $FliY_{M}$ (lane 8), or $FliY_{NM}$ (lane 9) in the absence of acetyl phosphate. Reduced interaction was seen with $FliM_{NM}$ in the absence of acetyl phosphate (lane 7). (B) Pull-down assay of $FliY_{NM}$ (100 μM, lane 1) and variants (100 μM, lane *2*, E35S/N38S; lane 3, E132S/N135S; lane 4, E35S/N38S/E132S/N135S) with His-tagged CheY (75 μM) in the presence of acetyl phosphate demonstrate that both active sites bind CheY-P. (C) Pull-down assay of FliY (80 μM) with His-tagged $FliG_{MC}$ (40 μM, lane 5). Positive control is as follows: His-tagged $FliG_{MC}$ pull down of $FliM_{M}$ (80 μM, lane 2). Controls of $FliM_{M}$ without tag (lane 3) and FliY without tag (lane 6) show no interaction with the affinity beads. Upper pair of bands in lane 2 represents $FliG_{MC}$ ± His_6 tag, whereas a lower pair of bands represents $FliM_{M}$ and an N-terminal cleavage product. The presence of untagged $FliG_{MC}$ in the pull-down indicates a larger than dimeric complex formed by $FliG_{MC}$ and $FliM_{M}$.

2.3.5 Interaction of FliY with FliG: The C-terminal domain of FliY is homologous to FliN (and FliMc) and thus, FliY is thought to be located in the flagellar rotor (Szurmant et al., 2004;

Bischoff and Ordal, 1992b). Indeed, *B. subtilis* FliY was able to complement a *S. typhimurium fliN* amber mutant and restore motility (Bischoff and Ordal, 1992a). Furthermore, some FliY sequences conserve with FliM residues known to form an important loop for engaging FliG (MGGXGE; supplemental Fig. 2.8). In pull-down assays, $FliM_M$ shows a strong interaction with affinity-tagged *T. maritima* $FliG_{MC}$ (Fig. 2.4 (C)). But, FliY shows no such interaction with $FliG_{MC}$ (Fig. 2.4 (C)). We also investigated the interaction between $FliG_{MC}$ and $FliY_{NM}$ by site-specific spin-labeling and pulsed dipolar electron spin resonance spectroscopy (data not shown). Nitroxide spin-labels on $FliM_{NM}$ and $FliG_{MC}$ provided interaction distances that agreed with the FliG:FliM complex crystal structure (Paul et al., 2011). However, spin-labels at a similar position on FliY did not yield any observable interaction with spin-labeled FliG. These experiments suggest that $FliY_M$ cannot replace $FliM_M$ in its association with FliG and therefore has a unique position in the flagellar rotor.

2.4 Discussion:

2.4.1 Comparison with CheC/CheX and $FliM_M$: $FliY_M$ maintains the topology of the CheC/CheX family, although the overall resemblance to CheC is greater than to CheX (supplemental Fig. 2.9). The most notable difference is that $FliY_M$ does not have defined secondary structure between residues 165-178 (c2′) which corresponds to α2′ in CheC and βx2′ in CheX (Park et al., 2004) (supplemental Fig. 2.8). The α2′ helix in CheC mediates binding to the activator CheD (Chao et al., 2006) and βx2′ mediates dimerization in CheX (Park et al., 2004). In FliM, the small α2′ helix mediates contact to the α1/α1′ face of a neighboring FliM subunit within the rotor (Park et al., 2006). The α1/α1′ helices containing the active site residues of $FliY_M$ are similar in size as to those of CheC and superposition of the conserved motifs on

α1/α1′ from CheC and $FliY_M$ show similar spatial orientation of the residue side chains (supplemental Fig. 2.9). Structural variation in the c2′ region of FliY suggests that FliY has a distinct architectural role from FliM and does not undergo associations similar to those of CheC and CheX.

2.4.2 Phosphatase activity of FliY: FliY has been assigned to be the primary CheY phosphatase in *B. subtilis*, despite the presence of CheC (Szurmant et al., 2004; Chao et al., 2006). Unlike *B. subtilis*, *Thermotoga* encodes all three members of the CheC phosphatase family, and *T. maritima* CheC and CheX have been previously demonstrated to dephosphorylate CheY-P (Park et al., 2004). FliY also dephosphorylates CheY-P, which establishes three distinct chemotaxis phosphatases in *T. maritima*, despite the presence of only one CheY homolog per genome. Sequence conservation with CheX, CheC (and CheZ, see below) suggested the possibility of two active sites on FliY. The double mutant of the second putative active site (Glu132Ser/Asn135Ser) has low observable phosphatase activity (Fig. 2.3 (D), (E)). The Glu35Ser/Asn38Ser mutant also has reduced phosphatase activity, but not to the same extent as Glu132Ser/Asn135Ser. The combined effect of mutating both active sites is roughly cumulative (Fig. 2.3 (F)). The low phosphatase activity of the first site, though apparent in Figs. 2.3 (D), (E) may be masked somewhat by the coupled nature of the assay. CheY-P hydrolyzes relatively quickly ($t_{1/2}$ = 30-150 sec (Swanson et al., 1996)), and thus conditions were used where the mutant activities would distinguish steady-state levels of CheY-P in the presence of CheA. In the case of the Glu35Ser/Asn38Ser double mutant, CheY phosphorylation by CheA competes with FliY-catalyzed dephosphorylation, but the overall dephosphorylation rate has been reduced compared to WT due to loss of the first active site. Why FliY contains two active centers of differing activity is unclear, although two different sites may facilitate the optimum deactivation

rate of CheY in the confines of the flagellar switch complex, where many copies of CheY-P simultaneously contribute to switching the rotation sense (Khan et al., 2000; Sowa and Berry, 2008).

Given that both FliY active sites show a high degree of symmetry in sequence and structure, they both bind the substrate CheY-P, but not the product CheY, and that conservative mutations of suspected catalytic residues in either site lower phosphatase activity, but mutations in both sites are needed to abolish activity, it is very likely that FliY has two independent catalytic centers. The greater activity of the Glu132/Asn135 site compared to the Glu35/Asn38 site most likely stems from the peripheral regions surrounding the consensus motifs. Either single mutant Glu132Ser or Asn135Ser showed nearly the same loss in activity as the double mutant Glu132Ser/Asn135Ser (Fig. 2.3 (D)). However, the Asn38Ser mutation has a larger affect on dephosphorylation than the Glu35Ser. The requirement of Asn at positions 38 and 135 is most likely due to their role in aligning a catalytic water molecule, as seen in the structure of CheX:CheY3 (Pazy et al., 2010). Substitution of the conserved Asn residues from both active sites in *T. maritima* and *B. subtilis* CheC (with activating CheD present) removed all activity, whereas the double Glu mutant could dephosphorylate CheY-P to some extent (Park et al., 2004; Muff and Ordal, 2007b).

2.4.3 Implications for interaction with CheY: The FliY active sites are very similar to the active site of CheX and CheZ as revealed by the crystallographic structures of those proteins in complex with a phospho-mimic of CheY ($CheY{\bullet}BeF_3^-{\bullet}Mg^{2+}$) (Pazy et al., 2010). Superimposition of the α1 and α1′ helices of *T. maritima* $FliY_M$ with those of CheX in the *B. burgdorferi* $CheX{\bullet}CheY3{\bullet}BeF_3^-{\bullet}Mg^{2+}$ cocrystal structure (PDB 3HZH) generated a clash free model with the Glu35 (or Glu132) and Asn38 (or Asn135) aligned with Glu96 and Asn99 of

CheX respectively (Fig. 2.5 (A)). Although the side chain of FliY Glu132 is directed away from the predicted location of the CheY-phosphate in the structure, the presence of CheY-P likely produces the proper disposition (Pazy et al., 2010). CheZ also projects acid and amide-containing side-chains from an α-helix to bind and hydrolyze the CheY phosphoryl group (Zhao et al., 2002). Superposition of α1 and α1' helices of *T. maritima* FliY on to the active-site helix of *E. coli* CheZ•CheY•BeF_3^-•Mg^{2+} (PDB 1KMI) led to a clash free model that superimposed Asp31 (or Ser128) to Asp143 of CheZ but it did not align the essential *T. maritima* FliY Asn38 (or Asn135) near the active site (Fig. 2.5 (B)). Shifting down the FliY helices to superimpose Asn38 (or Asn135) with Gln147 of CheZ generated some clashes and mismatched the side-chain lengths. Thus, the chemical mechanism of hydrolysis is likely similar in CXY and CheZ phosphatases (Pazy et al., 2010), although the reactive residues are supplied somewhat differently (Park et al., 2004).

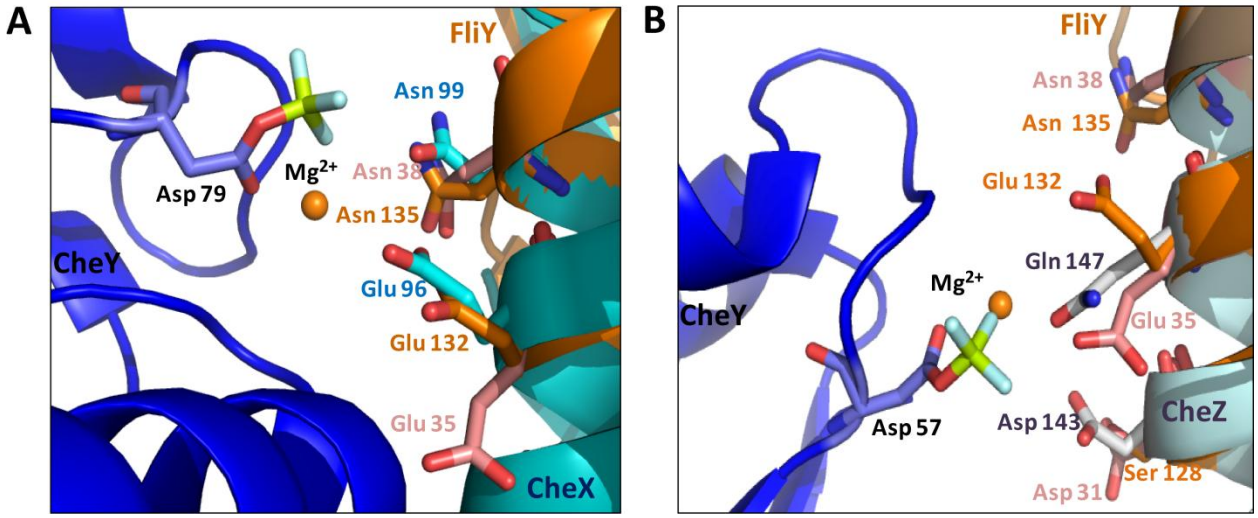

Figure 2.5. **Structural comparison of FliY to CheX and CheZ.** Comparison of the active center residues of FliY (site 1 in pink, site 2 in orange) and *B. burgdorferi* CheX (cyan) in complex with CheY·BeF_3^-·Mg^{2+} (blue) (A) and *E. coli* CheZ (light blue) in complex with CheY·BeF_3^-·Mg^{2+} (B).

2.4.4 The N-terminal CheY binding domain is not essential for phosphatase activity: FliY has an N-terminal CheY binding peptide which is homologous to the N-terminus of FliM. Crystal structures of activated CheY in complex with the $FliM_N$ peptide have shown that upon CheY phosphorylation Tyr106 changes conformation from an exposed to a partially buried position to facilitate the packing of the helical $FliM_N$ binding motif against the α4-β5-α5 region of CheY (Lee et al., 2001b; Lee et al., 2001a; Dyer et al., 2004). The residues involved in binding CheY are well conserved in FliM and FliY and a similar motif is found in the C-terminus of CheZ (supplemental Fig. 2.11; (Silversmith, 2005; Guhaniyogi et al., 2006)). Isothermal titration calorimetric measurements demonstrated a much higher affinity interaction for *T. maritima* CheY binding to $FliM_{NM}$ compared to $FliM_M$ (Park et al., 2004). The affinity between CheY and $FliM_{NM}$ is increased by orders of magnitude in the presence of the phosphor-mimic BeF_3^-. We have also demonstrated here that CheY-P binds to $FliM_{NM}$ more strongly than does CheY and that neither CheY-P nor CheY binds to $FliM_M$ under these conditions (Fig. 2.4 (A)). Given that the N-terminal peptides of FliM and FliY have conserved binding regions (supplemental Fig. 2.11) it is surprising that the *in vitro* phosphatase activity of FliY does not depend on $FliY_N$ (Fig. 2.3 (B)). Indeed, $FliY_{NM}$ or $FliY_M$ show the same degree of binding to CheY-P, which is contrary to what has been observed for the *B. subtilis* proteins (Szurmant et al., 2004). Thus, $FliY_N$ is not necessary to recruit CheY-P to the FliY active site, although it may interact weakly with CheY in the phosphorylated forms (the latter of which would be masked by the strong direct binding to $FliY_M$ in Fig. 2.4 (A)). Notably, if CheY were bound to $FliY_N$ in the same mode as found in the CheY-FliM peptide cocrystal structures the short linker between $FliY_N$ and $FliY_M$ would prevent the CheY aspartyl phosphate residue from accessing the FliY active center. The short linker of ~9 residues between the conserved CheY binding motif of

$FliY_N$ and the central domain (α1) in *T. maritima* FliY compared to the > 20 residues linkers of *B. subtilis* FliY, *E. coli* FliM and *T. maritima* FliM (supplemental Fig. 2.11) likely restrict CheY-P from accessing the dephosphorylation centers of *T. maritima* FliY. Thus, binding of *T. maritima* $FliY_N$ to CheY may be more important for switching the rotor direction (in assistance to $FliM_N$) than dephosphorylation of CheY-P.

2.4.5 Implications for rotor assembly: The structure of the flagellar rotor in genera like *Thermotoga* or *Bacillus* may be different from that in *Escherichia* and *Salmonella* due to the presence of FliY. Previous studies have shown that *T. maritima* FliN forms intertwined dimmers (Brown et al, 2005), which is consistent with FliY forming a dimer mediated by $FliY_C$ (i.e. FliN). Computational methods (with Psipred; (Buchan et al., 2010; Jones, 1999)) predict that the ~30 residue region connecting $FliY_M$ and $FliY_C$ does not have defined secondary structure and would allow substantial flexibility between the C-terminal and middle domains (Fig. 2.6). EM images and biochemical studies localize FliN to the bottom of the C-ring in *Salmonella* (Brown et al., 2005). Given the size of FliY (more than twice that of *E. coli* FliN), we predict $FliY_C$ to be also present as a rigid structure at the base of the C-ring with the $FliY_{NM}$ region extending out of the base. The inability of $FliY_M$ to bind $FliG_{MC}$ suggests that it does not substitute for $FliM_M$ in the center of the rotor. If the additional $FliY_M$ domain were to be fixed in position it may partly account for the larger diameter of the rotor in FliY-containing bacterial such as *Treponema primitia* (Murphy et al., 2006) and the extra electron density clearly visible at the bottom of the C-ring in *Leptospira interrogans* (Raddi et al., 2012).

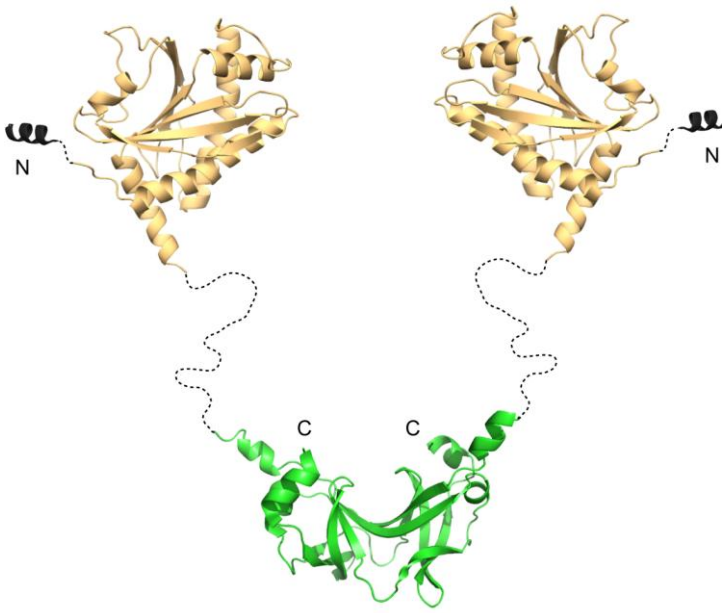

Figure 2.6. **Model of FliY.** Model derives from crystal structures of the middle domain (Protein Data Bank code 4HYN) and the C-terminal 100 residues (Protein Data Bank code 1YAB). Secondary structure prediction suggests that the long linker is unstructured. The color pattern as defined in Fig. 2.1.

The structure of *T. maritima* $FliY_M$ provides an atomic resolution model for a key component of the flagellar rotor of many bacteria and will aid the further exploration of rotor architecture in these species.

References:

Bilwes, A. M., Park, S. Y., Quezada, C. M., Simon, M. I., and Crane, B. R. (2003) Structure and Function of CheA, the Histidine Kinase Central to Bacterial Chemotaxis. in *Histidine Kinases in Signal Transduction.* (Inouye, M., and Dutta, R. ed.), Academic Press, San Diego, CA. pp 48-74

Bischoff, D. S., and Ordal, G. W. (1992a) Bacillus subtilis chemotaxis: a deviation from the Escherichia coli paradigm. Molecular microbiology *6*, 23-28.

Bischoff, D. S., and Ordal, G. W. (1992b) Identification and characterization of FliY, a novel component of the Bacillus subtilis flagellar switch complex. Molecular microbiology *6*, 2715-2723.

Brown, P.N., Hill, C.P., and Blair, D.F. (2002). Crystal structure of the middle and C-terminal domains of the flagellar rotor protein FliG. The EMBO journal *21*, 3225-3234.

Brown, P.N., Mathews, M.A., Joss, L.A., Hill, C.P., and Blair, D.F. (2005). Crystal structure of the flagellar rotor protein FliN from Thermotoga maritima. J Bacteriol *187*, 2890-2902.

Brown, P.N., Terrazas, M., Paul, K., and Blair, D.F. (2007). Mutational analysis of the flagellar protein FliG: sites of interaction with FliM and implications for organization of the switch complex. J Bacteriol *189*, 305-312.

Brunger, A. T. (2007) Version 1.2 of the Crystallography and NMR system. Nature Protocols *2*, 2728-2733.

Buchan, D. W. A., Ward, S. M., Lobley, A. E., Nugent, T. C. O., Bryson, K., and Jones, D. T. (2010) Protein annotation and modelling servers at University College London. Nucleic Acids Res. *38*, W563-W568.

Chao, X., Muff, T. J., Park, S. Y., Zhang, S., Pollard, A. M., Ordal, G. W., Bilwes, A. M., and Crane, B. R. (2006) A receptor-modifying deamidase in complex with a signaling phosphatase reveals reciprocal regulation. Cell *124*, 561-571.

Clausznitzer, D., Oleksiuk, O., Lovdok, L., Sourjik, V., and Endres, R. G. (2010) Chemotactic Response and Adaptation Dynamics in Escherichia coli. Plos Computational Biology *6*, e1000784.

Dyer, C. M., Quillin, M. L., Campos, A., Lu, J., McEvoy, M. M., Hausrath, A. C., Westbrook, E. M., Matsumura, P., Matthews, B. W., and Dahlquist, F. W. (2004) Structure of the constitutively active double mutant cheY(D13K) Y-106W alone and in complex with a flim peptide. J Mol Biol *342*, 1325-1335.

Dyer, C.M., Vartanian, A.S., Zhou, H., and Dahlquist, F.W. (2009). A molecular mechanism of bacterial flagellar motor switching. J Mol Biol *388*, 71-84.

Glekas, G. D., Plutz, M. J., Walukiewicz, H. E., Allen, G. M., Rao, C. V., and Ordal, G. W. (2012) Elucidation of the multiple roles of CheD in Bacillus subtilis chemotaxis. Molecular Microbiology *86*, 743-756.

Guhaniyogi, J., Robinson, V. L., and Stock, A. M. (2006) Crystal structures of beryllium fluoride-free and beryllium fluoride-bound CheY in complex with the conserved C-terminal peptide of CheZ reveal dual binding modes specific to CheY conformation. J Mol Biol *359*, 624-645.

Jones, D. T. (1999) Protein secondary structure prediction based on position-specific scoring matrices. J Mol Biol *292*, 195-202.

Khan, S., Pierce, D., and Vale, R. D. (2000) Interactions of the chemotaxis signal protein CheY with bacterial flagellar motors visualized by evanescent wave microscopy. Curr Biol *10*, 927-930.

Kirby, J. R., Kristich, C. J., Saulmon, M. M., Zimmer, M. A., Garrity, L. F., Zhulin, I. B., and Ordal, G. W. (2001) CheC is related to the family of flagellar switch proteins and acts independently from CheD to control chemotaxis in *Bacillus subtilis*. Molecular Microbiology *42*, 573-585.

Kuo, S. C., and Koshland, D. E. J. (1987) Roles of CheY and CheZ gene products in controlling flagellar rotation in bacterial chemotaxis of *Escherichia coli*. J Bacteriol *169*, 1307-1314.

Lee, L. K., Ginsburg, M. A., Crovace, C., Donohoe, M., and Stock, D. (2010) Structure of the torque ring of the flagellar motor and the molecular basis for rotational switching. Nature *466*, 996-1000.

Lee, S. Y., Cho, H. S., Pelton, J. G., Yan, D. L., Berry, E. A., and Wemmer, D. E. (2001a) Crystal structure of activated CheY - Comparison with other activated receiver domains. J Biol Chem *276*, 16425-16431.

Lee, S. Y., Cho, H. S., Pelton, J. G., Yan, D. L., Henderson, R. K., King, D. S., Huang, L. S., Kustu, S., Berry, E. A., and Wemmer, D. E. (2001b) Crystal structure of an activated response regulator bound to its target. Nat Struct Biol *8*, 52-56.

Liao, S., Sun, A., Ojcius, D.M., Wu, S., Zhao, J., and Yan, J. (2009). Inactivation of the fliY gene encoding a flagellar motor switch protein attenuates mobility and virulence of Leptospira interrogans strain Lai. BMC microbiology *9*, 253.

Lloyd, S. A., Whitby, F. G., Blair, D. F., and Hill, C. P. (1999) Structure of the C-terminal domain of FliG, a component of the rotor in the bacterial flagellar motor. Nature *400*, 472-475.

Lowenthal, A. C., Hill, M., Sycuro, L. K., Mehmood, K., Salama, N. R., and Ottemann, K. M. (2009) Functional Analysis of the Helicobacter pylori Flagellar Switch Proteins. J Bacteriol *191*, 7147-7156.

Mathews, M. A., Tang, H. L., and Blair, D. F. (1998) Domain analysis of the FliM protein of Escherichia coli. J Bacteriol *180*, 5580-5590.

McRee, D. E. (1999) XtalView Xfit - A versatile program for manipulating atomic coordinates and electron density. Journal of Structural Biology *125*, 156-165.

Minamino, T., Imada, K., Kinoshita, M., Nakamura, S., Morimoto, Y.V., and Namba, K. (2011). Structural insight into the rotational switching mechanism of the bacterial flagellar motor. Plos Biol *9*, e1000616.

Muff, T. J., and Ordal, G. W. (2007a) Assays for CheC, FliY, and CheX as representatives of response regulator phosphatases.Methods in enzymology *423*, 336-348.

Muff, T. J., and Ordal, G. W. (2007b) The CheC phosphatase regulates chemotactic adaptation through CheD. J Biol Chem *282*, 34120-34128.

Muff, T.J., and Ordal, G.W. (2008). The diverse CheC-type phosphatases: chemotaxis and beyond. Molecular microbiology *70*, 1054-1061.

Muff, T.J., Foster, R.M., Liu, P.J.Y., and Ordal, G.W. (2007).CheX in the three-phosphatase system of bacterial chemotaxis. J Bacteriol *189*, 7007-7013.

Murphy, G. E., Leadbetter, J. R., and Jensen, G. J. (2006) In situ structure of the complete Treponema primitia flagellar motor. Nature *442*, 1062-1064.

Otwinowski, Z., and Minor, W. (1997) Processing of X-ray diffraction data in oscillation mode. Methods Enzymol *276*, 307-325.

Park, S.Y., Chao, X., Gonzalez-Bonet, G., Beel, B.D., Bilwes, A.M., and Crane, B.R. (2004). Structure and function of an unusual family of protein phosphatases: the bacterial chemotaxis proteins CheC and CheX. Molecular cell *16*, 563-574.

Park, S.Y., Lowder, B., Bilwes, A.M., Blair, D.F., and Crane, B.R. (2006). Structure of FliM provides insight into assembly of the switch complex in the bacterial flagella motor. Proc Natl Acad Sci U S A *103*, 11886-11891.

Paul, K., Gonzalez-Bonet, G., Bilwes, A.M., Crane, B.R., and Blair, D. (2011). Architecture of the flagellar rotor. The EMBO journal *30*, 2962-2971.

Pazy, Y., Motaleb, M. A., Guarnieri, M. T., Charon, N. W., Zhao, R., and Silversmith, R. E. (2010) Identical phosphatase mechanisms achieved through distinct modes of binding phosphoprotein substrate. Proc Natl Acad Sci U S A *107*, 1924-1929.

Raddi, G., Morado, D.R., Yan, J., Haake, D.A., Yang, X.F., and Liu, J. (2012). Three-dimensional structures of pathogenic and saprophytic Leptospira species revealed by cryo-electron tomography. J Bacteriol *194*, 1299-1306.

Sarkar, M.K., Paul, K., and Blair, D. (2010). Chemotaxis signaling protein CheY binds to the rotor protein FliN to control the direction of flagellar rotation in Escherichia coli. Proc Natl Acad Sci U S A *107*, 9370-9375.

Silversmith, R.E. (2010). Auxiliary phosphatases in two-component signal transduction. Current opinion in microbiology *13*, 177-183.

Silversmith, R. E. (2005) High mobility of carboxyl-terminal region of bacterial chemotaxis phosphatase CheZ is diminished upon binding divalent cation or CheY-P substrate. Biochemistry *44*, 7768-7776.

Silversmith, R. E., Guanga, G. P., Betts, L., Chu, C., Zhao, R., and Bourret, R. B. (2003) CheZ-mediated dephosphorylation of the Escherichia coli chemotaxis response regulator CheY: role for CheY glutamate 89. J Bacteriol *185*, 1495-1502.

Sockett, H., Yamaguchi, Shigeru, Kihara, May, Irikura, Vera M. and Macnab, Robert M. (1992) Molecular Analysis of the Flagellar Switch Protein FliM of *Salmonella typhimurium*. J Bacteriol *174*, 793-806.

Sourjik, V., and Berg, H. C. (2002) Receptor sensitivity in bacterial chemotaxis. Proc Natl Acad Sci U S A *99*, 123-127.

Sowa, Y., and Berry, R.M. (2008). Bacterial flagellar motor. Quarterly reviews of biophysics *41*, 103-132.

Swanson, R. V., Sanna, M. G., and Simon, M. I. (1996) Thermostable chemotaxis proteins from the hyperthermophilic bacterium *Thermotoga maritima*. J Bacteriol *178*, 484-489.

Szurmant, H., and Ordal, G.W. (2004). Diversity in chemotaxis mechanisms among the Bacteria and Archaea. Microbiol Mol Biol Reviews *68*, 301-319.

Szurmant, H., Bunn, M.W., Cannistraro, V.J., and Ordal, G.W. (2003). Bacillus subtilis hydrolyzes CheY-P at the location of its action, the flagellar switch. J Biol Chem *278*, 48611-48616.

Szurmant, H., Muff, T. J., and Ordal, G. W. (2004) Bacillus subtilis CheC and FliY are members of a novel class of CheY-P-hydrolyzing proteins in the chemotactic signal transduction cascade. J Biol Chem *279*, 21787-21792.

Terwilliger, T. C. and Berendzen, J. (1999) Automated MAD and MIR structure solution. Acta Crystallography D Biol Crystallography *55*, 849-861.

Thomas, D.R., Francis, N.R., Xu, C., and DeRosier, D.J. (2006). The three-dimensional structure of the flagellar rotor from a clockwise-locked mutant of Salmonella enterica serovar Typhimurium. J Bacteriol *188*, 7039-7048.

Toker, A.S., and Macnab, R.M. (1997). Distinct regions of bacterial flagellar switch protein FliM interact with FliG, FliN and CheY. J Mol Biol *273*, 623-634.

Vartanian, A.S., Paz, A., Fortgang, E.A., Abramson, J., and Dahlquist, F.W. (2012). Structure of flagellar motor proteins in complex allows for insights into motor structure and switching. J Biol Chem *287*, 35779-35783.

Wadhams, G.H., and Armitage, J.P. (2004). Making sense of it all: bacterial chemotaxis. Nature reviews Molecular cell biology *5*, 1024-1037.

Wuichet, K., and Zhulin, I. B. (2010) Origins and Diversification of a Complex Signal Transduction System in Prokaryotes. Science Signaling *3.*

Zhao, R., Collins, E. J., Bourret, R. B., and Silversmith, R. E. (2002) Structure and catalytic mechanism of the E-coli chernotaxis phosphatase CheZ. Nature Structural Biology *9*, 570-575.

Supplemental Information

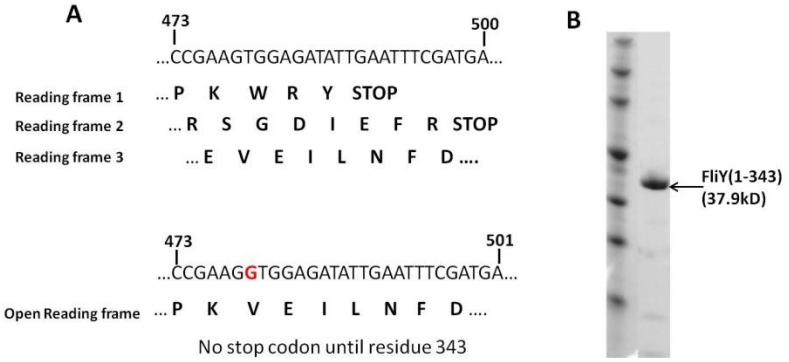

Figure 2.7. **$FliY_{FL}$ cloning and expression.** (A) The reported genomic DNA sequence of FliY lacked a guanine base which led to the disruption of the open reading frame. On sequencing PCR cloned genomic DNA a guanine base (# 479, shown in bold) was found intervening the genes. This lead to the expression of a fusion protein ending at residue 343. (B) SDS PAGE gel showing the expression of full length TmFliY.

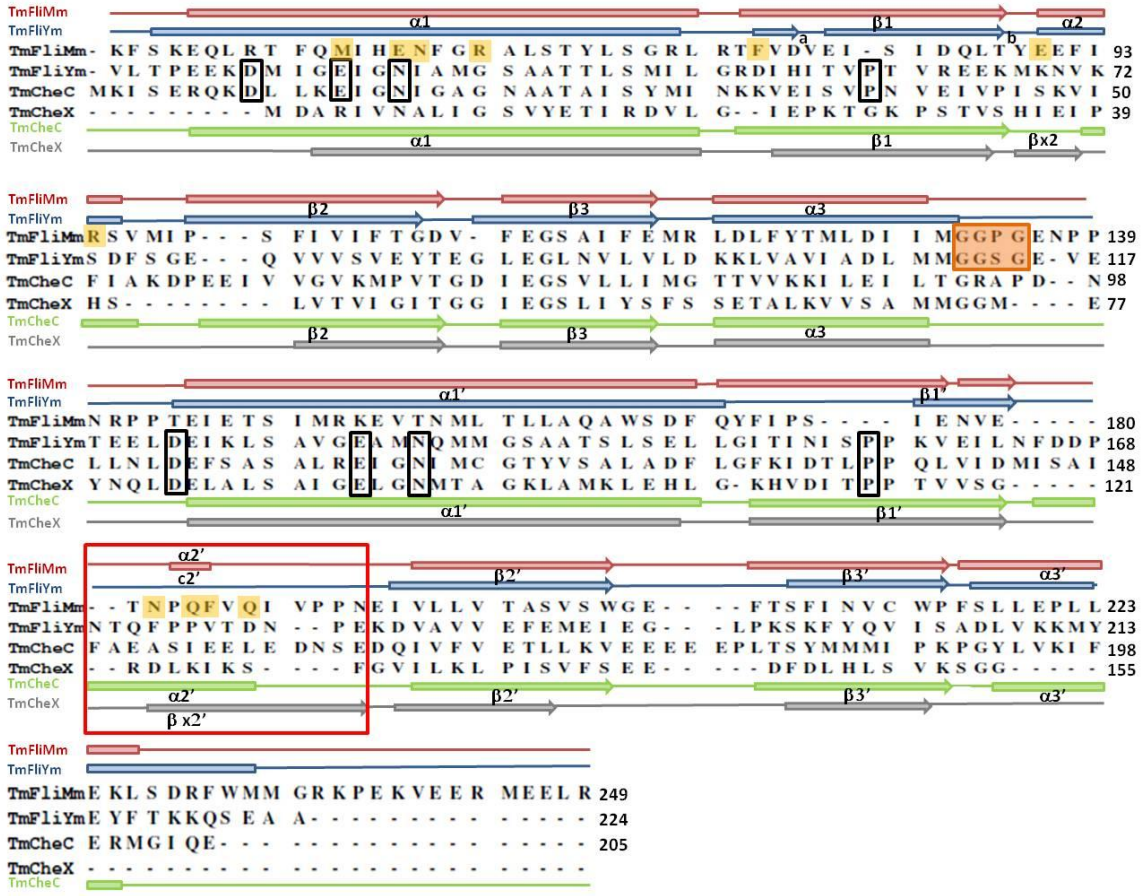

Figure 2.8. **Sequence alignment of *T. maritima* $FliM_M$, $FliY_M$, CheC, and CheX**. Secondary structure elements of $FliY_M$ are similar to $FliM_M$ and CheC than CheX except for in the region

c2′/α2′/βx2′ (red box). The conserved active site residues are highlighted in black boxes. Highlighted in orange is the conserved FliG binding motif GGXG of FliM aligned to the GGXG motif of FliY. Residues involved in FliM:FliM contacts in the rotor are highlighted in yellow (Park et al., 2006).

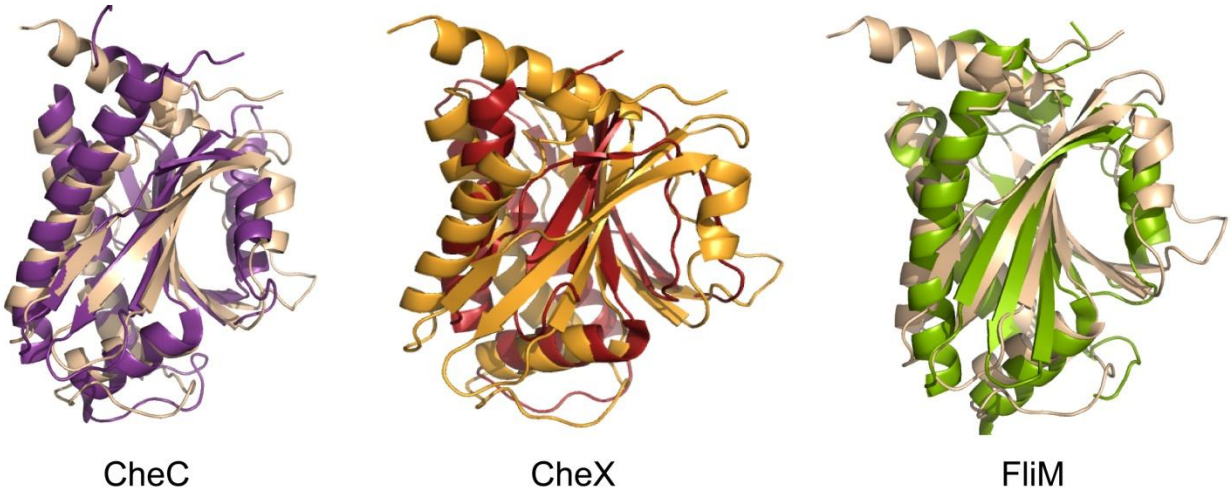

Figure 2.9. **Superposition of $FliY_M$ on CheC (dark purple), CheX (red), and FliM (green).** Superpostions were carried out by aligning the conserved β-strands of the central β-sheet.

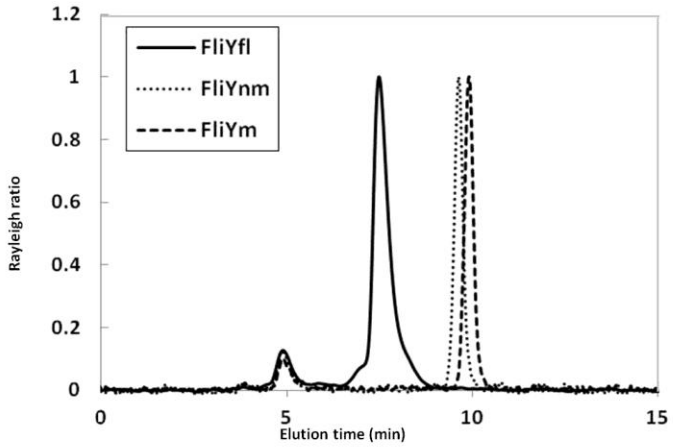

Figure 2.10. **Chromatogram of the light scattering data of $FliY_{FL}$ (solid line), $FliY_{NM}$ (dotted line), and $FliY_M$ (dashed line).**

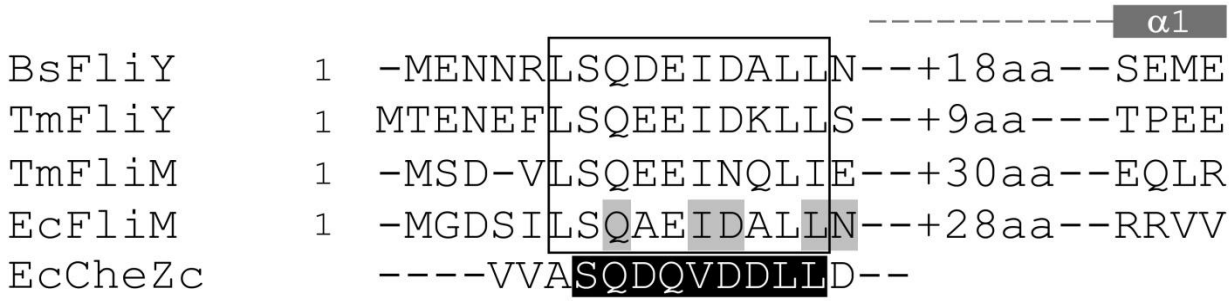

Figure 2.11. **Sequence alignment of the CheY binding motifs of *B. subtilis* FliY, *T. maritima* FliY, *T. maritima* FliM, *E. coli* FliM, and *E. coli* CheZ**. The linker region to the first helix in the middle domain is indicated. The span of residues that encompass the CheY binding motif are boxed. Highlighted in gray are residues involved in interaction with CheY, as observed in the *E. coli* CheY $FliM_N$ cocrystal structure (Lee et al., 2001a; Lee et al., 2001b; Dyer et al., 2004).

References:

Dyer, C. M., Quillin, M. L., Campos, A., Lu, J., McEvoy, M. M., Hausrath, A. C., Westbrook, E. M., Matsumura, P., Matthews, B. W., and Dahlquist, F. W. (2004) Structure of the constitutively active double mutant cheY(D13K) Y-106W alone and in complex with a flim peptide. J. Mol. Biol. *342*, 1325-1335.

Lee, S. Y., Cho, H. S., Pelton, J. G., Yan, D. L., Berry, E. A., and Wemmer, D. E. (2001a) Crystal structure of activated CheY - Comparison with other activated receiver domains. J. Biol. Chem. *276*, 16425-16431.

Lee, S. Y., Cho, H. S., Pelton, J. G., Yan, D. L., Henderson, R. K., King, D. S., Huang, L. S., Kustu, S., Berry, E. A., and Wemmer, D. E. (2001b) Crystal structure of an activated response regulator bound to its target. Nat. Struct. Biol. *8*, 52-56.

Park, S.Y., Lowder, B., Bilwes, A.M., Blair, D.F., and Crane, B.R. (2006). Structure of FliM provides insight into assembly of the switch complex in the bacterial flagella motor. Proc Natl Acad Sci U S A *103*, 11886-11891.

Chapter 3

Structural studies on ternary and binary complexes formed by *Thermotoga maritima* switch complex proteins

3.1 Introduction:

Biochemical assays have revealed interaction between the switch complex proteins FliG, FliM, and FliN, but structure of the ternary complex is unknown (Brown et al., 2005; Mathews et al., 1998; Passmore et al., 2008; Sarkar et al., 2010; Toker and Macnab, 1997). Switching of the motor rotation sense is the terminal step in the chemotaxis signaling pathway, however its mechanism of switching remains unclear largely due to the lack of detailed structural information on how the switch is constructed. As mentioned in Chapter 2, the switch complex in Gram-positive bacteria is different from the model system *Escherichia coli* due to the presence of the rotor protein FliY. Not much is known about the arrangement of FliY in the switch complex as a high resolution image of the rotor is not available from species that contain FliY. Cryo electron microscope (EM) images of the cytoplasmic C-ring in Gram-positive bacteria shows a larger diameter than found in C-rings of Gram-negative bacteria. This larger diameter may be attributed to the bulk caused by a large protein present at the base, i.e. FliY (Murphy et al., 2006; Raddi et al., 2012). We have aimed to reconstitute the ternary complex comprising of $FliG_{MC}$, $FliM_{FL}$, and $FliY_{FL}$ from *Thermotoga maritima* to study its structure and biophysical properties. A low-resolution structure of crystals grown from the ternary complex reveals a curved assembly of FliG and FliM.

3.2 Experimental Procedures:

3.2.1 Protein preparation: The genes encoding $TmFliY_{FL}$ (residues 1-343), $TmFliM_{FL}$ (residues 1- 328), $TmFliM_{M}$ (residues 46-242), $TmFliG_{MC}$ (residues 104 -335), and $TmFliG_{M}$ (residues 117-195), were cloned from *T. maritima* genomic DNA (obtained from American Type Culture Collection). For co-expression purposes $TmFliM_{FL}$ was digested into the dual vector pCDF (Novagen) using NdeI and XhoI restriction sites. It was co-transformed with $TmFliY_{FL}$ in pET28a vector (Novagen) into *E. coli* strain BL21-DE3 for co-expression.

Cells were induced with 100 μM Isopropyl β-D-1-thiogalactopyranoside (IPTG) at optical density 0.6 and were grown overnight at 25 °C. Proteins were purified using Nickel-NTA affinity chromatography and the His_6-tag on $TmFliY_{FL}$ was cleaved using thrombin overnight. The co-expressed proteins were further purified using size-exclusion chromatography (SEC, Superdex 200; Pharmacia Biotech). Fractions that correspond to two bands of the appropriate molecular weight on the SDS PAGE gel were concentrated in GF buffer (50 mM TRIS, pH=7.5, 150 mM NaCl) containing 5mM dithiothreitol (DTT).

For co-crystallization efforts with truncated proteins $TmFliM_{M}$, $TmFliG_{M}$, and $TmFliY_{FL}$, each protein was purified separately using Ni-NTA column chromatography, and SEC following overnight cleavage of the His_6-tag with thrombin. Samples were concentrated in GF buffer (50 mM TRIS, pH=7.5, 150 mM NaCl) with $TmFliM_{M}$ having an additional 2mM DTT in the buffer.

3.2.2 Crystallization and data collection: Crystals were obtained by vapor diffusion method at room temperature from a 2 μL drop containing 1 μL of well solution (0.1M imidazole, pH 6.5, 1.0 M sodium acetate trihydrate; Hampton research) and 1 μL of a mixture of three proteins $TmFliY_{FL}$, $TmFliM_{M}$, and $TmFliG_{M}$. Crystals were observed in 5 days. Crystals were optimized

by varying precipitant concentration and pH of buffer to obtain better diffraction quality crystals. Data was collected at Cornell High Energy Synchrotron Source (CHESS), station A1 using the ADSC Quantum 210 CCD detector. Crystals were briefly soaked in 30 % glycerol before data collection.

3.2.3 Structure determination and refinement: HKL2000 (Otwinowski and Minor, 1997) was used to scale the data set. The structure of the complex was obtained by PHENIX AutoMR (Adams et al., 2010). PDB entries 3SOH ($TmFliM_M$:$TmFliG_M$ structure) and 4HYN ($TmFliY_M$) were used as search models. Solutions were obtained with only 3SOH. There were 11 $TmFliM_M$:$TmFliG_M$ subunits in the asymmetric unit. No residual density was found to fit in TmFliY. The structure was refined using autorefine in PHENIX (Adams et al., 2010).

3.3 Results:

3.3.1 Reconstituting the ternary complex in *T. maritima*: Expression level of $TmFliM_{FL}$ is very low by itself. We therefore tried to express $TmFliM_{FL}$ with $TmFliY_{FL}$ which interacts with TmFliM via the C-terminal domain ($TmFliM_C$). This interaction between $TmFliM_C$ and C-terminus of TmFliY (also known as FliN in *E. coli*) is very strong and survived through different purification procedures (Brown et al., 2005). $TmFliY_{FL}$ was co-expressed with $TmFliM_{FL}$ as described under experimental procedures.

To reconstitute the ternary complex, $TmFliG_{MC}$ and $TmFliY_{FL}$:$TmFliM_{FL}$ were separately grown and purified using affinity column. His-tags on $TmFliG_{MC}$ and $TmFliY_{FL}$ in $TmFliY_{FL}$:$TmFliM_{FL}$ were cleaved using thrombin. They were then mixed and incubated for few hours before passing it through the size exclusion column. We observed a shift in the elution peak towards higher molecular weight indicating an interaction between $TmFliG_{MC}$ and $TmFliY_{FL}$:$TmFliM_{FL}$ (Fig.

3.1). Crystallization efforts using reconstituted $TmFliY_{FL}$:$TmFliM_{FL}$:$TmFliG_{MC}$ were unsuccessful despite several attempts with a large range of precipitants and buffers.

The molecular weights of $TmFliY_{FL}$ and $TmFliM_{FL}$ are very similar, 37.9 and 37.8 kDa respectively, which makes it difficult for us to decipher if both the proteins are co-expressed using a SDS PAGE analysis. TmFliY does not interact with TmFliG as shown in Chapter 2 and it is a known fact that FliM interacts with FliG very strongly (Brown et al., 2002; Brown et al., 2007; Lam et al., 2013; Passmore et al., 2008; Sircar et al., 2013; Vartanian et al., 2012). Co-elution of $TmFliG_{MC}$ with $TmFliY_{FL}$:$TmFliM_{FL}$ served as a proof that TmFliM is expressed (Fig. 3.1).

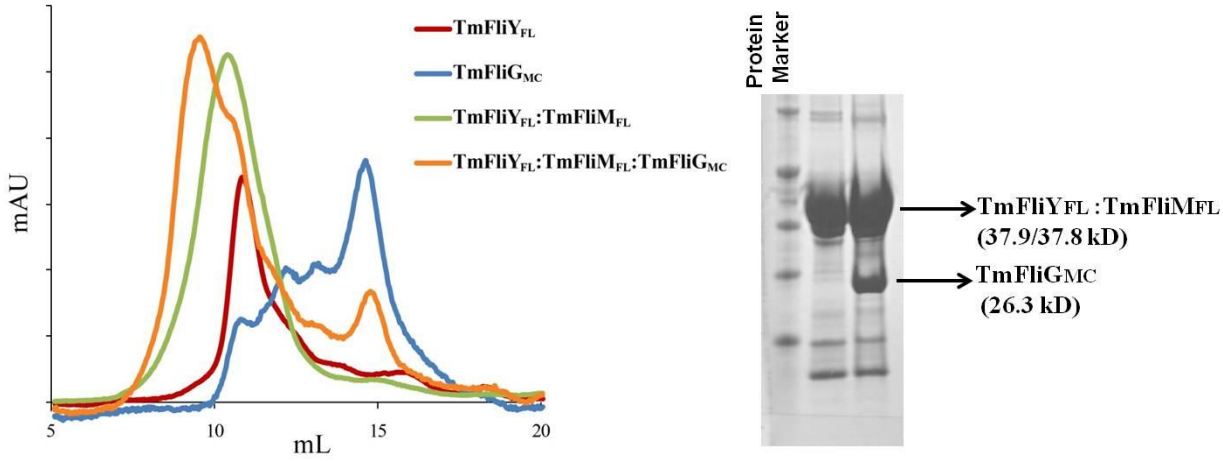

Figure 3.1. **Size exclusion chromatography of ternary protein complex.** Size exclusion column chromatography of $TmFliG_{MC}$ (blue), $TmFliY_{FL}$ (red), $TmFliY_{FL}$:$TmFliM_{FL}$ (green), $TmFliY_{FL}$:$TmFliM_{FL}$:$TmFliG_{MC}$ (orange). Shift in the elution peak of $TmFliY_{FL}$:$TmFliM_{FL}$:$TmFliG_{MC}$ from $TmFliY_{FL}$:$TmFliM_{FL}$ towards higher molecular weight suggests the interaction between the components. Samples corresponding to the main peaks were run on SDS PAGE gel showing the expression of $TmFliY_{FL}$:$TmFliM_{FL}$ and $TmFliY_{FL}$:$TmFliM_{FL}$:$TmFliG_{MC}$ respectively.

3.3.2 Structure of the $TmFliG_{M}$:$TmFliM_{M}$ binary complex: It is difficult to crystallize the switch complex composed of full length proteins. The full length proteins do not express well.

The flexible linkers connecting the domains of the proteins are possible sites for cleavage. Crystallization efforts involving larger fragments of rotor protein resulted in crystals of smaller fragments which resulted after tryptic digestion of the flexible linkers. We thus aimed to crystallize certain domains of the protein which are known to interact, obtain information from those complexes and then attempt to weave in the missing information together by lower resolution structural techniques. In an effort to crystallize $TmFliM_M$, $TmFliG_M$ and $TmFliY_{FL}$ we crystallized the binary complex of $TmFliG_M$ and $TmFliM_M$ instead. The crystals diffracted to 4.3 Å but molecular replacement (MR) worked successfully due to the availability of a search model. As known through various biochemical experiments $FliM_M$ interacts with $FliG_M$ through the GGPG motif of FliM. The electron density of the GGXG motif was absent in the crystal structure of $TmFliM_M$ (Park et al., 2006). However, this motif was ordered in presence of the binding partner in the co-crystal (Paul et al., 2011). The surface of contact between $TmFliG_M$ and $TmFliM_M$ involved the EHPQR motif of TmFliG and the loop containing the GGXG motif. In the asymmetric unit the $TmFliM_M$ molecules are arranged in an antiparallel fashion interacting through the long helices, α1 and α1′ from each molecule. This leads to the arrangement of two TmFliG binding regions to opposite extremes (Fig. 3.2).

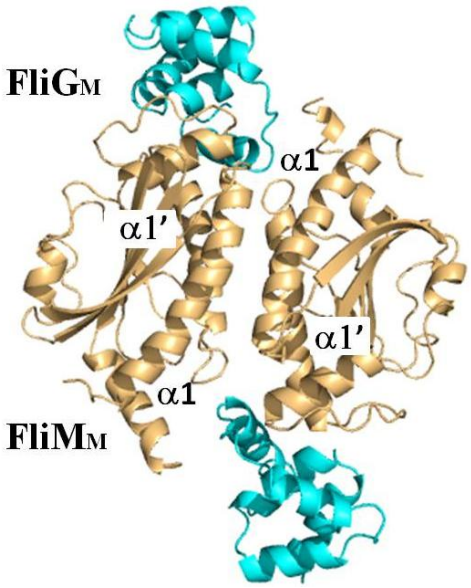

Figure 3.2. **Antiparallel arrangement of $TmFliM_M$:$TmFliG_M$ heterodimer.** Cartoon representation of the heterotetramer of $TmFliM_M$ (tan) and $TmFliG_M$ (aqua). The interaction is mediated via the α1 and α1′ helices of each TmFliM molecule.

3.4 Discussion:

$TmFliM_M$:$TmFliG_M$ crystallizes with 11 molecules present in the asymmetric unit. Interestingly, seven such subunits generated a curvature which mimicked a portion of a ring. Generation of five equivalent segments created a closed ring of diameter ~ 43 nm. This value is very close to the 45 nm diameter of the C-ring observed in the EM image (Thomas et al., 2006). A ring of radius and stoichiometry consistent with the C-ring (15 $TmFliM_M$:$TmFliG_M$ heterotetramers in an antiparallel arrangement and five $TmFliG_M$:$TmFliM_M$ heterodimer in a parallel arrangement) is quite surprising given the orientation of the subunits and current thinking regarding C-ring architecture (Fig. 3.3).

An EM image of the flagellar rotor from *Salmonella typhimurium* showed the symmetry to fluctuate between 32- to 36-fold (Thomas et al., 2006). Previous cross-linking experiment on TmFliM also shows that 35 copies of $TmFliM_M$ generate a C-ring of radius 45 nm (Park et al.,

2006). 35-fold symmetry of the ring observed here is in good agreement to what has been observed before.

This antiparallel arrangement was previously observed in $TmFliM_M$ and TmCheC (a phosphatase very similar in structure to $TmFliM_M$) crystal structures (Park et al., 2004; Park et al., 2006). The relevance of such an arrangement in the C-ring is questionable as it places alternating TmFliG molecules pointing upwards and downwards. The downward facing molecules are unavailable for binding to the stator (Lloyd et al., 1996). In the next chapter we have tested the relevance of such an arrangement in solution using a combination of pulsed dipolar electron spin resonance spectroscopy, cross-linking experiments.

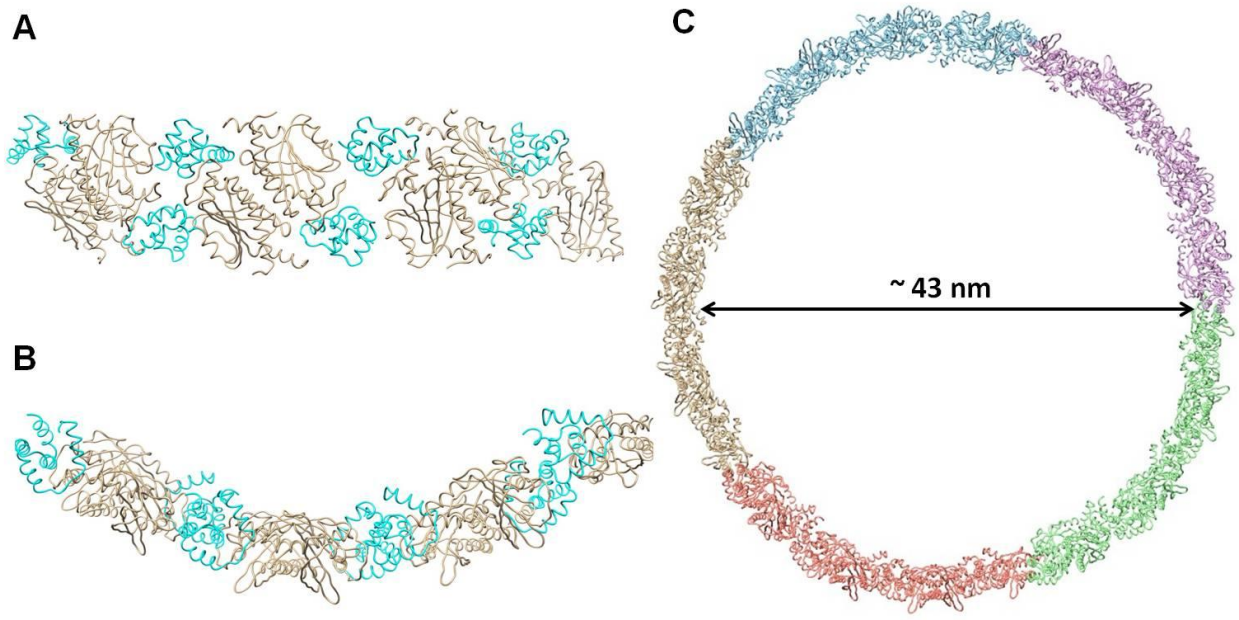

Figure 3.3. **Arrangement of $TmFliM_M$:$TmFliG_M$ in the asymmetric unit** (A) Ribbon representation of a segment of the asymmetric unit showing three $TmFliM_M$:$TmFliG_M$ heterotetramers in antiparallel arrangement and a heterodimer by itself (from left to right). $TmFliM_M$ is represented in tan and $TmFliG_M$ is represented in aqua (B) Top view of the segment showing the curvature. (C) Top view of the ring generated from this segment by applying an appropriate rotation matrix to generate a closed structure. The ring contains 35 copies of $TmFliG_M$:$TmFliM_M$.

Table 3.1. Data collection, phasing and refinement statistics

Data Collection	
Space group	$P2_12_12_1$
Unit cell (Å)	a = 105.40, b = 216.25, c = 262.21
Resolution range (Å)	50 – 4.3 (4.37- 4.3)[a]
[b]R_{merge}	0.105 (0.389) [a]
I/σI	11.7 (3.0) [a]
Completeness (%)	98.8 (98.7) [a]
Refinement	
No. of reflections	40483
R work/R free	0.241/0.281
No. of atoms	
Residues	186 (#46-231) for each chain of FliM, 75 (#113 -187) for each chain of FliG
Geometry (r.m.s.d.)[c]	
Bond lengths (Å)	0.008
Bond angles (°)	1.3

[a]Highest resolution range for compiling statistics

[b]$R_{merge} = \Sigma\Sigma_i |I_i - \langle I \rangle| / \Sigma\Sigma_i I_i$

[c]r.m.s.d., root mean square deviation

References:

Adams, P.D., Afonine, P.V., Bunkoczi, G., Chen, V.B., Davis, I.W., Echols, N., Headd, J.J., Hung, L.W., Kapral, G.J., Grosse-Kunstleve, R.W., *et al.* (2010). PHENIX: a comprehensive

Python-based system for macromolecular structure solution. Acta crystallographica Section D, Biological crystallography *66*, 213-221.

Brown, P.N., Hill, C.P., and Blair, D.F. (2002). Crystal structure of the middle and C-terminal domains of the flagellar rotor protein FliG. The EMBO journal *21*, 3225-3234.

Brown, P.N., Mathews, M.A., Joss, L.A., Hill, C.P., and Blair, D.F. (2005). Crystal structure of the flagellar rotor protein FliN from Thermotoga maritima. J Bacteriol *187*, 2890-2902.

Brown, P.N., Terrazas, M., Paul, K., and Blair, D.F. (2007). Mutational analysis of the flagellar protein FliG: sites of interaction with FliM and implications for organization of the switch complex. J Bacteriol *189*, 305-312.

Lam, K.H., Lam, W.W., Wong, J.Y., Chan, L.C., Kotaka, M., Ling, T.K., Jin, D.Y., Ottemann, K.M., and Au, S.W. (2013). Structural basis of FliG-FliM interaction in Helicobacter pylori. Molecular microbiology *88*, 798-812.

Lloyd, S.A., Tang, H., Wang, X., Billings, S., and Blair, D.F. (1996). Torque generation in the flagellar motor of Escherichia coli: evidence of a direct role for FliG but not for FliM or FliN. J Bacteriol *178*, 223-231.

Mathews, M.A., Tang, H.L., and Blair, D.F. (1998). Domain analysis of the FliM protein of Escherichia coli. J Bacteriol *180*, 5580-5590.

Murphy, G.E., Leadbetter, J.R., and Jensen, G.J. (2006). In situ structure of the complete Treponema primitia flagellar motor. Nature *442*, 1062-1064.

Otwinowski, Z., and Minor, W. (1997). Processing of X-ray diffraction data collected in oscillation mode. Methods Enzymol *276*, 307-326.

Park, S.Y., Chao, X., Gonzalez-Bonet, G., Beel, B.D., Bilwes, A.M., and Crane, B.R. (2004). Structure and function of an unusual family of protein phosphatases: the bacterial chemotaxis proteins CheC and CheX. Molecular cell *16*, 563-574.

Park, S.Y., Lowder, B., Bilwes, A.M., Blair, D.F., and Crane, B.R. (2006). Structure of FliM provides insight into assembly of the switch complex in the bacterial flagella motor. Proc Natl Acad Sci U S A *103*, 11886-11891.

Passmore, S.E., Meas, R., and Marykwas, D.L. (2008). Analysis of the FliM/FliG motor protein interaction by two-hybrid mutation suppression analysis. Microbiology *154*, 714-724.

Paul, K., Gonzalez-Bonet, G., Bilwes, A.M., Crane, B.R., and Blair, D. (2011). Architecture of the flagellar rotor. The EMBO journal *30*, 2962-2971.

Raddi, G., Morado, D.R., Yan, J., Haake, D.A., Yang, X.F., and Liu, J. (2012). Three-dimensional structures of pathogenic and saprophytic Leptospira species revealed by cryo-electron tomography. J Bacteriol *194*, 1299-1306.

Sarkar, M.K., Paul, K., and Blair, D.F. (2010). Subunit organization and reversal-associated movements in the flagellar switch of Escherichia coli. J Biol Chem *285*, 675-684.

Sircar, R., Greenswag, A.R., Bilwes, A.M., Gonzalez-Bonet, G., and Crane, B.R. (2013). Structure and activity of the flagellar rotor protein FliY: a member of the CheC phosphatase family. J Biol Chem *288*, 13493-13502.

Thomas, D.R., Francis, N.R., Xu, C., and DeRosier, D.J. (2006). The three-dimensional structure of the flagellar rotor from a clockwise-locked mutant of Salmonella enterica serovar Typhimurium. J Bacteriol *188*, 7039-7048.

Toker, A.S., and Macnab, R.M. (1997). Distinct regions of bacterial flagellar switch protein FliM interact with FliG, FliN and CheY. J Mol Biol *273*, 623-634.

Vartanian, A.S., Paz, A., Fortgang, E.A., Abramson, J., and Dahlquist, F.W. (2012). Structure of flagellar motor proteins in complex allows for insights into motor structure and switching. J Biol Chem *287*, 35779-35783.

Chapter 4

Probing the Structure of Flagellar Switch Complex from *Thermotoga maritima* using Pulsed ESR Spectroscopy

4.1 Introduction:

Bacteria move towards a favorable environment or away from an unfavorable one by switching the direction of flagellar rotation between clockwise and counter clockwise. Rotation of the flagellum is controlled by the switch complex of the cytoplasmic C-ring, a core rotor complex present at the base of flagella (Berg, 2003; Kojima and Blair, 2004; Sowa and Berry, 2008). The switch complex is composed of the three conserved proteins FliG, FliM, and FliN, each present in several copy numbers. This complex is essential for torque generation, switching and flagellar assembly. FliG functions directly in torque generation. The rotor protein FliM is the primary component involved in directional switching by interacting with the signaling protein phosphorylated CheY (CheY-P) and FliN is essential for flagellar export.

Rotation of the flagella involves the movement of the rotating part, the rotor, with respect to the stationary part, the stator. The stator, embedded in the membrane, is composed of MotA and MotB, which act as proton channels (Blair and Berg, 1991; Braun and Blair, 2001; Chun and Parkinson, 1988; Lloyd and Blair, 1997). The C-terminal domain of FliG ($FliG_C$) contains conserved charged residues that interact with MotA (Lloyd and Blair, 1997; Lloyd et al., 1999; Thormann and Paulick, 2010). FliG has two other conserved patches of residues for interaction with FliM: these are a conserved hydrophobic patch along the C-terminus and an EHPQR motif in the middle domain (Brown et al., 2007). Another conserved motif of FliG is the Gly-Gly

residues at the C-terminal end of the linker joining FliG middle domain ($FliG_M$) to $FliG_C$. This motif is thought to confer flexibility to the two domains (Brown et al., 2002; Lee et al., 2010).

Another component involved in switching is FliM (Sockett et al., 1992). Its amino terminal is known to interact with phosphorylated CheY (CheY-P) (Bren and Eisenbach, 1998; Park et al., 2006b; Toker and Macnab, 1997; Welch et al., 1993). CheA phosphorylates CheY at the poles. CheY-P then diffuses through the cytosol to the flagellar rotor (Armitage, 1999). When concentrations of CheY-P are low the cells continue to swim smoothly in a straight line. At higher concentrations of CheY-P the cells randomly reorient. Alternating between smooth swims and reorientation allows the bacteria to move up the attractant gradient (Berg and Brown, 1972; Macnab and Koshland, 1972). Binding of CheY-P to FliM (and FliN) is assumed to create a conformational change in FliG, resulting in a rearrangement at the FliG-MotA surface (Ahn et al., 2013; Lam et al., 2012; Park et al., 2006b; Sarkar et al., 2010a; Welch et al., 1993; Zhou et al., 1998). This causes the motor to rotate in clockwise direction. FliM is positioned right below FliG in the C-ring. The middle domain of FliM interacts with FliG through the conserved GGXG motif (Lam et al., 2013; Mathews et al., 1998; Paul et al., 2011b; Toker and Macnab, 1997; Vartanian et al., 2012). The C-terminal region of FliM interacts with FliN the other rotor protein and together they form the lower part of the C-ring (Brown et al., 2005; Sarkar et al., 2010b). In some genera like *Thermotoga* and *Bacillus,* the amino terminus of FliN is fused to an additional phosphatase domain, known as FliY (Bischoff and Ordal, 1992b; Bourret and Silversmith, 2010; Muff and Ordal, 2008; Silversmith, 2010; Sircar et al., 2013; Szurmant et al., 2003).

Structures of all the switch complex proteins are now available and an overall organization of the protein components was modeled based on co-crystal structures and biochemical assays (Brown et al., 2002; Brown et al., 2005; Lam et al., 2013; Lee et al., 2010; Lloyd et al., 1999; Lowder et

al., 2005; Lux et al., 2000; Mathews et al., 1998; Minamino et al., 2011; Park et al., 2006b; Paul et al., 2011b; Sourjik and Berg, 2000). Each switch complex protein is present in different copy numbers making their arrangement in the C-ring complex. Several models have been proposed to explain the symmetry mismatch between FliG (26 copies) and FliM (34 copies) but none have been fully tested and distinguished (Brown et al., 2007; Park et al., 2006b; Thomas et al., 2006). Extensive research on the flagellar motor gives us information about the molecular components involved but there is still much unanswered regarding the structure of the signaling complex and the molecular mechanism of rotational switching. The complex interactions involving a large number of membrane associated proteins makes it difficult to understand motor action and regulation.

X-ray crystallography allows us to obtain high-resolution structures of protein complexes; however direct measurements on how they assemble to form higher-order assemblies has not yet been achieved. Also, the solid state structure from crystals of components may not well represent the solution state structure, or the structure in the assembled flagella. Electron spin resonance (ESR) spectroscopy combined with site-directed spin labeling (SDSL) has emerged as one of the powerful techniques to study the structure and dynamic nature of the proteins (Columbus and Hubbell, 2002; Fanucci and Cafiso, 2006). SDSL is the method to introduce paramagnetic centers in to biomolecules which generally does not contain an endogenous paramagnetic center (Altenbach et al., 1989; Cornish et al., 1994; Steinhoff et al., 1994). The spin-labels are introduced in the protein by mutating a surface exposed residue to cysteine and treating it with 1-oxyl-2,2,5,5-tetramethylpyrolinyl-3-methyl)-methane sulphonate (MTSSL). This technique of SDSL is simple and is frequently used. The label is small enough to not affect the protein structure, however, the function of the labeled protein should always be compared to the WT to

check for any perturbation (McHaourab et al., 1996). These labels act as reporters for the surrounding environment, allowing us to measure the distances to other paramagnetic centers in the protein. SDSL combined with continuous wave ESR has been used for not over 20 years to measure distances up to 20 Å (Crane et al., 2005; Cuello et al., 2004; Dong et al., 2005). Double labeling combined with pulsed methods increases the distance range that can be measured (Borbat and Freed, 2007). Pulsed dipolar electron spin resonance spectroscopy (PDS) measures distances between specifically placed spin-labels using their magnetic dipolar coupling. By the application of PDS distances of up to 80 Å can be monitored under modified conditions (Borbat et al., 2004; Jeschke et al., 2004). This technique provides the long-range distance restraints necessary to map the architecture of multicomponent complexes. To investigate how individual domains are arranged and how conformational changes accompany switching in solution, we applied spin-labeling techniques with PDS (Bhatnagar et al., 2010; Borbat and Freed, 2007). Because PDS is not restricted by the size of the protein we can map higher order complexes (Jeschke, 2012). The time domain signal which reflects the dipolar coupling energy is processed to obtain the distance distribution data.

The low-resolution electron microscope (EM) images of the intact flagellar rotor from WT and the FliFFliG fusion deletion mutant from *Salmonella typhimurium*, and *Borrelia burgdorferi* further our understanding of the rotor architecture (Liu et al., 2009; Thomas et al., 2001; Thomas et al., 2006). These images along with protein binding assays, cross-linking experiments is indicative of the positions of the rotor proteins (Brown et al., 2007; Lowder et al., 2005; Park et al., 2006b; Paul and Blair, 2006; Paul et al., 2011b). However, the positions of the relative domains of the proteins are ambiguous (Brown et al., 2007; Paul et al., 2011b; Thomas et al., 2006). The structure of *Thermatoga maritima* (Tm) FliG middle domain ($FliG_M$) with TmFliM

middle domain ($FliM_M$) (Lam et al., 2013; Paul et al., 2011b), TmFliG middle and C-terminal domain ($FliG_{MC}$) with $TmFliM_M$ (Vartanian et al., 2012) gave us key insights into the association mode of two switch complex proteins. Using the FliM:FliG crystal structures and data based on cross-linking experiments (Park et al., 2006b) we built three models for parallel and antiparallel arrangement of the FliM:FliG heterotetramer. The first model is the antiparallel arrangement of FliM and FliG based on the crystal structure described in Chapter 3. The second model is the $FliM_M$:$FliG_{MC}$ co-crystal structure (PDB 4FHR) (Vartanian et al., 2012). For this crystal structure, the electron density for FliG residues 185 to 196 was missing. The third model is based on the $FliG_{MC}$ structure (PDB 3AJC) (Minamino et al., 2011). In this structure the electron density between residues 185 to 196 is not observed. The connection between $FliG_M$ and $FliG_C$ could be within the same molecule or with the adjacent molecule. Beneath the $FliG_M$ molecule the $FliM_M$ protomers are arranged in parallel arrangement. The heterotetramers in models II and III are generated based on cross-linking experiments on $FliM_M$ (Park et al., 2006b; Paul et al., 2011b) (Fig. 4.1). Using these models as our reference, PDS was conducted on spin-labeled FliM and FliG, individually or in mixture.

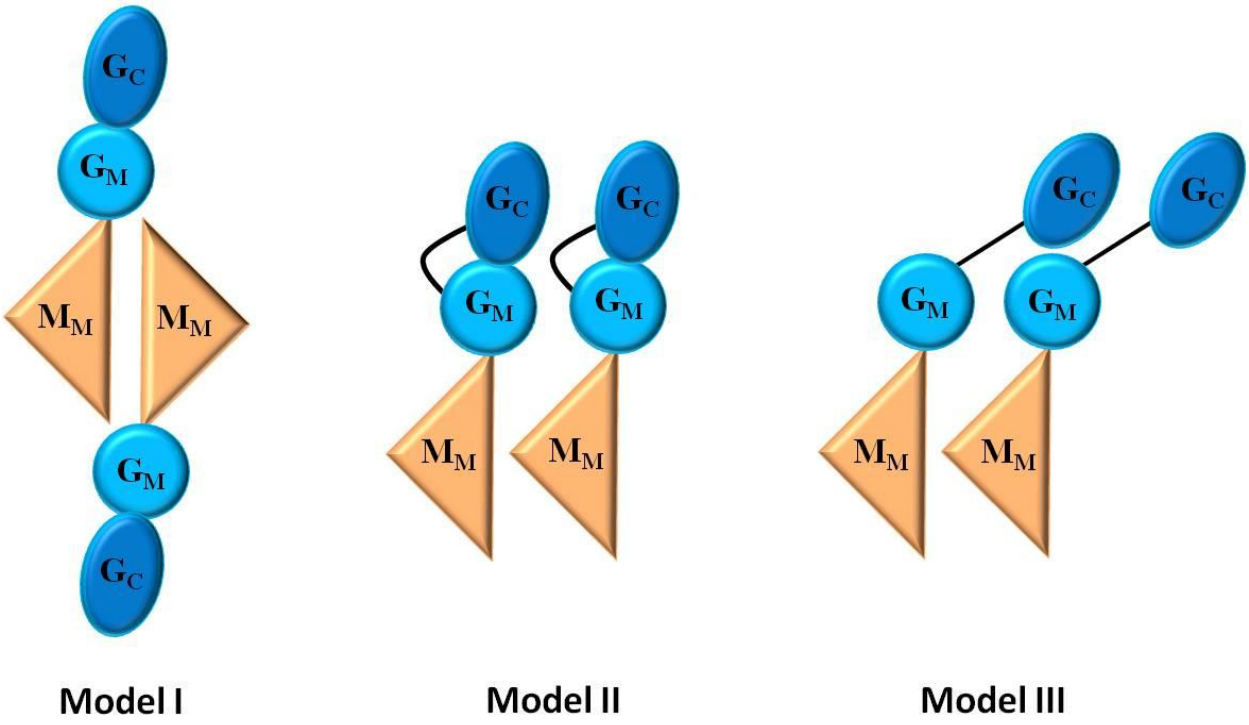

Figure 4.1: **Possible arrangements of FliM and FliG in the C-ring.** Model I is an antiparallel dimer of the heterodimer of FliM:FliG as observed in the structure mentioned in Chapter 3. Model II is a parallel dimer of heterodimer of FliM:FliG as seen in the $FliM_M$:$FliG_{MC}$ crystal structure (PDB 4FHR). Model III is based on the $FliG_{MC}$ crystal structure (PDB 3AJC), with a parallel arrangement of FliM under it.

In this study we have probed the association properties of *T. maritima* FliG and FliM using PDS, cross-linking, and multiangle light scattering (MALS) experiments. Mutations in the C-terminal domain of FliG affected the domain interface of a FliG dimer that forms in solution. These observations were complemented by MALS, which provided similar support for a FliG dimer. We herein report that in the soluble complexes, FliG and FliM interacts through their middle domains in a 1:1 mode, but higher order structures involve contacts made by $FliG_C$ The interaction between $FliG_M$ and the $FliG_C$ of the adjacent molecule results in the generation of an array in the C-ring and would explain the high degree of cooperativity observed on switching.

4.2 Experimental procedures:

4.2.1 Cloning, mutagenesis and spin labeling: The genes encoding *T. maritima* $FliG_{MC}$ (residues 116-335), $FliM_{NM}$ (residues 1-249), and CheY were PCR cloned from *T. maritima* genomic DNA (obtained from the American Type Culture Collection) into the vector pET28a (Novagen) and expressed with a His_6-tag in an *E. coli* strain BL21-DE3. Point mutations to cysteine residues on $FliG_{MC}$ (K160, K174, L208, E305), and $FliM_{NM}$ (E60, D121, M131, R141, S167) and tryptophan residues on $FliG_{MC}$ (Q129, I204, L227) were introduced by QuikChange (Stratagene) or overlap extension and mutations were confirmed by sequencing. *E. coli* cultures transformed with our vectors were grown overnight at room temperature after induction with 100 μM Isopropyl β-D-1-thiogalactopyranoside (IPTG) at the optical density of 0.6 at 25 °C. Cells were collected by centrifugation, frozen and stored in -80 °C. Frozen cells were thawed and resuspended in lysis buffer (25 mM HEPES, pH 7.5, 500 mM NaCl, 5 mM imidazole). Cells were sonicated and centrifuged at 22000 rpm for 1 hr at 4 °C. The wild type protein samples were purified by Ni-NTA affinity chromatography and further purified by size exclusion chromatography after cleaving the His_6-tag with thrombin. *E. coli* cultures expressing cysteine mutants were processed as described above. Cell lysates were applied to the Ni-column. 5-10 mM MTSSL (Toronto research, Toronto, ON) spin-label was added to the column, incubated at room temperature for 4 hrs then overnight at 4 °C. The next day thrombin was added to cleave the His_6-tag. Samples were eluted after overnight incubation with thrombin. They were further purified on size-exclusion column (Superdex 75 or Superdex 200; Pharmacia Biotech) and concentrated in GF buffer (50 mM TRIS, pH=7.5, 150 mM NaCl).

4.2.2 Sample preparation for PDS: Spin-labeled proteins as well as unlabeled proteins were aliquoted in small volumes and stored at -80 °C after flash freezing. The samples were prepared

by incubating $FliG_{MC}$ (50 μM) and $FliM_{NM}$ (50 μM) (labeled or unlabeled proteins) for 30 minutes on ice in GF buffer with 40% glycerol before flash-freezing them in liquid N_2 for the PDS measurement.

4.2.3 PDS Measurement: The experiments were carried out at 60 K. The magnetic dipolar coupling **A** (r, θ) between two spin labels A and B, separated by a distance, r, is given by

$$\mathbf{A}\,(r,\theta) = \omega_d\,(1 - 3\cos^2\theta).$$

The dipolar coupling constant, ω_d is, defined as $\gamma_e^2\hbar/r^3$ (γ_e is the gyromagnetic ratio of the electron, $\hbar$ is the Plank's constant divided by 2π, and θ is the angle between the external magnetic field $\mathbf{B}_o$ and the vector r). Primary echo is applied to spins A, which resonates at ωA. A second pump pulse of frequency ωB (value different from ωA) is applied only to excite spins B at varying time delays during the evolution of the A spin echoes. This inverts the coupling with A and changes the frequency of A such that the amplitude of the A echo is modulated at a frequency dependent on the dipole coupling strength.

Four pulse double electron electron resonance (DEER) experiment were conducted on a 17.3 GHz FT ESR spectrometer, which is modified to perform PDS experiments (Bhatnagar et al., 2010; Borbat et al., 1997; Park et al., 2006a). The baseline used for data processing was approximated by a linear polynomial. Distance distributions of spin separations within the sample were calculated by the Tikhonov method (Chiang et al., 2005a) and refined by the maximum entropy regularization method (MEM) (Chiang et al., 2005b).

4.2.4 Spin-labeling efficiency: The modulation depth for N-coupled spins represents the fraction of A spins effected by B-spin pumping and is given by $\Delta(p) = (1-(1-p))^{N-1}$. For a pair of spins,

modulation depth becomes p provided there is 100% spin-labeling. For incomplete spin labeling the modulation depth is a function of spin-labeling efficiency (f), Δ (p,f) = $(1- (1-fp))^{N-1}$. The pulse sequence used for the control experiments to calculate the spin-labeling efficiency had pulse widths of 16 ns -32 ns -32 ns and a pump p pulse of 32 ns. For the 17.3 GHz spectrometer, p is approximately 0.23 for the above mentioned pulse sequence. The spin-labeling efficiency was calculated for the control experiments using the modulation depth for those experiments.

4.2.5 Disulfide cross-linking studies: Cross-linking studies on FliM and FliG were performed according to Bass, et al. with minor modifications (Bass et al., 2007). Copper-phenanthroline was used as the oxidant. Concentrated proteins were in GF buffer. However, the volume of the reaction mixture was made up with disulfide reaction buffer, as mentioned in (Bass et al., 2007). Final concentration of each protein was kept at 6 µM with the Copper-phenanthroline concentration at 2 mM. The reaction volume for each reaction was kept constant at 10 µL. 8 µL of the reaction was quenched with equal volume of 2X SDS with 10 mM imidazole after 1 hr of incubation. 15 µL of this mixture was run on the SDS gel after heat treatment at 90 °C for 2 minutes. For each sample, a control at the zero time point was collected and quenched before the addition of the initiator stock.

4.3 Results:

4.3.1 Spin-label positions: Here, we are exploring the arrangement of the switch components in soluble complexes. For labeling sites, we mutated five residues on $FliM_{NM}$ (E60, D121, M131, R141, S167) and four residues on $FliG_{MC}$ (K160, K174, L208, E305) to cysteine (Fig. 4.2). It is important to mention here that FliM has a native buried cysteine (Cys 214), which was not mutated. Spin-labeling efficiency of this native cysteine is ~ 5 %, hence this position does not

contribute to the PDS signal. Experiments on singly labeled proteins with unlabeled partners were performed first. Under these conditions, oligomerization of the FliM:FliG heterodimer to generate the heterotetramer would yield one distance. This would allow us to obtain FliM:FliM and FliG:FliG distances in the higher order complexes.

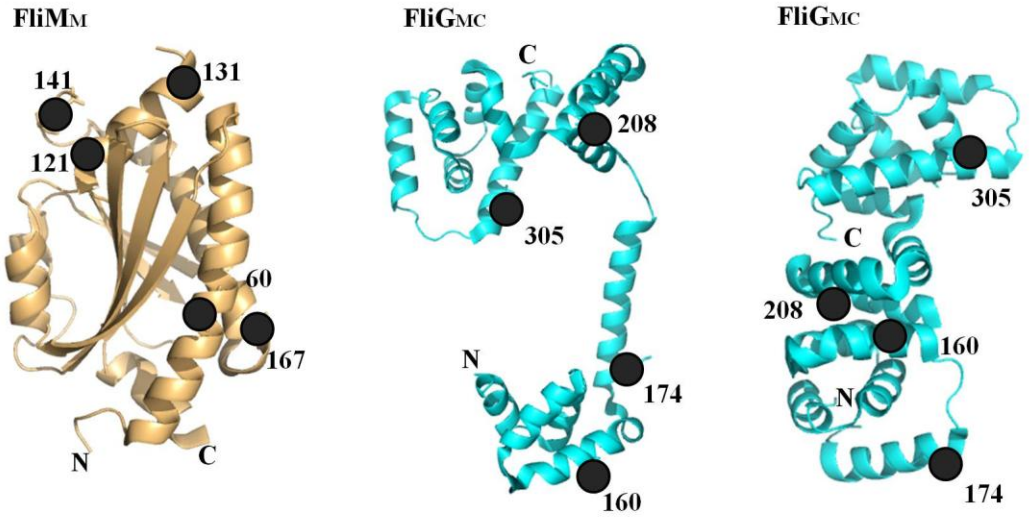

Figure 4.2. **Spin-label positions on FliM and FliG.** Ribbon representation of $FliM_M$ (tan) and $FliG_{MC}$ (aqua) indicating the positions of the spin-labels (grey spheres) Positions of spin-label on $FliM_M$ (PDB 2HP7) and two different $FliG_{MC}$ structures (PDB 1LKV, center and PDB 4FHR, right) are shown. The structures differ with respect to the position of the helix joining the two domains.

4.3.2 Spin-labels on $FliG_M$: Two surface-exposed residues K160 and K174 were chosen in the middle domain of FliG such that the parallel and antiparallel arrangements of the FliM:FliG complex would yield different distances. The distance distribution data of FliG K160 with unlabeled FliM yields a distance of about 47 Å, close to that expected for a parallel arrangement but too short for the distance expected from an antiparallel arrangement (Table 4.1). For FliG K174 we observed a very wide distance distribution with R_{max} of 32 Å, which is close to the distance expected for a parallel arrangement (Table 4.1). Based on those results from FliG K160

and FliG K174, the parallel arrangement is likely present in solution. However, the possibility of a mixture of both parallel and antiparallel arrangement cannot be ruled out as extracting an accurate distance of 70 Å in the presence of a shorter distance is difficult. The broad distribution for K174 could result from a mixture of distances from two different arrangements. Nonetheless, we can conclude that the major configuration is parallel.

4.3.3 Spin-labels on FliM$_M$: PDS was performed with spin-labels on three sites of FliM$_M$. Two sites, E60 and S167 are present along the helices α1 and α1′, respectively. These residues are located close to the edge of the molecule. The third site D121 is present along α3, close to the center of the molecule. All three sites produce only very weak dipolar signals when FliM is alone, which indicates that the protein is monomeric. Both the middle domain and C-terminus of FliG is necessary to see a strong dipolar signal as shown by the time domain signal of FliM E60 (Fig. 4.3). This indicated FliG$_{MC}$ associates the FliM molecules (Bonet, 2010).

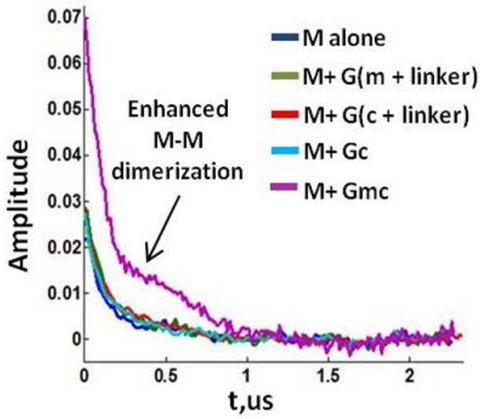

Figure 4.3. **FliG dependent oligomerization of FliM.** Time domain data of FliM E60 showing increase in FliM dimerization in presence of both the domains of FliG, but not FliG$_M$ or FliG$_C$. Figure adapted from Bonet, 2010.

When FliM is in complex with unlabeled FliG$_{MC}$, the spin-label on FliM E60 leads to a peak in the distance distribution of around 30 Å and a smaller peak around 46 Å. The spin-label on D121

gave a distance distribution with the R_{max} of 54 Å. Results obtained from spin-labels on FliM were not conclusive about the nature of the FliM arrangement (Bonet, 2010).

Table 4.1: The C_β-C_β distances as expected from different models. The experimentally observed ESR distances are tabulated in the last column. Provided are the ESR distances in which there are closely related multiple peaks and the R_{max} of the major peak along with the distance range. Semicolons separate multiple distances within the same distance distribution.

	Model I distances (Å)	Model II distances (Å)	Model III distances (Å)	ESR distances (Å)
M_M:M_M				
60:60	26	31.9	31.2	30; 46
121:121	45.8	31.2	30.7	54
167:167	20.5	34.6	33.9	30, 21-38; 48
G_M:G_M				
160:160	67.0	31.3	31.3	48
174:174	41.9	35.5	31.9	32, broad
M_M:G_M				
60:160	40.4, 30.7	40.8, 56.1	40.5, 44.5, 56.9	31; 35;43
121:160	20.5, 31.1	20.8, 42	20.9, 40.6, 33.8	20; 47
167:160	44.5, 27.4	44.8, 60.9	44.5, 46.3, 62.4	31, 30-36; 44
60:174	36.7, 23.6	35.9, 52.3	25.4, 41.4, 39.4	31, 25-35; 44

4.3.4 Inter-protein dipolar coupling with spin pair, on FliM and on FliG: Spin-labels introduced at FliM D121 and FliG K160 showed two distinct distance contributions, a very short component at ~20 Å and a longer one at ~47 Å. The short distance when compared to the distances from the models, can be attributed to the $FliM_M$:$FliG_M$ intermolecular distance in a heterodimer (Table 4.1). This distance is present in all the models, as the $FliM_M$:$FliG_M$ interaction involving GGXG motif and EHPQR motif is conserved in all the models. The longer distance around 47 Å is a mixture of $FliG_M$:$FliG_M$ homodimer distance, $FliM_M$:$FliM_M$ homodimer distance and $FliG_M$:$FliM_M$ intermolecular distances (in the tetramer). For the FliM E60 and FliG K160 spin pair, we observed a very wide distribution. In spite of the wide distance distribution we were able to isolate the peaks that overlap at the base. Based on the control experiments we assigned the peaks to $FliM_M$:$FliM_M$ (32 Å), $FliG_M$:$FliG_M$ (48 Å) and $FliG_M$:$FliM_M$ (37 Å) distances. FliM S167 and FliG K160 showed a wide bimodal distribution spanning about 40 Å, with a peak around 44 Å and another peak around 34 Å.

4.3.5 Cross-linking experiments: In order to rule out the possibility of either parallel or antiparallel arrangement for the FliM:FliG heterotetramer, cross-linking experiments were performed. These experiments allowed us to test the proximity of cysteine residues on FliM in complex with FliG. The control experiment with WT FliM, which has a native cysteine did not show any cross-linked products in the presence or absence of $FliG_{MC}$ (data not shown). Targeted cross-linking was performed on single or doubly mutated FliM in presence of FliG, using residues that were previously identified to be cross-linked (Park et al., 2006b). We also tested FliM residue 164, which would cross-link only in the antiparallel arrangement. The cysteine pairs (64/185 and 57/185) in presence of an oxidant showed efficient cross-linking yielding dimers and multimers in presence of FliG. Cross-linking was also observed with the single

cysteine mutants (57, 64, and 164) in presence of FliG under identical experimental conditions. These cross-linked products however formed only dimers. For mutants 64 and 164, only an antiparallel arrangement of FliM (as expected from the C_β-C_β distances, Fig. 4.4 (C)) would allow the formation of cross-linked products. The antiparallel arrangement would also prevent the formation of multimers. Residue 57 is separated by a distance larger than the distance required for cross-linking in either the parallel or antiparallel arrangement (Fig. 4.4 (C)). The cross-linked product in that case could be a result from random collision. For the mutant 185 we did not observe any cross-linked product as expected from the C_β-C_β distance separation in either arrangement. Results of cross-linking experiments suggested a mixture of parallel and antiparallel arrangements in solution.

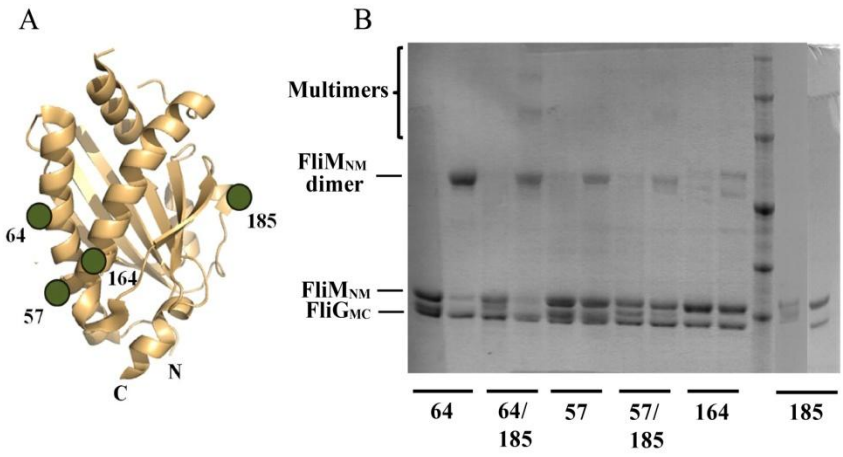

Residues on FliM	Parallel	Antiparallel
64/185	12	37.2
64	32.1	12.5
57/185	20	40.3
57	32.4	33.5
185	33.9	55.8
164	34.2	11.2

Figure 4.4. **Cross-linking studies on FliM in presence of FliG.** (A) Positions of Cysteine residues on $FliM_M$ used for cross-linking study. (B) SDS PAGE gel showing cross-linking between 64 (lanes 1 and 2), 64/185 (lanes 3 and 4), 57 (lanes 5 and 6), 57/185 (lanes 7 and 8), 164 (lanes 9 and 10), and 185 (lanes 11 and 12) Cys pairs. The odd numbered lane is the control for each pair, without the addition of initiator, the even numbered lanes denotes the product after 1 hr of incubation with the initiator. (C) Table denotes the distances in Å as expected for a parallel and antiparallel arrangement of FliM in presence of FliG.

4.3.6 PDS on FliG mutants: The effect of mutations in TmFliG (129, 204, 227) that were previously reported to have disrupted FliG:FliM interaction (Brown et al., 2007) were probed by spin-labeling and PDS (Fig. 4.5).

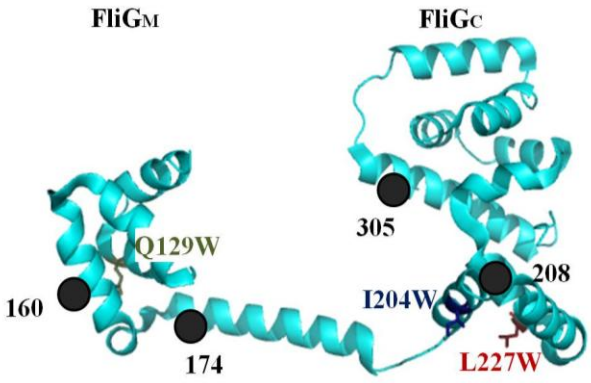

Figure 4.5. **Positions of mutation on FliG that affect FliM:FliG binding.** Positions of mutation (Q129, I204, and L227) and spin-label (K160, K174, L208, and E305) shown as grey spheres mapped on *T. maritima* $FliG_{MC}$ (PDB 1LKV).

Mutating the key residue (Q129) involved in the FliG:FliM interaction in the middle domain of FliG leads to the loss of the $FliG_M$:$FliM_M$ heterodimer distance as observed by the dipolar interactions of the FliG K160 and FliM D121 spin pair (Fig. 4.6) and the FliG K160 and FliM E60 spin pair (Fig. 4.7). However, for the other spin pair FliG K160 and FliM S167, overlap from the $FliM_M$:$FliM_M$ homodimer and $FliG_M$:$FliG_M$ homodimer distances made it difficult to isolate the effect of the mutation on the $FliG_M$:$FliM_M$ separation.

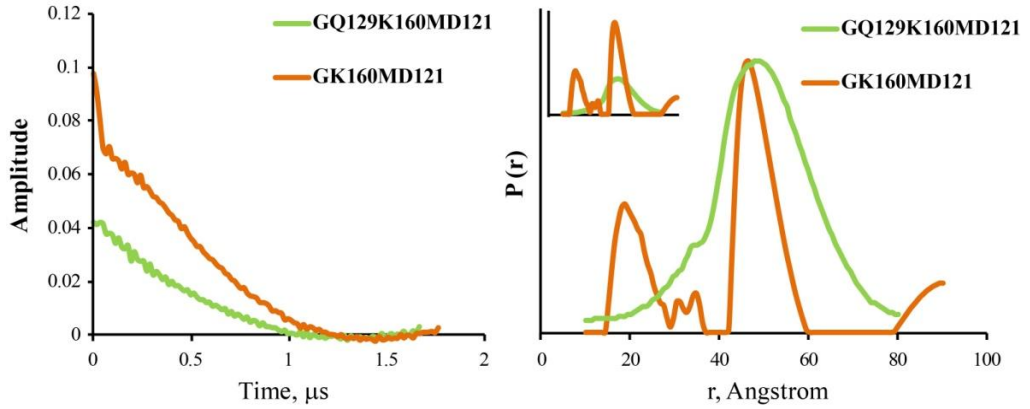

Figure 4.6. **Comparison of time domain signals and distance distributions for spin-labeled FliG K160:FliM D121 between WT and FliG Q129W.** Time domain data (left) and corresponding distance distribution (right) for spin-labels at FliG K160:FliM D121 spin pair (orange) and on the FliG Q129W K160:FliM D121 spin pair (green). Absence of the short distance component (20 Å) upon mutating the key interface residue FliG Q129W when compared to the WT clearly attributes that peak to the $FliG_M$:$FliM_M$ intermolecular distance in the heterodimer. All distance distribution signals are scaled to a common value for ease of comparison. Inset shows the same PDS data without scaling.

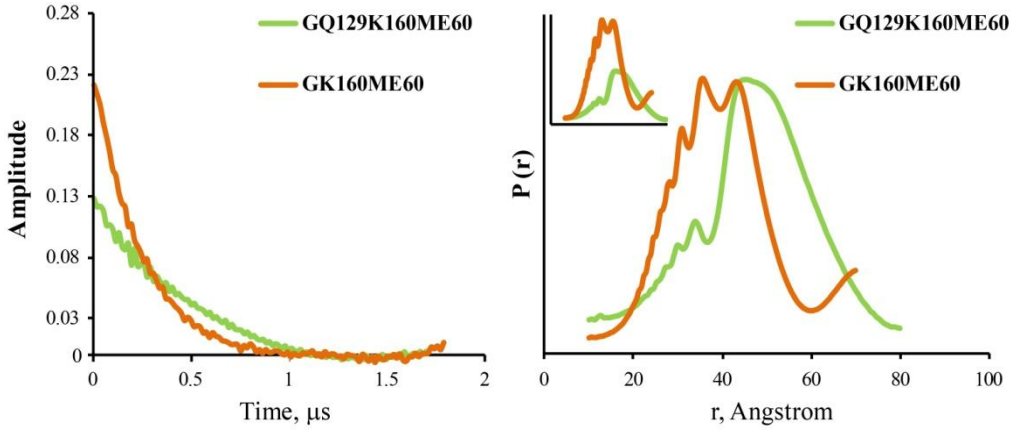

Figure 4.7. **Comparison of time domain signals and distance distributions for spin-labeled FliG K160:FliM E60 between WT and FliG Q129W.** Time domain data (left) and corresponding distance distribution (right) for spin-labels on the FliG K160:FliM E60 spin pair (orange) and on the mutant FliG Q129W K160:FliM E60 spin pair (green). A loss in a peak at distance 40 Å due to the mutation FliG Q129W is attributed to the $FliG_M$:$FliM_M$ intermolecular distance in the heterodimer. All distance distribution signals are scaled to a common value for ease of comparison. Inset shows the same PDS data without scaling.

For mutations in the C-terminal domain of FliG (I204 and L227), the $FliG_M$:$FliM_M$ distance was not affected. A decrease in the signal amplitude was observed, which indicates a decrease in the number of molecules participating in the interaction. Interestingly, for both the FliG C-terminal mutants, we saw the peak around 48 Å disappear as measured for the spin pair FliG K160:FliM E60 (Fig. 4.8). This peak was assigned to $FliG_M$:$FliG_M$ homodimer distance based on control experiments.

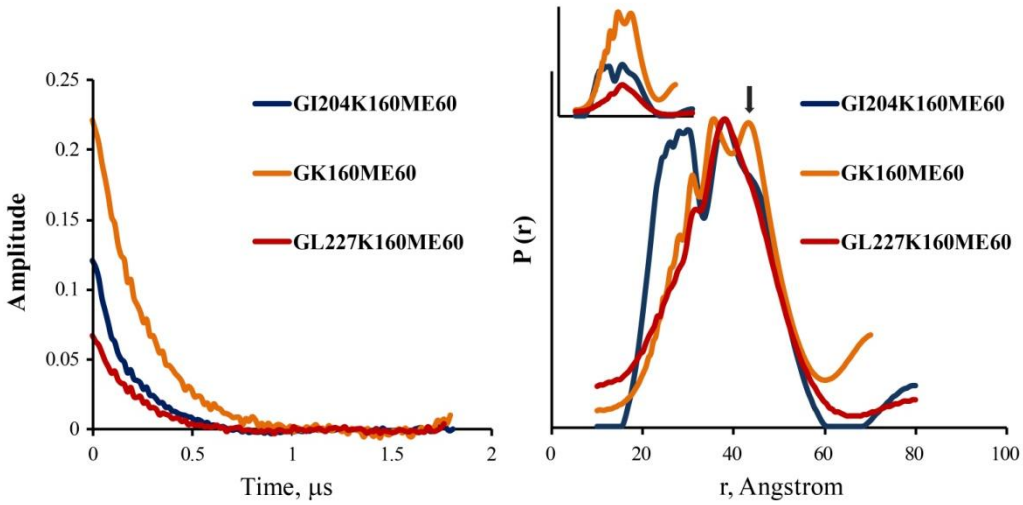

Figure 4.8. **Comparison of time domain signals and distance distributions for spin-labeled FliG K160:FliM E60 between WT and FliG I204W/ FliG L227W mutants.** Time domain data (left) and corresponding distance distributions (right) for spin-labels at FliG K160:FliM E60 spin pair (orange), FliG L227W K160:FliM E60 (red) and FliG I204W K160:FliM E60 spin pair (blue). A loss in a peak at distance 48 Å (indicated by arrow) due to the mutation is attributed to the $FliG_M$:$FliG_M$ homodimer distance. All distance distribution signals are scaled to a common value for ease of comparison. Inset shows the same PDS data without scaling.

In the crystal structure of the CW locked FliG (ΔPEV) mutant from *Thermotoga maritima*, residues 204 and 227 are involved in a hydrophobic interaction in the domain interface between $FliG_M$ and $FliG_C$ (Minamino et al., 2011). The $FliG_M$:$FliG_C$ intermolecular interaction of adjacent molecules is also observed in crystal structures of $TmFliG_{MC}$ (PDB 1LKV) and *Aquifex aeolicus* $FliG_{FL}$ (PDB 3HJL). Mutating these residues to the bulky tryptophan disrupted the domain

interface. Multiangle light scattering experiments on these FliG mutants confirmed the loss of higher oligomeric states of the protein. Such a $FliG_C$:$FliG_{M+1}$ interaction is impossible in the antiparallel arrangement, disfavoring model I. Amongst the other two models, the loss of the $FliG_C$:$FliG_{M+1}$ stacking on mutation can only be explained by the intermolecular interaction between $FliG_M$ and $FliG_C$ of an adjacent molecule as might be possible in model III.

4.3.7 Model validation: Based on results from the mutational studies we could further clarify the nature of the arrangement between FliG and FliM in solution, with model III providing the best fit to the available data. According to model III, PDS experiments with spin-labels on FliM and FliG respectively, would generate five distinct spin-spin separations upon oligomerization (Fig. 4.9). FliG:FliG homodimer distance (d1) would be generated by spin-labels only on FliG. Similarly spin-labels on FliM would generate the $FliM_M$:$FliM_M$ homodimer distance (d2). These distances were measured as the control experiments before with PDS on spin-labeled protein with its unlabeled partner. Presence of both spins in a FliM:FliG heterodimer would generate the intermolecular distance d3. The other heterodimer in the tetramer would yield the same distance d3. Thus d3 contributes twice to the probability term (see equation below). The domains are arranged in a non-symmetrical fashion, generating two different intermolecular distances d4 and d5 in the tetramer.

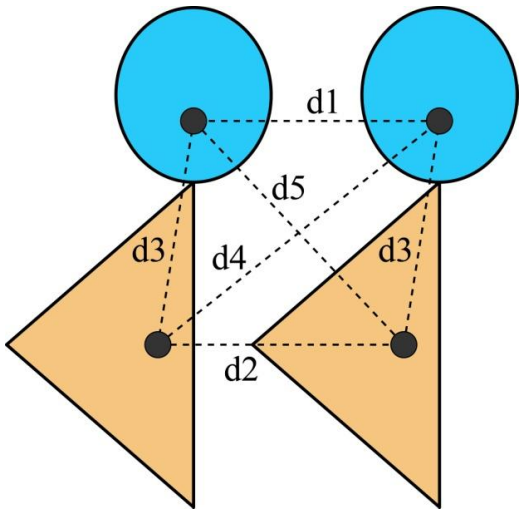

Figure 4.9. **Schematic representation of five distances in FliM (tan):FliG (aqua) tetramer.** Grey spheres indicate the position of the spin-label on the proteins. d1 denotes the FliG:FliG homodimer distance, d2 the FliM:FliM homodimer distance, d3 the FliG:FliM intermolecular distance in the heterodimer, d4 and d5 designate two FliG:FliM intermolecular distances in the heterotetramer.

For qualitative analysis we modeled our experimental data as the sums of five Gaussian functions. The probability of spin separation is then defined as

$$P(r) = S \times \{(f1^2/\sigma1)G1 + (f2^2/\sigma2)G2 + (2f1f2/\sigma3)G3 + (f1f2/\sigma4)G4 + (f1f2/\sigma5)G5\}$$

where S is a normalization factor, G1, G2, G3, G4, and G5 are Gaussian means, σ1, σ2, σ3, σ4, and σ5 are standard deviations for the five distinct distance distributions respectively. f1 and f2 are spin-labeling efficiencies for each spin. Non-linear curve fitting algorithm in OriginLab software was used to fit the experimental distance distribution into a sum of five Gaussian distributions. The C_β-C_β distances from the model and distances from control experiments were used as initial guesses for Gaussian means. They were changed in subsequent steps to improve the fitting. For the fitting process, widths were constrained to 6 Å or lower except for one spin that had a very wide distribution. For distance distributions from structured residues this value serves as the upper limit (Borbat et al., 2002).

For spin pairs FliG K160:FliM S167 and FliG K160:FliM E60 the distance d5 is large (62.4 Å and 56.9 Å respectively). For fitting purposes we did not consider those long distances as under the conditions of the experiment distances around 60 Å or larger cannot be measured accurately. For those spin pairs we used four Gaussian functions instead of five. The spin-labeling efficiency was obtained from the control experiment for one labeled site in the presence of the unlabeled partner as described in the experimental procedure section. Parameters used in one fit were simultaneously used to fit multiple distributions involving the same spin site. The overall good fit allowed us to gauge the quality of the parameters.

The results obtained from the Gaussian fits matched well with the experimental distance distribution data. The consistency of the Gaussian fits was estimated from the adjusted R^2 parameter in the OriginLab software. This parameter ranged from 0.85 to 0.97 and indicated that the Gaussians agreed well to the observed distance distribution data. The small discrepancies between the calculated curve and the experimental distance distribution can be explained by the fact that the distance distributions are probably not exactly Gaussian, for reasons such as the spin-labels have preferred orientations in a given environment (Borbat and Freed, 2007).

We extracted a total of 19 distances that were in good agreement with the C_β distances, yielding a rmsd of 7.0 Å. In T4 Lysozyme, 20 different distance measurements between residues yielded a rmsd of 6.9 Å; this indicates that our deviations arise due to inherent differences between C_β distances and the paramagnetic atoms of the spin-label (Kazmier et al., 2011). It is interesting to note that d1 and d2 are not the same. Based on how the models II and III were generated we would expect them to be the same. The adjacent heterodimer was generated by simple translation of the molecule based on cross-linking experiments (Park et al., 2006b). Crystal structures

suggest a rigid arrangement but in solution the domains are very flexible as observed here by different d1 and d2 values.

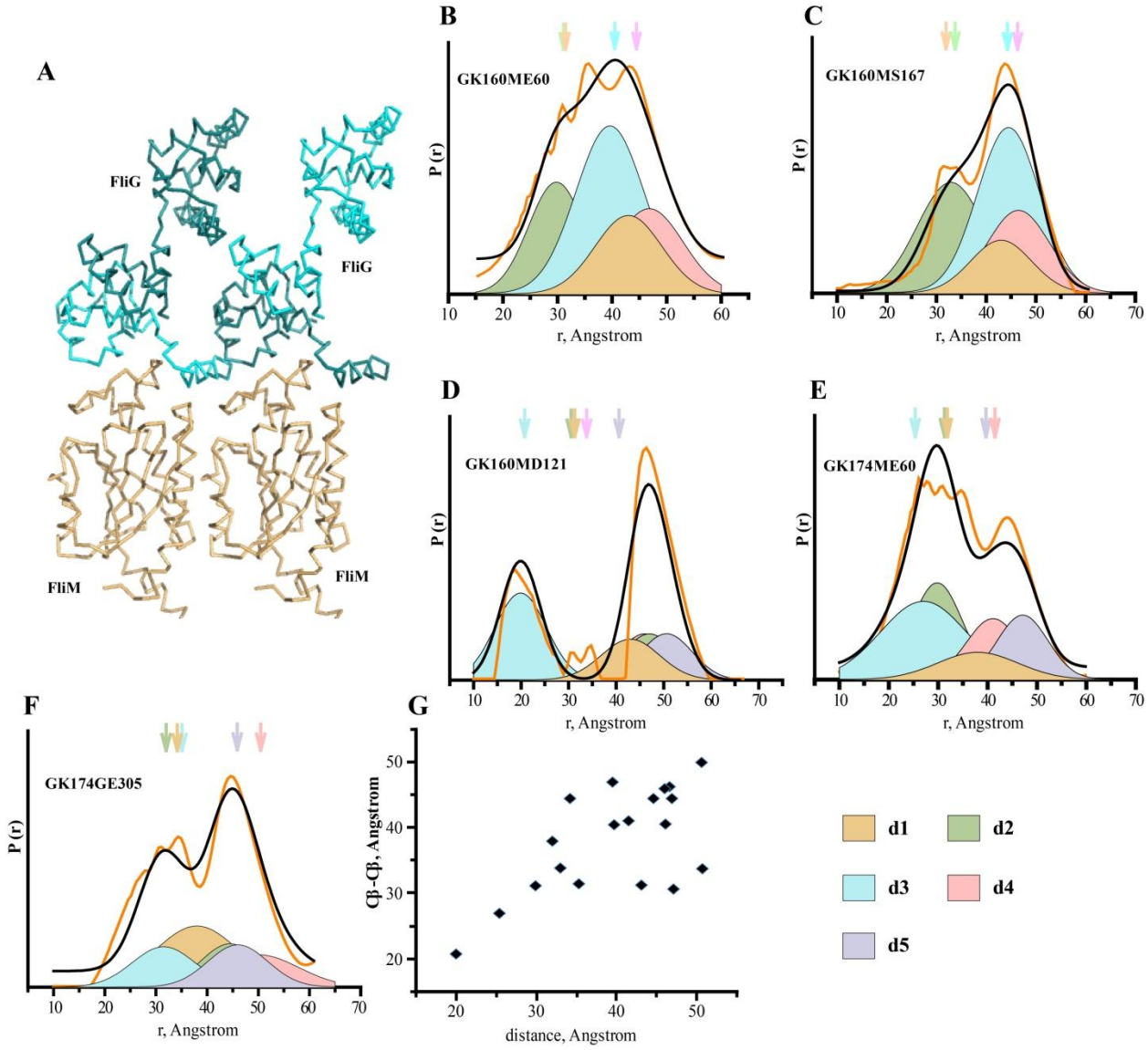

Figure 4.10. **Qualitative analysis of distance distribution data.** (A) Ribbon representation of the $FliM_M$:$FliG_{MC}$ model used in fitting. The lighter teal color indicates the interaction between $FliG_M$ domain and $FliG_C$ domain of the neighboring molecule. Broad distance distributions of spin pairs (B) FliG K160:FliM E60, (C) FliG K160:FliM S167, (D). FliG K160:FliM D121, (E) FliG K174:FliM E60, and (F) FliG K174:FliG E305. The orange line is the experimental distance distribution. The black line is the envelope of the four or five fitted Gaussians. Single Gaussians represents distances d1 (solid beige), d2 (solid green), d3 (solid blue), d4 (solid pink) and d5 (solid grey). The arrows on top indicate the C_β–C_β distances as measured from the model. Only for (B) and (C) the distance distribution is fitted to four Gaussian functions instead

of five. For (F) d1 represents the FliG E305:FliG E305 distance, d2 represents the FliG K174:FliG K174 distance, d3 represents the FliG E305:FliG K174 intramolecular distance, d4 and d5 represent intermolecular distances between the two sites. (G) Distances obtained from the Gaussian fits versus those measured from model III.

4.3.8 Probing the interaction between $TmFliG_C$ and $TmFliM_M$: In model III $FliG_C$ interacts primarily with $FliG_M$ of the adjacent subunit in a parallel arrangement. Mutational studies and cross-linking experiments clearly indicate the role of the conserved hydrophobic patch of $FliG_C$ in the interaction with FliM (Brown et al., 2007; Paul et al., 2011a; Paul et al., 2011b). Studies also suggest that the presence of CheY or CheY-P leads to alteration of the interaction between $FliM_M$ and $FliG_C$ (Dyer et al., 2009). To investigate the interaction between $FliM_M$ and $FliG_C$ in the *T. maritima* system, we performed pull-down assays with two $FliG_C$ variants 195-335 (construct includes Gly-Gly motif) and 204-335 with $FliM_{NM}$. No interaction was observed in the absence and presence of CheY or CheY-P (Fig. 4.11). We also investigated the interaction between $FliG_C$ and $FliM_{NM}$ using PDS by placing spin-labels on $FliG_C$ (E305) and FliM (E60, D121, S167) (data not shown). For most of the spin pairs, distance distributions obtained were weak and broad, making it difficult for us to isolate a $FliG_C$:$FliM_M$ distance from $FliM_M$:$FliM_M$ and $FliG_C$:$FliG_C$ distances. Based on the cross-linking data from David Blair's lab (Paul et al., 2011a) we selected the same residues for SDSL hoping to observe a short distance indicative of a $FliM_M$:$FliG_C$ contact. But we did not observe any short distance in such experiments. Unfortunately, the cysteine pair (M131 or R141 on FliM) was very close to the $FliM_M$:$FliG_M$ interaction surface and introduction of the bulky MTSSL group disrupted the formation of FliG:FliM entirely.

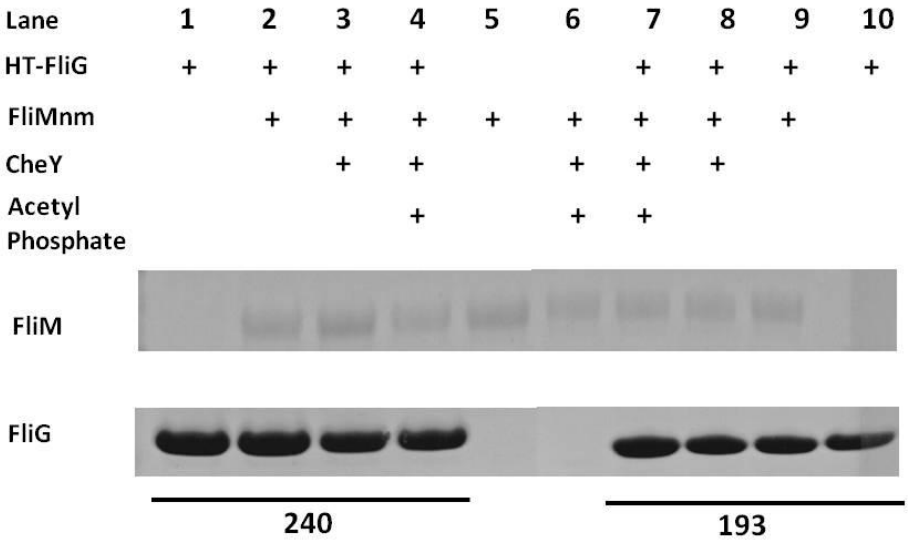

Figure 4.11. **Interaction between FliM and $FliG_C$.** Pull-down assay of $FliM_{NM}$ with $FliG_C$ 240 (lanes 1-4) and $FliG_C$ 193 (lanes 7-10) in presence of CheY or CheY-P where indicated. Controls of $FliM_{NM}$ without tag (lane 5) in presence of CheY-P (lane 6) show some non specific binding to the affinity beads. No apparent binding is observed between $FliM_{NM}$ and $FliG_C$ (240 in lane 2 and 193 in lane 9) nor was it observed in presence of CheY (240 in lane 3 and 193 in lane 8) or CheY-P (240 in lane 4 and 193 in lane 7).

4.3.9 Effects of CheY or CheY-P on the FliM:FliG complex: Pulsed ESR experiments provide us with information as to how the individual domains change juxtaposition when CheY/CheY-P (or activated CheY) binds to the amino terminus of FliM. Spin-labels on different positions of $FliM_M$ shows differential changes when CheY/CheY-P is present along with unlabeled $FliG_{MC}$. An increase in signal amplitude with spin-label at position FliM E60 (Fig. 4.12 (A)) and FliM D121 (Fig. 4.12 (C)) with CheY (purple) and CheY-P (yellow) indicates that CheY brings two FliM molecules in close proximity and this interaction decreases the flexibility making the $FliM_M$ domains very rigid. A weak, broad signal is observed with FliM E60 and unlabeled $FliG_{MC}$. Addition of CheY or CheY-P to the system resulted in a sharp peak around 30 Å and a tiny peak around 47 Å. For FliM D121 and unlabeled $FliG_{MC}$ the peak is slightly sharpened in presence of CheY or CheY-P. Spin-label at S167 showed the opposite effect. The peak was

flattened in presence of CheY-P indicating increased conformational flexibility (Fig. 4.12 (B)) (Bonet, 2010).

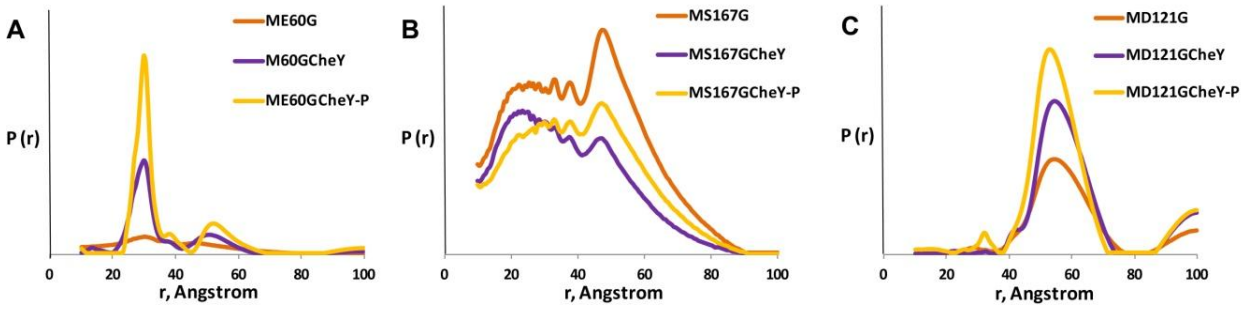

Figure 4.12. **Conformational changes FliM undergoes in presence of CheY and CheY-P using PDS:** Distance distribution for spin-label at (A) FliM E60:FliG (orange) spin pair, in presence on CheY (purple) and CheY-P (yellow) (B) FliM S167:FliG (orange) spin pair in presence of CheY(purple) and CheY-P (yellow) (C) FliM D121:FliG (orange) spin pair in presence of CheY(purple) and CheY-P (yellow). For this set of experiments phosphono CheY was used as the activated CheY. Figure adapted from Bonet, 2010.

4.4 Discussion:

Combining data from PDS, cross-linking and MALS experiments, a model was built for the FliM:FliG arrangement in the upper region of the C-ring. Our mutational study clearly indicates that FliM and FliG interact in the ratio of 1:1 via their middle domains. Higher oligomeric structures are mediated through interaction between $FliG_C$ and $FliG_{M+1}$ as observed before in crystal structures of FliG by numerous groups (Brown et al., 2002; Lee et al., 2010).

4.4.1 Parallel arrangement of FliM and FliG mediated by the $FliG_C$:$FliG_{M+1}$ interaction:

We have shown here that the antiparallel arrangement of FliM and FliG as observed in the crystal structure is not prevalent in solution. The antiparallel arrangement placed FliG on opposite extremes making some copies of it inaccessible to its binding partner –MotA (Lloyd et al., 1996; Zhou et al., 1998). Though the placement of 30 units of FliM:FliG in antiparallel arrangement along with five units in parallel arrangement generated a ring of ~43 nm diameter,

the positioning of FliG dictated by such an arrangement seems unlikely. This arrangement could be an artifact of working with truncated protein or a result of crystal packing. Addition of the C-terminal domain of FliM could prevent the anti-parallel stacking of this arrangement.

The building block of this model is the strong interaction between $FliG_C$ and $FliG_{M+1}$ which essentially polymerizes the FliG molecules into an array. The $FliG_C$:$FliG_{M+1}$ interaction was observed before in the structure of *A. aeolicus* FliG (Lee et al., 2010). The arm stacking in their structure forms a continuous hydrophobic core that extends through the superhelix (Lee et al., 2010). The interaction allows oligomerization of FliM as seen by the increase in signal amplitude in presence of both the middle and C-terminal domains of FliG (Bonet, 2010). The FliM:FliG interaction via the middle domains is observed in crystal structures and by numerous biochemical assays. Unable to observe any interaction between $FliG_C$ and $FliM_M$, we predict that FliG interacts with FliM through the middle domain, which is the higher affinity site. The parallel arrangement of FliM in the C-ring has already been shown through cross-linking experiments (Park et al., 2006b; Paul et al., 2011b) and also here. The cross-linked product in this study, indicative of the antiparallel arrangement, could be a result of random collision or an arrangement favored by the truncated proteins.

4.4.2 Distances are consistent with the model: From the Gaussian fit, 19 distances were extracted and are in good agreement with the C_β–C_β distances from the model with an rmsd of 7 Å. This is consistent with the differences observed in literature between the C_β–C_β distances and spin-labels in single proteins of defined structure. The distances which show the maximum discrepancy involve the FliG:FliG contact. Control experiments on spin-labeled FliG K160 yielded a distance of 48 Å. The C_β-C_β distance used in our fitting is 43 Å whereas the distance from the model would be 32 Å. Distances obtained from ESR experiments are typically longer

than the C_β distances by 5-7 Å (Airola et al., 2013; Bhatnagar et al., 2010; Georgieva et al., 2013). On a closer examination of the molecular structure of the final model it was observed that K160 is present along the interface of $FliG_C$:$FliG_{M+1}$, where its aliphatic side chain participates in a hydrophobic interface. Adding a bulky spin-label to this interface may well affect the interaction between subunits and leading to broadening and increased distances between neighboring $FliG_M$ domains.

In the C-ring three proteins assemble to form the switch complex. In this study we worked with two truncated proteins because the full length proteins do not have high expression levels. It is clear that the FliM:FliG complexes were formed in solution in absence of a membranous structure. The absence of FliN or FliY at the base of the C-ring affected this complex formation. FliM did not have a platform to anchor itself to; this allowed some conformational flexibility to the lower part of the FliM domains. This resulted in slightly longer distances and wider distributions than would be expected in a rigid C-ring.

4.4.3 Interaction between $FliG_C$ and $FliM_M$: Uncertainty in the position of the domains of FliG needs to be addressed because FliG is the component of the rotor involved in torque generation. In the PDS experiments and the pull-down assays, we were unable to detect any interaction between $FliG_C$ and $FliM_M$. The only co-crystal structure of FliM and FliG, which includes the C-terminal domain of FliG, does not show any interaction between $FliM_M$ and $FliG_C$. Instead the interaction was observed only via the middle domains (Vartanian et al., 2012). Solution state NMR studies also could not detect an interaction between TmFliM and $TmFliG_C$ (Dyer et al., 2009). Furthermore in a recent study using pull-down assays and isothermal calorimetric experiments from *Helicobacter pylori* no evidence for interaction between FliM and $FliG_C$ was observed (Lam et al., 2013). On the other hand, the Blair group was able to show the interaction

between $FliM_M$ and $FliG_C$ by cross-linking experiments. Most of the experiments performed by the Blair group were in intact rotors within cells (Paul et al., 2011a; Paul et al., 2011b). It may be possible that the $FliG_C$:$FliM_M$ interaction is only observed in fully assembled rotors.

Due to restrictions of our experiment we could not isolate any distance between $FliM_M$ and $FliG_C$, but the presence of FliG C-terminus is necessary for formation of the higher oligomers as evidenced from previous work by our lab (Bonet, 2010). Based on the EM image, the C-ring has 34-fold symmetry and MS ring has 26-fold symmetry. Since FliG acts as the mediator between the C-ring and the MS-ring, it is believed to have 26 copies. Based on previous study, 34 copies of FliM can fit in to the C-ring (Park et al., 2006b). Extrapolating that result and our finding we would expect 34 copies of FliM to interact with 34 copies of FliG. However with only 26 copies of FliG being present and to explain the symmetry mismatch we hypothesize only 26 copies of $FliM_M$ interact with 26 copies of $FliG_M$ and the remaining eight copies of FliM interact with FliGc. This contact via the C-terminal domain might only be observed under the context of assembled rotors.

4.4.4 CheY-P interactions with FliM: Chemotactic signal is highly amplified within the switch. The reason for this amplification is not very clear. Studies have shown switching to be a highly cooperative event having a hill coefficient of 10 (Cluzel et al., 2000). However, FRET results show that binding of CheY-P to FliM is about fivefold less cooperative than switching (Sourjik and Berg, 2002). In this study we observed changes that occur during the early stages of switching.

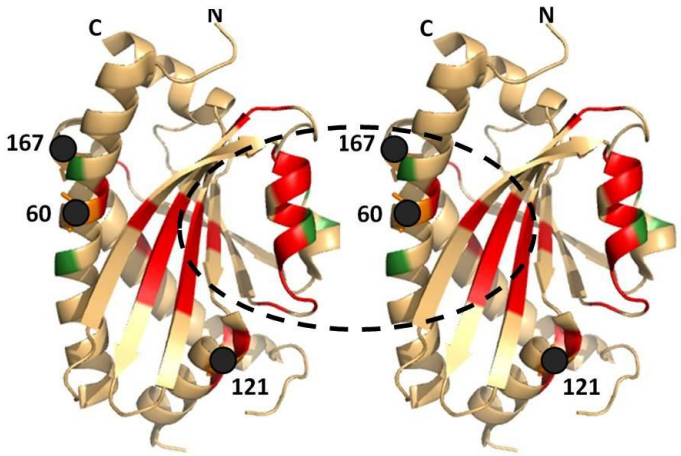

Figure 4.13. **Residues on $FliM_M$ affected by CheY-P binding.** Residues affected by CheY-P binding mapped on to the FliM surface in the assembled subunits are shown in red. Positions of spin-label are shown in grey. Residues involved in cross-linking the FliM monomers are shown in green (Dyer et al., 2009; Park et al., 2006b). Dotted lines indicate the region of CheY-P binding to dimerize FliM and induce rotation of the domains.

PDS experiments on spin-labeled FliM indicate that CheY or CheY-P binds to FliM and brings about conformational changes to $FliM_M$. Previous studies have shown that CheY binds more tightly to FliM full length than $FliM_N$ indicating a second binding site (McEvoy et al., 1999; Sourjik and Berg, 2002). Deletion mutant studies on FliM have implied an interaction between FliM and activated CheY (Mathews et al., 1998). A NMR study from the Dahlquist group isolated residues on FliM that were perturbed in presence of CheY-P (Dyer et al., 2009). Those residues are dispersed along the surface. Residues 59 and 96, which were perturbed the most in the presence of CheY-P, are located near the $FliM_M$:$FliM_M$ interface (Fig. 4.13). Residues 96 and adjacent residues 95, 97, and 98 present along α2 form a solvent exposed hydrophobic patch for binding the response regulator. The CheY binding site 59 is close to the spin-label site 60. We hypothesize that the CheY-P binding causes FliM to rotate. This rotation causes spin-labels present along the periphery to be affected in such a way that it brings the 60 sites together and

the 167 sites further apart. Spin-label 121 is present along α3, more towards the center of the molecule that is not affected much by the rotation, hence we see a slight sharpening of the peak.

This conformational change on FliM resulting from the interaction with CheY-P would induce conformational change to the $FliG_M$ surface via its interacting site. The helix connecting $FliG_M$ to $FliG_C$ would propagate this change to $FliG_C$. Once this conformational change takes place in one unit it would propagate to the neighboring FliG molecule. This would alter the interaction between FliG and MotA resulting in a switch of rotor rotation sense. Further PDS experiments on spin-labeled FliG will help us understand the conformational change it undergoes in the presence of CheY-P and FliM.

References:

Ahn, D.R., Song, H., Kim, J., Lee, S., and Park, S. (2013). The crystal structure of an activated Thermotoga maritima CheY with N-terminal region of FliM. International journal of biological macromolecules *54*, 76-83.

Airola, M.V., Huh, D., Sukomon, N., Widom, J., Sircar, R., Borbat, P.P., Freed, J.H., Watts, K.J., and Crane, B.R. (2013). Architecture of the Soluble Receptor Aer2 Indicates an In-Line Mechanism for PAS and HAMP Domain Signaling. Journal of Molecular Biology *425*, 886-901.

Altenbach, C., Flitsch, S.L., Khorana, H.G., and Hubbell, W.L. (1989). Structural studies on transmembrane proteins. 2. Spin labeling of bacteriorhodopsin mutants at unique cysteines. Biochemistry *28*, 7806-7812.

Armitage, J.P. (1999). Bacterial tactic responses. Advances in microbial physiology *41*, 229-289.

Bass, R.B., Butler, S.L., Chervitz, S.A., Gloor, S.L., and Falke, J.J. (2007). Use of site-directed cysteine and disulfide chemistry to probe protein structure and dynamics: applications to soluble and transmembrane receptors of bacterial chemotaxis. Methods in enzymology *423*, 25-51.

Berg, H.C. (2003). The rotary motor of bacterial flagella. Annual review of biochemistry *72*, 19-54.

Berg, H.C., and Brown, D.A. (1972). Chemotaxis in Escherichia coli analysed by three-dimensional tracking. Nature *239*, 500-504.

Bhatnagar, J., Borbat, P.P., Pollard, A.M., Bilwes, A.M., Freed, J.H., and Crane, B.R. (2010). Structure of the ternary complex formed by a chemotaxis receptor signaling domain, the CheA histidine kinase, and the coupling protein CheW as determined by pulsed dipolar ESR spectroscopy. Biochemistry *49*, 3824-3841.

Bischoff, D.S., and Ordal, G.W. (1992). Identification and characterization of FliY, a novel component of the Bacillus subtilis flagellar switch complex. Molecular microbiology *6*, 2715-2723.

Blair, D.F., and Berg, H.C. (1991). Mutations in the MotA protein of Escherichia coli reveal domains critical for proton conduction. J Mol Biol *221*, 1433-1442.

Bonet, G.G. (2010). Structural, biochemical and biophysical studies of bacterial flagellar switch complex. Doctoral Dissertation, Cornell University, NY, USA.

Borbat, P.P., Crepeau, R.H., and Freed, J.H. (1997). Multifrequency two-dimensional Fourier transform ESR: an X/Ku-band spectrometer. J Magn Reson *127*, 155-167.

Borbat, P.P., Davis, J.H., Butcher, S.E., and Freed, J.H. (2004). Measurement of large distances in biomolecules using double-quantum filtered refocused electron spin-echoes. J Am Chem Soc *126*, 7746-7747.

Borbat, P.P., and Freed, J.H. (2007). Measuring distances by pulsed dipolar ESR spectroscopy: spin-labeled histidine kinases. Methods in enzymology *423*, 52-116.

Borbat, P.P., McHaourab, H.S., and Freed, J.H. (2002). Protein structure determination using long-distance constraints from double-quantum coherence ESR: study of T4 lysozyme. J Am Chem Soc *124*, 5304-5314.

Bourret, R.B., and Silversmith, R.E. (2010). Two-component signal transduction. Current opinion in microbiology *13*, 113-115.

Braun, T.F., and Blair, D.F. (2001). Targeted disulfide cross-linking of the MotB protein of Escherichia coli: evidence for two H(+) channels in the stator Complex. Biochemistry *40*, 13051-13059.

Bren, A., and Eisenbach, M. (1998). The N terminus of the flagellar switch protein, FliM, is the binding domain for the chemotactic response regulator, CheY. J Mol Biol *278*, 507-514.

Brown, P.N., Hill, C.P., and Blair, D.F. (2002). Crystal structure of the middle and C-terminal domains of the flagellar rotor protein FliG. The EMBO journal *21*, 3225-3234.

Brown, P.N., Mathews, M.A., Joss, L.A., Hill, C.P., and Blair, D.F. (2005). Crystal structure of the flagellar rotor protein FliN from Thermotoga maritima. J Bacteriol *187*, 2890-2902.

Brown, P.N., Terrazas, M., Paul, K., and Blair, D.F. (2007). Mutational analysis of the flagellar protein FliG: sites of interaction with FliM and implications for organization of the switch complex. J Bacteriol *189*, 305-312.

Chiang, Y.W., Borbat, P.P., and Freed, J.H. (2005a). The determination of pair distance distributions by pulsed ESR using Tikhonov regularization. J Magn Reson *172*, 279-295.

Chiang, Y.W., Borbat, P.P., and Freed, J.H. (2005b). Maximum entropy: a complement to Tikhonov regularization for determination of pair distance distributions by pulsed ESR. J Magn Reson *177*, 184-196.

Chun, S.Y., and Parkinson, J.S. (1988). Bacterial motility: membrane topology of the Escherichia coli MotB protein. Science *239*, 276-278.

Cluzel, P., Surette, M., and Leibler, S. (2000). An ultrasensitive bacterial motor revealed by monitoring signaling proteins in single cells. Science *287*, 1652-1655.

Columbus, L., and Hubbell, W.L. (2002). A new spin on protein dynamics. Trends in biochemical sciences *27*, 288-295.

Cornish, V.W., Benson, D.R., Altenbach, C.A., Hideg, K., Hubbell, W.L., and Schultz, P.G. (1994). Site-specific incorporation of biophysical probes into proteins. Proc Natl Acad Sci U S A *91*, 2910-2914.

Crane, J.M., Mao, C., Lilly, A.A., Smith, V.F., Suo, Y., Hubbell, W.L., and Randall, L.L. (2005). Mapping of the docking of SecA onto the chaperone SecB by site-directed spin labeling: insight into the mechanism of ligand transfer during protein export. J Mol Biol *353*, 295-307.

Cuello, L.G., Cortes, D.M., and Perozo, E. (2004). Molecular architecture of the KvAP voltage-dependent K+ channel in a lipid bilayer. Science *306*, 491-495.

Dong, J., Yang, G., and McHaourab, H.S. (2005). Structural basis of energy transduction in the transport cycle of MsbA. Science *308*, 1023-1028.

Dyer, C.M., Vartanian, A.S., Zhou, H., and Dahlquist, F.W. (2009). A molecular mechanism of bacterial flagellar motor switching. J Mol Biol *388*, 71-84.

Fanucci, G.E., and Cafiso, D.S. (2006). Recent advances and applications of site-directed spin labeling. Current opinion in structural biology *16*, 644-653.

Georgieva, E.R., Borbat, P.P., Ginter, C., Freed, J.H., and Boudker, O. (2013). Conformational ensemble of the sodium-coupled aspartate transporter. Nature structural & molecular biology *20*, 215-221.

Jeschke, G. (2012). DEER distance measurements on proteins. Annual review of physical chemistry *63*, 419-446.

Jeschke, G., Bender, A., Paulsen, H., Zimmermann, H., and Godt, A. (2004). Sensitivity enhancement in pulse EPR distance measurements. J Magn Reson *169*, 1-12.

Kazmier, K., Alexander, N.S., Meiler, J., and McHaourab, H.S. (2011). Algorithm for selection of optimized EPR distance restraints for de novo protein structure determination. Journal of structural biology *173*, 549-557.

Kojima, S., and Blair, D.F. (2004). The bacterial flagellar motor: structure and function of a complex molecular machine. International review of cytology *233*, 93-134.

Lam, K.H., Ip, W.S., Lam, Y.W., Chan, S.O., Ling, T.K., and Au, S.W. (2012). Multiple conformations of the FliG C-terminal domain provide insight into flagellar motor switching. Structure *20*, 315-325.

Lam, K.H., Lam, W.W., Wong, J.Y., Chan, L.C., Kotaka, M., Ling, T.K., Jin, D.Y., Ottemann, K.M., and Au, S.W. (2013). Structural basis of FliG-FliM interaction in Helicobacter pylori. Molecular microbiology *88*, 798-812.

Lee, L.K., Ginsburg, M.A., Crovace, C., Donohoe, M., and Stock, D. (2010). Structure of the torque ring of the flagellar motor and the molecular basis for rotational switching. Nature *466*, 996-1000.

Liu, J., Lin, T., Botkin, D.J., McCrum, E., Winkler, H., and Norris, S.J. (2009). Intact flagellar motor of Borrelia burgdorferi revealed by cryo-electron tomography: evidence for stator ring curvature and rotor/C-ring assembly flexion. J Bacteriol *191*, 5026-5036.

Lloyd, S.A., and Blair, D.F. (1997). Charged residues of the rotor protein FliG essential for torque generation in the flagellar motor of Escherichia coli. J Mol Biol *266*, 733-744.

Lloyd, S.A., Tang, H., Wang, X., Billings, S., and Blair, D.F. (1996). Torque generation in the flagellar motor of Escherichia coli: evidence of a direct role for FliG but not for FliM or FliN. J Bacteriol *178*, 223-231.

Lloyd, S.A., Whitby, F.G., Blair, D.F., and Hill, C.P. (1999). Structure of the C-terminal domain of FliG, a component of the rotor in the bacterial flagellar motor. Nature *400*, 472-475.

Lowder, B.J., Duyvesteyn, M.D., and Blair, D.F. (2005). FliG subunit arrangement in the flagellar rotor probed by targeted cross-linking. J Bacteriol *187*, 5640-5647.

Lux, R., Kar, N., and Khan, S. (2000). Overproduced Salmonella typhimurium flagellar motor switch complexes. J Mol Biol *298*, 577-583.

Macnab, R.M., and Koshland, D.E., Jr. (1972). The gradient-sensing mechanism in bacterial chemotaxis. Proc Natl Acad Sci U S A *69*, 2509-2512.

Mathews, M.A., Tang, H.L., and Blair, D.F. (1998). Domain analysis of the FliM protein of Escherichia coli. J Bacteriol *180*, 5580-5590.

McEvoy, M.M., Bren, A., Eisenbach, M., and Dahlquist, F.W. (1999). Identification of the binding interfaces on CheY for two of its targets, the phosphatase CheZ and the flagellar switch protein fliM. J Mol Biol *289*, 1423-1433.

McHaourab, H.S., Lietzow, M.A., Hideg, K., and Hubbell, W.L. (1996). Motion of spin-labeled side chains in T4 lysozyme. Correlation with protein structure and dynamics. Biochemistry *35*, 7692-7704.

Minamino, T., Imada, K., Kinoshita, M., Nakamura, S., Morimoto, Y.V., and Namba, K. (2011). Structural insight into the rotational switching mechanism of the bacterial flagellar motor. Plos Biol *9*, e1000616.

Muff, T.J., and Ordal, G.W. (2008). The diverse CheC-type phosphatases: chemotaxis and beyond. Molecular microbiology *70*, 1054-1061.

Park, S.Y., Borbat, P.P., Gonzalez-Bonet, G., Bhatnagar, J., Pollard, A.M., Freed, J.H., Bilwes, A.M., and Crane, B.R. (2006a). Reconstruction of the chemotaxis receptor-kinase assembly. Nature structural & molecular biology *13*, 400-407.

Park, S.Y., Lowder, B., Bilwes, A.M., Blair, D.F., and Crane, B.R. (2006b). Structure of FliM provides insight into assembly of the switch complex in the bacterial flagella motor. Proc Natl Acad Sci U S A *103*, 11886-11891.

Paul, K., and Blair, D.F. (2006). Organization of FliN subunits in the flagellar motor of Escherichia coli. J Bacteriol *188*, 2502-2511.

Paul, K., Brunstetter, D., Titen, S., and Blair, D.F. (2011a). A molecular mechanism of direction switching in the flagellar motor of Escherichia coli. Proc Natl Acad Sci U S A *108*, 17171-17176.

Paul, K., Gonzalez-Bonet, G., Bilwes, A.M., Crane, B.R., and Blair, D. (2011b). Architecture of the flagellar rotor. The EMBO journal *30*, 2962-2971.

Sarkar, M.K., Paul, K., and Blair, D. (2010a). Chemotaxis signaling protein CheY binds to the rotor protein FliN to control the direction of flagellar rotation in Escherichia coli. Proc Natl Acad Sci U S A *107*, 9370-9375.

Sarkar, M.K., Paul, K., and Blair, D.F. (2010b). Subunit organization and reversal-associated movements in the flagellar switch of Escherichia coli. J Biol Chem *285*, 675-684.

Silversmith, R.E. (2010). Auxiliary phosphatases in two-component signal transduction. Current opinion in microbiology *13*, 177-183.

Sircar, R., Greenswag, A.R., Bilwes, A.M., Gonzalez-Bonet, G., and Crane, B.R. (2013). Structure and activity of the flagellar rotor protein FliY: a member of the CheC phosphatase family. J Biol Chem *288*, 13493-13502.

Sockett, H., Yamaguchi, S., Kihara, M., Irikura, V.M., and Macnab, R.M. (1992). Molecular analysis of the flagellar switch protein FliM of Salmonella typhimurium. J Bacteriol *174*, 793-806.

Sourjik, V., and Berg, H.C. (2000). Localization of components of the chemotaxis machinery of Escherichia coli using fluorescent protein fusions. Molecular microbiology *37*, 740-751.

Sourjik, V., and Berg, H.C. (2002). Binding of the Escherichia coli response regulator CheY to its target measured in vivo by fluorescence resonance energy transfer. Proc Natl Acad Sci U S A *99*, 12669-12674.

Sowa, Y., and Berry, R.M. (2008). Bacterial flagellar motor. Quarterly reviews of biophysics *41*, 103-132.

Steinhoff, H.J., Mollaaghababa, R., Altenbach, C., Hideg, K., Krebs, M., Khorana, H.G., and Hubbell, W.L. (1994). Time-resolved detection of structural changes during the photocycle of spin-labeled bacteriorhodopsin. Science *266*, 105-107.

Szurmant, H., Bunn, M.W., Cannistraro, V.J., and Ordal, G.W. (2003). Bacillus subtilis hydrolyzes CheY-P at the location of its action, the flagellar switch. J Biol Chem *278*, 48611-48616.

Thomas, D., Morgan, D.G., and DeRosier, D.J. (2001). Structures of bacterial flagellar motors from two FliF-FliG gene fusion mutants. J Bacteriol *183*, 6404-6412.

Thomas, D.R., Francis, N.R., Xu, C., and DeRosier, D.J. (2006). The three-dimensional structure of the flagellar rotor from a clockwise-locked mutant of Salmonella enterica serovar Typhimurium. J Bacteriol *188*, 7039-7048.

Thormann, K.M., and Paulick, A. (2010). Tuning the flagellar motor. Microbiology *156*, 1275-1283.

Toker, A.S., and Macnab, R.M. (1997). Distinct regions of bacterial flagellar switch protein FliM interact with FliG, FliN and CheY. J Mol Biol *273*, 623-634.

Vartanian, A.S., Paz, A., Fortgang, E.A., Abramson, J., and Dahlquist, F.W. (2012). Structure of flagellar motor proteins in complex allows for insights into motor structure and switching. J Biol Chem *287*, 35779-35783.

Welch, M., Oosawa, K., Aizawa, S., and Eisenbach, M. (1993). Phosphorylation-dependent binding of a signal molecule to the flagellar switch of bacteria. Proc Natl Acad Sci U S A *90*, 8787-8791.

Zhou, J., Lloyd, S.A., and Blair, D.F. (1998). Electrostatic interactions between rotor and stator in the bacterial flagellar motor. Proc Natl Acad Sci U S A *95*, 6436-6441.

Chapter 5

Conclusion and Outlook

The bacterial flagellar motor is considered by many to be the first nanoscale molecular machine discovered. The intricate and complicated designs of these motors have been the source of debate between the proponents of intelligent design and the school of Darwinism. Over forty years of research on the flagellar motor provided information about the molecular components involved, but there is much still unanswered regarding the molecular mechanisms of torque generation and rotational switching (Berg, 2003; Kojima and Blair, 2004; Sowa and Berry, 2008). This is largely because the motor action and regulation require complex interactions among a large number of membrane associated proteins. Understanding the architecture and molecular interactions of the flagellar motor promises to aid in the design of artificial nanomachines.

Chemotaxis and motility are essential for intestinal pathogens like *Helicobacter pylori* to move through the mucous layer of the stomach and find optimum sites of attachment (Howitt et al., 2011; Rolig et al., 2011). Spirochetes, such as *Leptospira, Borrellia*, and *Treponema*, the causative agents of leptospirosis, lyme disease, and syphilis, respectively, penetrate deep into the tissues and blood stream to circulate to sites of infection (Liao et al., 2009). In these cases, directional motility is necessary to survive in the host environment and reach the target site. Disruption of bacterial motility is a possible avenue to mitigate infection. Indeed, mutations in motility apparatuses often render pathogentic bacteria non-infectious. The flagellar motor is unique to prokaryotes and thus may serve as a useful target for antibiotics (Okada et al., 2007). Furthermore, understanding the motility mechanism, will aid in designing new therapeutic agents.

The chemotaxis pathway in *E. coli* has been studied extensively, but in Gram-positive bacteria or spirochetes to a lesser extent. These bacteria have features that are significantly different from *E. coli*. The switch proteins FliM and FliG are common to all the species, the primary difference in Gram-positive bacteria and spirochetes is the replacement of FliN with FliY in the switch (Szurmant and Ordal, 2004). Recent studies on the genera *Leptospira* and *Campylobacter* have identified the role of *fliY* gene in pathogenicity (Liao et al., 2009; Lou et al., 2013). The structure of FliY presented here furthers our understanding of the Gram-positive switch complex and moreover broadens the knowledge about motility and pathogenicity in bacteria. Nonetheless, numerous questions about the switch remain unanswered. For instance, the position of FliY is not clear. It is believed to be positioned in close proximity to FliM, however the functional role of localizing a phosphatase to the switch itself is not understood (Bischoff and Ordal, 1992b; Szurmant et al., 2003). The low-resolution cryo EM image of flagella from *Leptospira interrogans* shows an increase in the C-ring diameter, which may be attributed to the presence of FliY (Raddi et al., 2012). *Leptospira*, encodes both FliN and FliY, and the resolution of the image is not high enough to clearly indicate the postion of FliY with respect to the other rotor proteins. Positioning of FliY could come from a higher resolution EM image of the intact flagella in Gram-positive bacteria. Targeted cross-linking, as has been done for the *E. coli* flagella, or perhaps PDS on intact Gram-positive rotors could also lend insight to FliY positioning.

A study on *Bacillus subtilis* using heterologous CheX expression has shown that compared to CheC and FliY, CheX has the maximum phosphatase activity of all three phosphatases (Muff et al., 2007). In our study we have shown that FliY from *Thermotoga maritima* behaves differently from *Bacillus subtilis* in terms of its ability to interact with other switch components and CheY-P (Sircar et al., 2013). Experiments that compare relative phosphatase activities of *Thermotoga*

maritima phosphatase would be interesting as this bacterial species naturally encodes all the three proteins of the CheC, FliY, and CheX family.

Why FliY has two phosphatase active centers is also not clear. The structure of FliY reveals two active sites situated on two different helices. Interestingly, we have also shown that one active site is more reactive than the other (Sircar et al., 2013). The detailed interactions between FliY and its substrate, activated CheY, are not known. A co-crystalized structure of FliY with CheY gives insight to the system.

Crystal structures of the switch protein components and complexes aided in understanding the architecture of the rotor and how the proteins interact to produce a functional switch. The structure of the binary complex of FliM and FliG presented here has a unique antiparallel arrangement. Subsequently, we showed that this arrangement is not favored in solution. Consequently, we have presented a structural model for FliM:FliG association and arrangement in the C-ring based on results from a combination of spectroscopic techniques and biochemical assays. Ultimately, the model is not perfect and has scope for improvement. A next step to improve the model is to increase the amount of distant restraint data by investigating more spin-label sites specifically on the C-terminal domain of FliG to probe the distance between $FliG_C$ and FliM. However, the limits of studying soluble complexes should be recognized and the greatest impact of extended spin-labeled experiments would involve measurements on intact rotors. It would be a challenge to specifically spin-label a cysteine mutant protein in the intact rotor and isolate the signal, but it would remain as a long term goal for future work.

In this dissertation, the structure of FliY was determined and a model was proposed on how it might be arranged in the C-ring based on our experimental data. In the preceding chapters, the

arrangement of FliM and FliG in the C-ring was shown. We have added two essential pieces to the puzzle about the arrangement of the components in the C-ring: 1) the structure of the non-conserved rotor protein FliY and its interaction with other rotor proteins, and 2) parallel alignment of FliM:FliG dimer in the array. Higher order FliM:FliG complexes are formed by interaction between $FliG_C$ and $FliG_M$ of the adjacent molecule. This information gained here in combination with previously acquired knowledge will collectively facilitate substantial refinement of pre-existing models and lead towards a better understanding of the flagellar switch complex.

References:

Berg, H.C. (2003). The rotary motor of bacterial flagella. Annual review of biochemistry *72*, 19-54.

Bischoff, D.S., and Ordal, G.W. (1992). Identification and characterization of FliY, a novel component of the Bacillus subtilis flagellar switch complex. Molecular microbiology *6*, 2715-2723.

Howitt, M.R., Lee, J.Y., Lertsethtakarn, P., Vogelmann, R., Joubert, L.M., Ottemann, K.M., and Amieva, M.R. (2011). ChePep controls Helicobacter pylori Infection of the gastric glands and chemotaxis in the Epsilonproteobacteria. mBio 2.

Kojima, S., and Blair, D.F. (2004). The bacterial flagellar motor: structure and function of a complex molecular machine. International review of cytology *233*, 93-134.

Liao, S., Sun, A., Ojcius, D.M., Wu, S., Zhao, J., and Yan, J. (2009). Inactivation of the fliY gene encoding a flagellar motor switch protein attenuates mobility and virulence of Leptospira interrogans strain Lai. BMC microbiology *9*, 253.

Lou, H., Ge, Y., Zhang, J., Yan, J., and Zhao, J. (2013). [Role of fliY gene in pathogenicity-associated chemotaxis and colonization of Campylobacter jejuni]. Zhejiang da xue xue bao Yi xue ban = Journal of Zhejiang University Medical sciences *42*, 141-148.

Muff, T.J., Foster, R.M., Liu, P.J.Y., and Ordal, G.W. (2007).CheX in the three-phosphatase system of bacterial chemotaxis. J Bacteriol *189*, 7007-7013.

Okada, A., Gotoh, Y., Watanabe, T., Furuta, E., Yamamoto, K., and Utsumi, R. (2007). Targeting Two-Component Signal Transduction: A Novel Drug Discovery System. Methods Enzymol *422*, 386-395.

Raddi, G., Morado, D.R., Yan, J., Haake, D.A., Yang, X.F., and Liu, J. (2012). Three-dimensional structures of pathogenic and saprophytic Leptospira species revealed by cryo-electron tomography. J Bacteriol *194*, 1299-1306.

Rolig, A.S., Carter, J.E., and Ottemann, K.M. (2011). Bacterial chemotaxis modulates host cell apoptosis to establish a T-helper cell, type 17 (Th17)-dominant immune response in Helicobacter pylori infection. Proc Natl Acad Sci U S A *108*, 19749-19754.

Sircar, R., Greenswag, A.R., Bilwes, A.M., Gonzalez-Bonet, G., and Crane, B.R. (2013). Structure and activity of the flagellar rotor protein FliY: a member of the CheC phosphatase family. J Biol Chem *288*, 13493-13502.

Sowa, Y., and Berry, R.M. (2008). Bacterial flagellar motor. Quarterly reviews of biophysics *41*, 103-132.

Szurmant, H., Bunn, M.W., Cannistraro, V.J., and Ordal, G.W. (2003). Bacillus subtilis hydrolyzes CheY-P at the location of its action, the flagellar switch. J Biol Chem *278*, 48611-48616.

Szurmant, H., and Ordal, G.W. (2004). Diversity in chemotaxis mechanisms among the Bacteria and Archaea. Microbiol. Mol. Biol. Reviews *68*, 301-319.